

POROUS METAL COMPLEXES FOR CO₂ CAPTURING



UNIVERSITY *of the*
WESTERN CAPE

By

Christophe Adrien Ndamyabera

M.Sc. thesis submitted in fulfilment of the requirement for the degree of Magister Scientiae,
in the Faculty of Natural Sciences, Department of Chemistry,



Supervisors

Prof. Salam Titinchi

Dr. Hanna Abbo

2017

DECLARATION

I declare that “**Porous metal complexes for CO₂ capturing**” is my own work, that it has not been submitted for any degree or examination in any other university and that all the sources I used or quoted have been indicated and acknowledged by appropriate references.

Full name: Christophe Adrien NDAMYABERA...

Signed:

Date:



KEY WORDS

Carbon dioxide

Porous materials

Metal organic frameworks

Microwave

Cobalt succinates

Nickel hydroxy-terephthalates

CO₂ adsorption capacity



ABSTRACT

The need in energy has resulted in the burning of fossil fuels at an increasingly high level. The consequence is a release of high volumes of carbon dioxide gas (CO₂) in the atmosphere. This gas is a major greenhouse gas which causes global warming. There is therefore a great need to efficiently sequester this gas (CO₂) for a sustainable economic development and environment. A new class of metal organic frameworks (MOFs) is a promising high potential application in carbon dioxide capture.

In the current study, synthetic methods were developed for the design of porous cobalt succinates and nickel hydroxy-terephthalates for CO₂ adsorption. The methods developed and interrogated include, sonication, hydrothermal synthesis (at room temperature, reflux and Parr reactor), and microwave synthesis. The conventional cobalt chloride hexahydrate was substituted by cobalt acetate for synthesis at room temperature. Cobalt acetate was used to replace cobalt chloride in the synthesis of cobalt succinate at room temperature and led to a new cobalt succinate complex (CoS-Ac). The complex CoS-Ac differs from CoS synthesized from cobalt chloride hexahydrate. Synthesis of cobalt succinate via sonication (CoS-sn) was achieved in 45 min and the structure of the complex was different when synthesized via the hydrothermal route (under reflux) abbreviated CoS-th.

Cobalt succinates were also synthesized under autogenous pressure (pr) using different reaction conditions. The obtained complexes are abbreviated as CoS-pr1, CoS-pr2 and CoS-pr3. Pores were observed in these compounds as shown by SEM. Thermo-gravimetric analysis showed that weight loss of guest molecules increased using hexane in the following order: CoS-pr3>CoS-pr2>CoS-pr1. On the other hand, microwave synthesis (mw) was used to prepare cobalt succinates complexes under different reaction conditions. It was found that two of the obtained complexes i.e. CoS-mw1 and CoS-mw2 were similar. The EDS results of these complexes showed the presence of chlorine and potassium. This

confirms that their structures are different from cobalt succinates synthesized through the other synthesis routes.

In this study, additional porous complexes i.e. nickel hydroxy-terephthalates, were synthesized via a thermal route using different reaction conditions and abbreviated as Nitp-1, Nitp-2, and Nitp-3. The synthesis of Nitp-2 and Nitp-3 involved the use of hexane to assist in the purification of Nitp-2 and Nitp-3 by removal of unreacted terephthalic acid.

All the synthesized complexes were carefully characterized using various techniques viz., FTIR, UV-Vis, TGA, XRD, SEM, and EDS. The CO₂ adsorption study was carried out using TGA. The results obtained showed that CoS-mw2 achieved the highest adsorption capacity of 0.074 mmol of CO₂/g among the synthesized cobalt succinates. The effect of using hexane in the synthesis of CoS-pr2, and CoS-pr3 led to a higher adsorption capacity compared to CoS-pr1. The regeneration process i.e. adsorption-desorption was performed for three cycles using CoS-pr2. Among Nitp-1, Nitp-2, and Nitp-3, Nitp-2 showed the highest adsorption capacity of 0.16 mmol of CO₂/g. It is also concluded from the CO₂ regeneration process using Nitp-2 as a representative adsorbent for three cycles that these adsorbents can be recycled and reused.

DEDICATION

This thesis is dedicated to my mother T. NYIRABARUNDI, J. UKWIZAGIRA and my family in general.



UNIVERSITY *of the*
WESTERN CAPE

ACKNOWLEDGEMENT

The support from many people contributed a lot to achieve the completion of my thesis with helpful criticism and assistance, and references. These people's contribution made this thesis meaningful and their support is highly appreciated.

I am greatly thankful to my supervisors Prof. Salam Titinchi and Dr. Hanna Abbo, for their guidance, insights, thoughtful suggestions, and continuous support during the progress of this research. I thank you for your practical assistance and encouragement. I would like to express my strong appreciation for the financial support from the EnPe-Programme, The Norwegian University of Science and Technology (NTNU). Also, I would like to acknowledge all the assistance and support from the University of the Western Cape (UWC) specifically the department of chemistry for providing machines, laboratories and conducive environment for research.

I highly appreciate the advice from Mr. Ayabei, Dr. G. Ndayambaje, E. Tuyishimire and E. Ameh. Your encouragement for my journey in the master was great. In addition, I would like to thank Ms. E. Gabriella, P. Ms. Veruscha and other colleagues from Catalysis Research Group, my colleague Mr. H. Kipruto and my colleagues at the UWC in general for their academic support.

I would like to express my deep gratitude to my mother, T. Nyirabarundi for your parenthood cares, kind love, and support. You are my mother. I express my deep gratitude to my friend J. Ukwizagira for your brotherhood support, caring, strong advice and sacrifice. You have made it. This work is acknowledged to my brother and sisters in Rwanda I thank you for your support.

I cannot stop to thank J. Umunyurwa, Dr. S. Ndimurugero, and Ms O. Murara for your advice and different supports. I also thank very much Mr. J. Biraguma and L. Mukaruzima your support is highly appreciated.

This master's thesis is acknowledged to the family of KAMOSO through Sister G. Mukamarara for your parenthood cares and financial support during my high school studies which are the foundation of this achievement.

I thank all lecturers at the former National University of Rwanda for your academic support during my bachelor's studies. I thank the teachers at Nyamasheke high school for your work that empowered me to have the foundation of my studies. I thank teachers who taught me at Shara primary school including A. Mukantagara and J.P. Sindikubwabo.



CONTENTS

DECLARATION	i
KEY WORDS	ii
ABSTRACT	iii
DEDICATION	v
ACKNOWLEDGEMENT	vi
CONTENTS	viii
LIST OF FIGURES	x
LIST OF TABLES	xi
ABBREVIATION	xii
CHAPTER 1: INTRODUCTION	1
1.1 Introduction	1
1.2 Background	1
1.2.1 Impacts caused by CO ₂ emission	2
1.2.2 Reduction of CO ₂ emission	2
1.3 Problem statement	5
1.4 Research question of the study	6
1.5 Hypothesis	6
1.6 Objectives	7
1.7 Research approach	7
1.8 Research outlines	8
CHAPTER 2: LITERATURE REVIEW	10
2.1 Introduction	10
2.2 T Background of CCS and fators influencing it	10
2.2.1 Pre-combustion CO ₂ capture	11
2.2.2 Oxy-fuel combustion capture	12
2.2.3 Post-combustion capture	12
2.3 Carbon dioxide capture by absorption	14
2.3.1 Amine-based solvents	14
2.3.2 Ionic liquids	15
2.4 Carbon dioxide capture by membranes	16
2.5 Carbon dioxide capture by adsorption	17
2.5.1 Zeolites	17
2.5.2 Metal-organic frameworks MOFs	18
2.5.3 Adsorption capacity	33
2.6 Chapter summary	35
CHAPTER 3: EXPERIMENTAL	37
3.1 Introduction	37
3.2 Materials	37
3.3 Synthesis of cobalt succinates	37
3.4 Synthesis of Nickel hydroxy-terephthalates	39
3.5 Characterization techniques	40

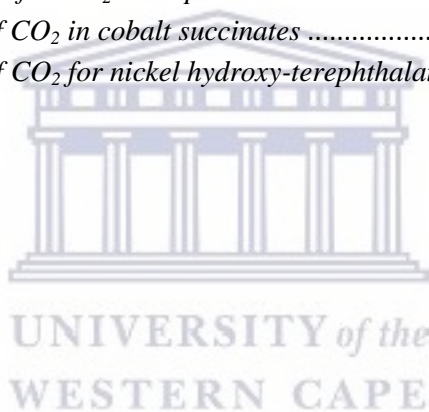
3.5.1	Fourier Transform Infrared (FTIR) Spectroscopy	40
3.5.2	Ultraviolet-Visible spectroscopy (UV-Vis)	40
3.5.3	Thermal gravimetric analysis (TGA)	40
3.5.4	X-ray powder diffraction (XRD)	41
3.5.5	Scanning electron microscopy and Energy dispersive X-ray spectroscopy (EDS).....	41
3.6	Adsorption and desorption process of carbon dioxide	42
3.7	Chapter summary	43
CHAPTER 4: RESULTS AND DISCUSSION: COBALT SUCCINATES		44
4.1	Introduction.....	44
4.2	FTIR characterisation.....	45
4.3	Ultraviolet and Visible (UV-Vis) characterization	49
4.4	Thermal gravimetric analysis (TGA) characterisation.....	52
4.5	Scanning electron microscopy (SEM) and energy dispersive X-ray spectroscopy (EDS) ...	57
4.6	X-ray diffraction (XRD) characterisation	62
4.7	Chapter summary	65
CHAPTER 5: RESULTS AND DISCUSSION: NICKEL HYDROXY-TEREPHTHALATES		67
5.1	Introduction.....	67
5.2	Fourier transform infrared (FTIR)	68
5.3	Ultraviolet and visible (UV-VIS).....	69
5.4	Thermal gravimetric analysis (TGA).....	71
5.5	Scanning electron microscopy spectroscopy (SEM) and energy dispersive X-ray spectroscopy (EDS)	73
5.6	X-ray diffraction analysis (XRD)	76
5.7	Chapter summary	78
CHAPTER 6: CARBON DIOXIDE (CO₂) ADSORPTION		79
6.1	Introduction.....	79
6.2	Adsorption capacity of CO ₂ for the cobalt succinates.....	80
6.3	Adsorption capacity of CO ₂ for the nickel hydroxyl-terephthalates	82
6.4	Recycling CO ₂ from adsorbent	84
6.5	Summary of the chapter	86
CHAPTER 7: CONCLUSION AND RECOMMENDATIONS		88
7.1	Conclusion	88
7.2	Recommendations and future work	90
REFERENCES		91
APPENDIX.....		105

LIST OF FIGURES

Figure 2.1: Three options for CO ₂ capture from power plant generation [20].....	13
Figure 2.2: Formation of new chemical bonds in amine during CO ₂ absorption process [8].....	15
Figure 2.3: Coordination mode in which carboxylates can be linked to metal center or node [78].....	19
Figure 2.4: Coordination polymer MOFs with different coordination mode [69].....	20
Figure 2.5: Evolution of the five phases of cobalt succinates, from low temperature (far left) to high temperature (far right).....	27
Figure 4.1: FTIR spectra of cobalt succinates a) from Co(CH ₃ COO) ₂ ·4H ₂ O and CoCl ₂ ·6H ₂ O at rt, sonication & thermal reaction, b) Parr reactor and c) microwave	46
Figure 4.2: Proposed structure for the compound CoS-mw1 and CoS-mw2 [152]	48
Figure 4.3: UV-Vis spectra of cobalt succinates a) from Co(CH ₃ COO) ₂ ·4H ₂ O or CoCl ₂ ·6H ₂ O at rt, sonication & thermal reaction, b) Parr reactor and c) microwave.	50
Figure 4.4: Thermal behaviour under air of cobalt succinates a) from Co(CH ₃ COO) ₂ ·4H ₂ O and CoCl ₂ ·6H ₂ O at rt, sonication & thermal reaction, b) Parr reactor, and c) microwave.	53
Figure 4.5: SEM images of CoS-pr1 synthesized using only water, showing a) the surface morphology b) the aggregate particles filled in pores	58
Figure 4.6: SEM images of CoS-pr2 synthesized using water and 1.25 ml of hexane a) surface morphology and shape and b) free pores and very few aggregate particles at the surface.	58
Figure 4.7: SEM image of CoS-pr3 synthesized using water and 2.5 ml of hexane a) Surface morphology and shape and b) free pores and aggregate particles at the surface	58
Figure 4.8: SEM image of CoS-mw1 showing a) surface morphology b) open pore structures.....	59
Figure 4.9: EDS spectra of cobalt succinates a) Parr reactor b) Parr reactor and adding 1.25 ml of hexane to the reaction mixture, and c)Parr reactor and adding 2.5 ml of hexane to the reaction mixture, and d) by microwave.	61
Figure 4.10: XRD spectra of cobalt succinates a) from (CH ₃ COO) ₂ Co·4H ₂ O and CoCl ₂ ·6H ₂ O at rt, using sonication and thermal reaction, b) using Parr reactor and c) using microwave.	64
Figure 5.1: FTIR spectra of nickel hydroxy-terephthalates and TPA.....	68
Figure 5.2: UV-Vis spectra of a) nickel hydroxy-terephthalates synthesized along with parent compound TPA.....	70
Figure 5.3: TGA of nickel hydroxy-terephthalates synthesized Nitp-1, Nitp-2 and Nitp-3.....	71
Figure 5.4: SEM images of nickel hydroxy-terephthalates synthesized a) Nitp-1, b) (Nitp-2, and c) Nitp-3.	74
Figure 5.5: EDS spectra of nickel hydroxy-terephthalates a) Nitp-1, b) Nitp-2 and c) Nitp-3.	75
Figure 5.6: XRD diffractograms of nickel hydroxy-terephthalates Nitp-1 Nitp-2 and Nitp-3.....	77
Figure 6.1: CO ₂ Adsorption of cobalt succinates at 33 °C (a) at rt, sonication, and thermal reaction (b): by Parr reactor and microwave.	81
Figure 6.2: Adsorption process of CO ₂ at 33 °C for nickel hydroxy-terephthalates.	83
Figure 6.3. a and b: cyclic adsorption-desorption of CO ₂ by CoS-pr2 and Nitp-2.	85

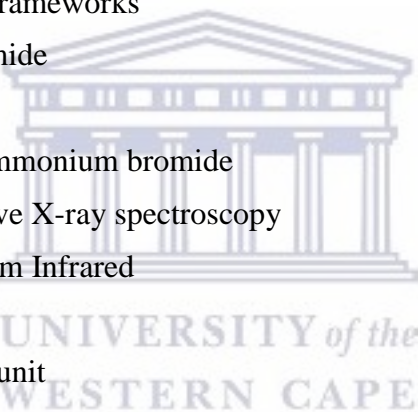
LIST OF TABLES

<i>Table 2.1: Comparison of crystal size of MOFs synthesized from conventional and microwave synthesis</i>	25
<i>Table 2.2: List of synthesized metal organic complexes with their metal sources and reaction conditions</i>	30
<i>Table 3.1: Chemical reagents</i>	37
<i>Table 3.2: Abbreviations of cobalt succinate complexes and synthesis conditions</i>	38
<i>Table 3.3: Abbreviations of the synthesized nickel terephthalates</i>	39
<i>Table 4.1: Compound codes and their corresponding explanation</i>	44
<i>Table 4.2: UV-Vis spectra observed for cobalt succinates</i>	51
<i>Table 4.3: Weight loss analysis for cobalt succinates</i>	54
<i>Table 4.4: EDS states quantitative elemental analysis of compounds CoS-pr1, CoS-pr2, CoS-pr3, and CoS-mw1</i>	60
<i>Table 5.1: Table of abbreviations of nickel terephthalates according to the synthetic conditions</i>	67
<i>Table 5.2: TGA results of nickel hydroxy-terephthalates</i>	72
<i>Table 5.3: The elemental composition of Nitp-1, Nitp-2, and Nitp-3 from EDS analysis</i>	76
<i>Table 6.1: Experimental condition for CO₂ adsorption</i>	79
<i>Table 6.2: Adsorption capacity of CO₂ in cobalt succinates</i>	80
<i>Table 6.3: Adsorption capacity of CO₂ for nickel hydroxy-terephthalates</i>	83



ABBREVIATION

Ac:	Acetate
bi-pyren:	1,2-Bis(4-pyridyl)-ethylene
bipy:	2,2'-Bipyridine
BTC:	Benzene tricarboxylic acid
CCS:	Carbon Capture and Storage
IPCC:	Intergovernmental Panel on Climate Change
rt:	Room Temperature
ILs:	Ionic liquids
RTIL:	Room temperature ionic liquids
TSA:	Temperature Swing Adsorption
PSA:	Pressure Swing Adsorption
MOFs:	Metal Organic Frameworks
DMF:	Dimethylformamide
CoS:	Cobalt succinate
CTAB:	Cetyltrimethylammonium bromide
EDS:	Energy Dispersive X-ray spectroscopy
FTIR:	Fourier Transform Infrared
GHG:	Greenhouse gas
GPU:	Gas permeation unit
H ₂ BDC:	Benzene dicarboxylic acid
ndc:	2,6-Naphtha-lenedicarboxylate
pH:	Power of hydrogen
pr:	Parr reactor
SDA:	Structure-directing agent
SEM:	Scanning electron microscopy
sn:	Sonication
TGA:	Thermal gravimetric Analysis
th:	Thermal reaction
TMB:	1,3,5-Trimethylbenzene
UV-Vis:	Ultraviolet-Visible
XRD:	X-Ray Diffraction



CHAPTER 1: INTRODUCTION

1.1 Introduction

This chapter briefly gives a background on the origin of carbon dioxide (CO₂), which is the main greenhouse gas and illustrates the hazards that might be caused by the high volume of CO₂ emitted in atmosphere. Several technologies used to sequester the subject gas are discussed herein. However, such technologies have been reported to present several drawbacks. Therefore, an alternative technology of using the emerging class of porous material, metal-organic frameworks (MOFs) has been used to capture CO₂ efficiently. Different materials are used for CO₂ capture and include amine-based solvents, ionic liquids, zeolites, ordered mesoporous silica, and membranes. The studies showed that MOFs offer more advantages over the others. Advanced properties of these compounds are developed through various synthetic methods some of which are described in this work.

1.2 Background

Global warming and its consequences are on the increase due to anthropogenic influences of carbon dioxide, the main cause of global warming and other greenhouse gases (GHG). In 2010, it was reported that CO₂ contributes up to 76% of the total global warming [1,2]. From the industrial revolution up to 2005, carbon dioxide concentration increased by about 36%. According to an intergovernmental panel on climate change (IPCC) estimations, the increase may even be as high as 95% by 2100 if no effective policy is instituted on carbon dioxide (CO₂) emission [1].

The increase in CO₂ emitted from anthropogenic influences where the sources are; energy, industry, transport and building sectors. Pachauri *et al.* reported that the burning of fossil fuel in power plants makes the highest contribution towards CO₂ emission among those sectors [1]. In 2006, world energy was dependant on 95% from fossil fuels as reported by Owen [3]

while Menyah reported that South African's total energy supply depended on 70% being derived from burning fossil fuels [4].

IPCC announced that the increase in CO₂ emission is caused by population growth and industrial development, the latter being the main cause. It was noted that the population growth from 2000 to 2010 was approximately the same as the previous three decades while the industrial development increased sharply CO₂ emission by 22% [1]. The group of twenty countries including South Africa (G20), the world's leading industrialised and emerging economies was responsible for 81.5% of global CO₂ emissions in 2015 because of rapid industrialization [5].

1.2.1 Impacts caused by CO₂ emission

According to the IPCC, the temperature on the earth's surface area will likely increase by 2 °C in 2100 [1]. This would result in annual precipitation increase in some areas and a decrease in others. Consequently, this global warming could likely influence oceans and sea level rise in 2100 between 0.5 and 1.4 meters above 1990 [6]. Consequently, due to the rise in temperature arctic and antarctic ice will melt and decrease and life quality for humans and animals will suffer because water, food and air will be adversely affected [1,2]. Therefore, it is important to sequester CO₂ from flue gas released from power plants in order to counteract its contribution towards global warming.

1.2.2 Reduction of CO₂ emission

Research conducted on different methods to improve the efficient removal of CO₂ from the atmosphere has been a constant theme of huge value [7]. The liquid amines based absorption method was found to effectively capture CO₂ [8] but requires a high energy input for regeneration of the adsorbent [2,9]. Amine-based solvents easily deteriorate and are

somewhat corrosive and are easily oxidized [10,11], all of which limit their application. Ionic liquids were used as an alternative to amine solvents with increased absorption capacity and absence of volatility but their viscosity is a drawback [12]. Membranes were used for carbon capture as improved materials due to their selectivity but their limited permeability remained a challenge [13,14]. Research on alternative materials, viz., zeolites showed high adsorption and stability but overwhelming challenges are low CO₂ adsorption at high temperature, high temperature to regenerate the adsorbent and low stability in the presence of water [15]. In addition to these drawbacks, zeolites displayed a low selectivity for CO₂ adsorption [16]. A new class of hybrid material derived from metal ions with a well-defined coordination geometry and organic linkers was found to contribute to efficient CO₂ capture [16–18]. Porous materials referred to as Metal Organic Frameworks (MOFs) are reported as having a greater potential for CO₂ adsorption [9,18].

The research continues to investigate technologies that can effectively reduce CO₂ emission [19,20]. Several countries have developed technologies to capture CO₂ [21,22] including solvent systems based on amine adsorbents, chemical looping (metal oxides), and zeolites. In Korea, they developed the technology to capture CO₂ using dry potassium based sorbents [23]. Research on the use of Zeolitic Imidazolate Frameworks [24] and Porous Carbon Monoliths [25] to contribute to CO₂ sequestration in America, China and Germany. Adsorbents for CO₂ capture such as MOFs were developed, produced and commercialized all over the world [26]. In South Africa, a carbon capture policy plans to implement a CO₂ plant using amine base solvents by 2020 [27]. Research on the use of other techniques are an ongoing investigation; for example, the use of MOFs for gas adsorption is ongoing in South Africa [27]. Among the cases studied in South Africa, the syntheses of ZrMOFs for hydrogen storage [28] and $Zn_2(\mu_2\text{-OH}_2)(\text{HBTRI})(\text{BTRI})(\text{H}_2\text{O})_2 \cdot \text{DMA} \cdot 3\text{H}_2\text{O}$ and $\text{Gd}(\text{BTRI})(\text{H}_2\text{O})_6$ (HBTRI: 1,3,5-benzene tricarboxylic acid and BTRI its deprotonated unit)

using zinc(II) sulphate heptahydrate and gadolinium(III) nitrate heptahydrate mixed with HBTRI for the stability test is receiving much attention[29]. The investigations are on-going to find a materials that can efficiently contribute to the CO₂ capture.

Metal-organic frameworks (MOFs) are metal or metal oxide clusters connected by pillar-like ligands which serve as bridges [30]. This emerging class of MOFs is scientifically exciting due to their crystalline nature, pore tunability, large surface area, and thermal and chemical stability [30–33]. They have a wide range of application such as; gas storage, chemical separation, catalysis, drug delivery, and gas adsorption [32]. The good quality of MOFs depends on different synthetic parameters which offer good tailoring for the desired structure [34]. The high cavity and/or high surface area also depends on the length of the organic linker (ligand) [32] which may contain functionalities such as –OH, –COOH, and N-donating groups [32]. The source of metal salt also contributes to properties like purity and structure of the synthesized MOFs and these may have an impact on gas adsorption [34]. Furthermore, the concentration, solvent, and pH play important roles and have to be taken into account during preparation of these porous materials [34]. The effect of benzene as a template in the synthesis of MOFs resulted in porous non-interpenetrated compounds [35]. Temperature is the most important parameter reported to play a crucial role in designing MOFs to achieve a 3D (three dimension) structure [36]. An example of the effect of temperature on the MOFs structure is the synthesis of cobalt succinates at temperatures above 150 °C which leads to a 3D structure with an increase in the number of coordinated ligands on the metal centre and incorporation of hydroxyl groups [37,38]. The compound $\text{Co}(\text{H}_2\text{O})_4(\text{C}_4\text{H}_4\text{O}_4)_2$ was synthesized at temperatures below 100 °C while $\text{Co}_5(\text{OH})_2(\text{C}_4\text{H}_4\text{O}_4)_4$ was synthesized at temperatures above 150 °C using the same starting mixture.

Post-synthesis modifications of MOFs are done to provide purification, activation, and functionalization of synthesized MOFs in general. In light of these treatments, activation by

solvent exchange with low boiling point solvents which also removal guest molecules from pores results in a high surface area [7]. All of these treatments may be required to improve the quality of MOF to enhance the adsorption capacity and selectivity for gas [39]. In some cases the process of activation may result in pores collapsing or blockages according to the kind of MOFs [33] and thus it is important to search and try alternative parameters during synthesis and different ways of purification.

MOFs are investigated for their efficiency for carbon dioxide adsorption more often than other compounds generally in a laboratory [7]. In addition, MOFs require low energy for regeneration compared to other solid adsorbents [9,19]. Thus MOFs can be used for CO₂ capture to sustain an economy and development as well as to improve the environment. These good properties of MOFs prompt the study of porous metal organic complexes for CO₂ capture. In this regard, the synthesis of cobalt succinates and nickel hydroxy-terephthalates were optimized to enhance their CO₂ adsorption capacity and selectivity.

This study focuses on synthesizing porous metal organic complexes with enhanced CO₂ adsorption. Two porous metal-organic compounds were studied, cobalt succinates and nickel terephthalates. The syntheses are based on methods such as sonication, thermal, microwave, and hydrothermal preparation.

1.3 Problem statement

The South African Industrial enterprise, as well as other industrialized countries, emits huge amounts of carbon dioxide (CO₂) in the atmosphere. This gas is the major cause of global warming. The main cause is burning of fossil fuels due to the high demand of electricity. The sequestration of CO₂ to limit its emission is necessary at especially power plants. Different policies and technologies have been applied for CO₂ capture but still there are gaps and inefficiency due to the challenges of economic growth and high input energy for sorbents

regeneration. Porous Metal-Organic Frameworks (MOFs) are being developed around the world but are not widely tested for carbon capture.

Metal carboxylates including cobalt succinates and nickel terephthalates used in CO₂ adsorption have great promise. A family of cobalt succinates has been synthesized but no investigation on their ability to capture CO₂. Cobalt succinates were synthesized hydrothermally which takes three days [36]. However, a synthesis based on microwave technology can provide final products of MOFs about 10 min [30] and sonication has the potential to reduce reaction time and produce products in high yield and excellent crystallinity [40]. These two methods are not known in the synthesis of cobalt succinates. A study on nickel hydroxy-terephthalate was carried out but their potential on CO₂ adsorption is unknown.

1.4 Research question of the study

- i. Can cobalt acetate as the source of metal ion give cobalt succinate different from cobalt chloride hexahydrate?
- ii. Can the synthetic reaction using sonication, reflux, Parr reactor, and microwave result in different cobalt succinates?
- iii. Can the use of the no-polar solvent (hexane) results in new phases in the synthesis of cobalt succinates and nickel terephthalates?
- iv. Can the synthesized cobalt succinates and nickel terephthalates adsorb CO₂?

1.5 Hypothesis

- i. The use of cobalt acetate as metal source can contribute to the synthesis of new cobalt succinates.

- ii. The synthesis via sonication, reflux, Parr reactor, and microwave can give different cobalt succinates frameworks.
- iii. The use of hexane in the synthesis of cobalt succinates and nickel terephthalates can result in the new phases.
- iv. Cobalt succinates and nickel terephthalates can adsorb CO₂.

1.6 Objectives

- i. To evaluate the effect of using different metal source viz. cobalt acetate and cobalt chloride hexahydrate on the structure of the product, cobalt succinates.
- ii. To evaluate the effect of the synthesis method i.e. sonication, reflux, autogeneous heating (Parr reactor), and microwave on cobalt succinate structure.
- iii. To evaluate the effect of hexane on the structures of porous cobalt succinates and nickel hydroxy-terephthalates.
- iv. To evaluate CO₂ adsorption capacity of the synthesized adsorbents.

1.7 Research approach

The hydrothermal synthesis at autogenous pressure was performed to achieve a highly porous material. The use of cobalt acetate to produce new materials was performed. Sonication was one of the synthetic methods to synthesize cobalt succinates in 45 minutes. Non polar solvent, hexane, was used in the hydrothermal reaction to facilitate the synthesis of accessible porous cobalt succinates and nickel terephthalates. Microwave synthesis might also contribute to the preparation of the adsorbent materials in shorter periods of time i.e one hour, in order to increase surface area and increased porosity with high CO₂ adsorption capacity. The test of CO₂ adsorption in these compounds is compared with other metal

organic frameworks. The optimization of reaction conditions for the synthesis of these compounds may enhance the adsorption capacity of CO₂.

1.8 Research outlines

This thesis is composed of seven chapters including this first chapter.

Chapter one: This chapter introduces and provides a summary of the work. It states the purpose and the objectives of the project. Here is addressed the problem showing the different technologies used to address the issue. The general information on the use of porous metal organic complexes to limit carbon dioxide emission is also given in this section.

Chapter two: This Chapter report on technologies in the critical way that carbon capture should rely on one with low cost. It describes the materials used in CO₂ sorption and the relative drawbacks. The details are mainly given on the synthesis and application of MOFs as advanced materials for CO₂. The reaction condition like temperature is reported to favor the formation of porous products when well controlled. Example, interpenetration can be formed due to the high temperature. Different treatments to avoid this interpenetration were investigated. The use of microwave in different works leads to MOFs with increased surface area according to this literature. Furthermore, post-synthesis to enhance adsorption capacity, as well as selectivity, was also provided.

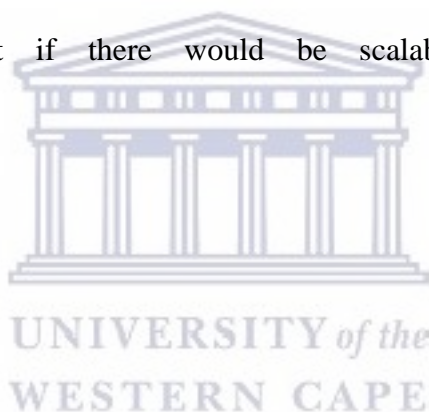
Chapter three: This chapter presents the materials and the actual methodology used to synthesize cobalt succinates and nickel hydroxy-terephthalates. It explains the research instruments and the characterisation techniques for analysis of the synthesized compounds. It also presents the experimental process used to test CO₂ adsorption in the synthesized compounds.

Chapter four: This chapter presents the characterization and discussion for the synthesized cobalt succinates.

Chapter five: Here, the characterization and the discussion have focused on the synthesized nickel hydroxy-terephthalates. It also discusses the effect of hexane used in the synthesis on resulting compounds.

Chapter six: The adsorption capacity of pure CO₂ on synthesized adsorbents was investigated using TGA instrument. The cyclical adsorption was investigated to evaluate the stability of compounds. This will allow us to compare which relevant synthetic that can be adopted to synthesize MOFs for further research and application. A brief conclusion will be stated at the end of this chapter.

Chapter seven: The summary of findings, in general, is outlined here including conclusion and recommendation. The achievements on hypothesis are mentioned and suggestions for future projects to suggest if there would be scalability from this research.



CHAPTER 2: LITERATURE REVIEW

2.1 Introduction

This chapter reviews the technology methods developed for carbon dioxide capture. Different processes and conditions used to capture and sequester CO₂ from flue gas are presented.

The parameters such as temperature, pressure, and humidity can be controlled to optimise operating conditions for CO₂ sorption process. The sorption process can involve absorption materials such as amine-based solvents, ionic liquids, membranes and adsorption solids such as zeolites and metal organic frameworks. One of the focuses of using these materials is the sorption selectivity. The problems associated with these materials for CO₂ capture are cost and efficiency. In this case, porous metal organic complexes known as metal-organic frameworks (MOFs) showed promise as being cost effective with a high capturing efficiency. The synthesis of MOFs can be developed in various ways to produce more efficient framework types. This synthesis may require the use of microwaves to enhance CO₂ capturing efficacy as discussed by a number of researchers. However, the emphasis must be placed on the reusability which is one of the key properties of excellent MOFs.

2.2 Background of CCS and factors influencing it

Carbon dioxide (CO₂) gas, as well as other greenhouse gases, are generated from burning fossil fuels and cement production [1,42] among many other sources. The combustion process produces CO₂ including other gases such as methane, SO₂ and N₂O [42,43]. This causes an increase in the amount of CO₂ present in the atmosphere and consequently results in global warming which has been implicated in current devastating global disasters such as desert encroachment and famine [43]. Therefore, it is necessary to develop a means of

capturing the CO₂ in order to reduce its emission [1]. According to Rao and Rubin, the separation process involves the adsorption process in which CO₂ from its gas phase is attached to the surface of solid adsorbents [44] such as MOFs [45] and zeolites [46]. There is another absorption process in which CO₂ is solubilized in chemical liquids such as amines and ionic liquid based solvents [46,49]. Temperature and pressure are limiting factors in the process [48]. The procedures of producing single and concentrated CO₂ from a dilute gas requires energy input [48]. The energy cost is typically referred to as the energy penalty as there is the portion of electricity or energy from a power plant which is additional energy required for the CCS process [44].

Produced carbon dioxide gas from power plants is an unwanted product from electricity production which increases expenses for CCS. Siriwardane *et al.* suggested condition for CO₂ separation from flue gas which involves a sequence of different conditions such as temperature and pressure that can also allow the recovery of the sorbents [15]. The research states that temperature swing adsorption (TSA), and pressure swing adsorption (PSA) offered an efficiency in CCS [49]. However, according to Merel *et al.*; TSA is more applicable to industrial conditions because it showed a reduction of the specific heat consumption [50]. The conditions such as temperature and pressure are the components of three basic CO₂ separation and capture options such as pre-combustion capture, oxy-fuel combustion, and post-combustion capture [19]. All the options use energy, but the energy differs in cost input from one option to another [11] due to the effort of input.

2.2.1 Pre-combustion CO₂ capture

Pre-combustion capture involves the de-carbonation by gasification of starting fuel like coal and biomass by reacting them with oxygen or air. There is separation of CO₂ at much higher

pressure from gasified coal syngas (largely H₂ and CO) prior to the gas going to a combustion turbine. H₂ is purified and then applied for different uses including electrical and thermal power [11]. Blomen *et al.* reported that the total input of this process is expensive, because it requires extended plant, complex instruments, low H₂ output and poor purification [11].

2.2.2 Oxy-fuel combustion capture

This approach consists of burning fuels using pure oxygen rather than air to produce nearly pure CO₂. During combustion H₂O also is produced and associated with some poisonous gases such as SO₂/SO₃ which have to be further removed and therefore oxy-fuel combustion limits emission of harmful compounds. Even though this process is associated with purification, its operability is limited by high cost due to the cryogenic distillation for the production of oxygen and cooling of CO₂ [11,20]. These limitations of high cost for producing pure oxygen and cooling capacity are always associated with high-cost input and practical installation of the CO₂ capture system.

2.2.3 Post-combustion capture

In this process, CO₂ is removed from a flue gas containing mainly N₂ and CO₂. Post-combustion capture provides removal of other contaminants such as oxygen, NO_x and SO_x gases [11,19]. The disadvantage of low partial pressure for CO₂ separation from flue gas requires large equipment to allow high gas loading resulting in an expensive process [50]. Moreover, the use of amine solvents for absorption require high energy for desorption due to chemical sorption [11,51], but solid adsorbents are promising since they require a low energy for regeneration [17]. However, despite disadvantages, post-combustion capture is the most feasible on a short time scale and is easily able to be fitted to existing power units [19]. This independent installation for post-combustion can allow the manipulation of each unit

separately. Blomen *et al.* reported that post-combustion can be less expensive [11]. Therefore the post-combustion capture can be considered to be the ideal for CO₂ capture among two other options [11]. Figure 2.1 illustrates the summary of the three options for CO₂ separation from flue gas in a power plant.

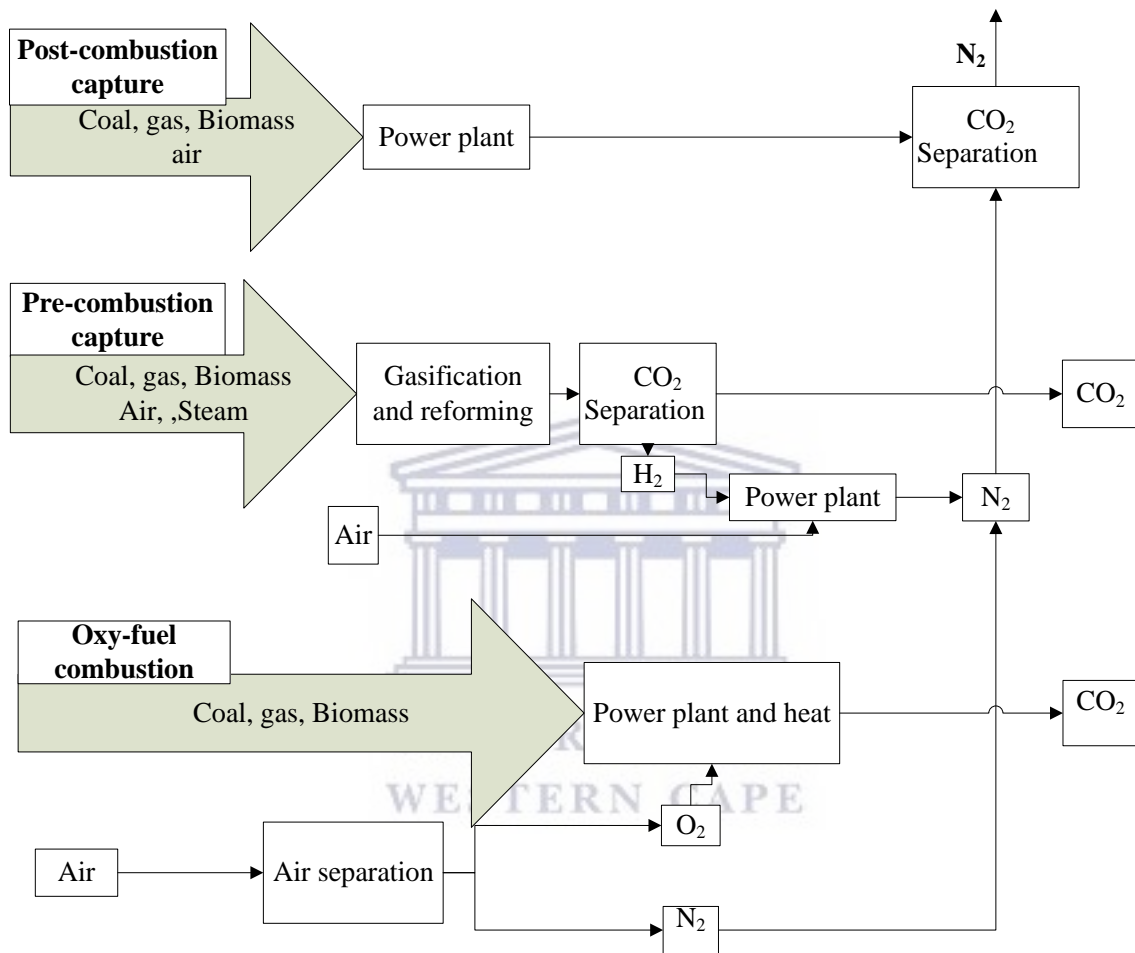


Figure 0.1: Three options for CO₂ capture from power plant generation [20]

Merkel *et al.* showed that post-combustion allows low-pressure sorption that can be applicable in amine-based absorption and ionic liquids [13]. Post-combustion can also be used in zeolite, activated carbon, and MOFs leading to lower cost effective strategies [13,52]. The sorbents used for CO₂ capture can be divided into liquids amines based solvents and

ionic liquids known for the absorption process and the solids such as zeolites and MOFs known for the adsorption process.

2.3 Carbon dioxide capture by absorption

The various types of sorbents such as amines based solvents, ionic liquids and membranes are used for the absorption process. Amine-based solvents and ionic liquids absorb CO₂ from flue gas by dissolution [45,53]. Once the solubility and compatibility of absorbents have been investigated, it can provide the best solution for the process for CCS techniques as this depends on the nature or content of absorbents [8]. Camper *et al.* found out that both ionic liquid and amine solvents have different absorption capacity and selectivity [8].

2.3.1 Amine-based solvents

The amine based solvents are amines designed to remove acidic gas impurities such as H₂S and CO₂ from natural gas streams [44]. Therefore, amine solvents are used for CO₂ capture. Examples of amine-based absorption solvents include a 30% monoethanolamine (MEA) in water successfully used to remove about 80% of CO₂ from flue gas [47]. The absorption of CO₂ in amines involves new strong chemical bond formation which requires high energy to break it [8,54]. Apart from high temperature for desorption there are other disadvantages such as solvent volatility, high energy required in regeneration and chemical deterioration in amines based solvents [52]. In conducted experiments by other groups it was found that an increase in the concentration of amine-based solvents minimizes the energy for sorbent regeneration but requires high amine loading and use of huge amounts of water to stabilize the temperature [10,48]. These processes illustrated certain effects on reduction of energy to regenerate sorbents, and solvent corrosion and degradation [10]. The use of high amine

loading and large amounts of water requires large equipment, complex processes and loss of absorbent resulting in high cost [44].

2.3.2 Ionic liquids

Ionic liquids (ILs) and room temperature ionic liquids (RTILs) derived from imidazolium, phosphonium, ammonium, and pyridinium compounds are studied for CO₂ capture [8]. Due to the tunability in these ionic ILs [8,55], their functionalization using phosphonium-based amino acids achieved a one mole of CO₂ per one mole of ILs stoichiometry, showing high CO₂ absorption [55]. In this regard, ionic liquids showed better manipulations than amine based absorbents due to the possibility of non-volatility, impregnation and adjustment of ions with side chains [8,55]. The polar functionalization in RTILs had shown noticeable enhancement of CO₂ solubility, however the increase in viscosity presented difficulties [8,57].

The sorption of CO₂ depends on interaction between absorbent and the gas [46,58]. Camper *et al.* stated that RTILs with acid gas (CO₂) form insoluble carbamate that helps to deliver the capture reaction [8] which is different from amine based sorbents. In addition, CO₂ absorbed by RTILs can be easily removed by the reduce pressure (Figure 2.2).

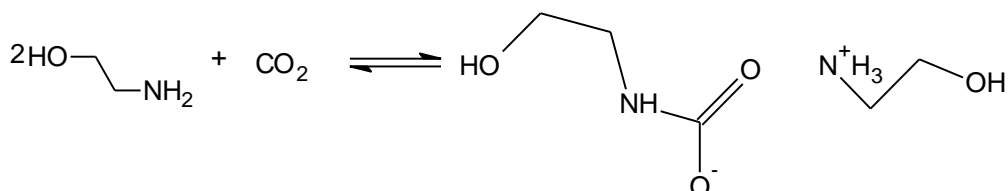


Figure 0.2: Formation of new chemical bonds in amine during CO₂ absorption process [8].

The gas can be absorbed by chemical or physical sorption phenomena [8,16,59]. Chemical sorption processes requires energy to break the formed bond [8,45] while physical sorption

does not involve chemical reaction [8,45]. The energy used to recover the functionalized RTILs is low compared to that of amine-based absorbents as there is no need for the additional heat for CO₂ desorption, therefore this reflects great promise for CO₂ capturing [8,54]. However, carbamates formed in the RTILs can remain soluble slowing CO₂ absorption [8].

2.4 Carbon dioxide capture by membranes

Membranes can be prepared by incorporating fine crystalline material such as MOFs and zeolites into polymeric matrixes forming a film layer that favours permeability [14,60,61]. The increase in permeability in membrane-based CO₂ separation represents a feasible energy cost saving [13,60]. The sequestration of CO₂ using membranes started early in the 1990s, where the use of membranes was proved to be more efficient than amine solutions for CCS but with low selectivity and permeability [13]. Carbon dioxide separation in membranes does not result in a new chemical bond [14]. Merkel *et al.* synthesized membranes with enhanced CO₂ permeances of capacity greater than 1000 gpu (gas permeation unit) and a CO₂/N₂ selectivity of 50 (in terms of Henry's constant). However, they realized that the requirements of feed compression to increase permeation results in high cost. Furthermore, Venna and Carreon demonstrated the draw-back of membranes, for example "zeolite imidazole frameworks-8" (ZIF-8) membranes had a low permeability and selectivity [14]. A study of developing high selective and permeability in ZIF-8 membranes may lead to materials with a high efficiency for CO₂ separation but the study is still ongoing. Therefore, alternative developments of solid adsorbents such as zeolites and MOFs for CO₂ are required.

2.5 Carbon dioxide capture by adsorption

Carbon dioxide is adsorbed through interaction of the adsorbent surface which does not alter the nature of adsorbed gas [15]. Britt *et al.* reported that such adsorbents (like zeolites and MOFs) can provide promising energy-efficient alternatives to the current amine-based absorption systems [9].

2.5.1 Zeolites

Zeolites are solid porous aluminosilicate materials [61] with a large external surface area, large pore volume [62] and thermal stability [63]. These properties give advantages for their application on CO₂ capture from post-combustion [60,62]. The adsorption of CO₂ on zeolites does not involve the formation of a strong chemical interaction as in amine based adsorbents. Thus less energy is needed for regeneration of adsorbents because high temperatures would not be required [64].

Zeolite adsorption capacity depends on their chemical composition [15]. Siriwardane *et al.*, showed that Zeolites rich in sodium have a high CO₂ adsorption capacity [15]. In general Zeolites have high adsorption for CO₂ depending on their chemical content but the presence of water molecules in gas mixtures impairs their efficiency [65]. Li *et al.*, showed that recovery of CO₂ from zeolite 13X decreased from 78.5 to 60% due to the presence of water molecules [66]. In addition, the study conducted by Brandani and Ruthven found that the adsorption capacity of CO₂ in CaX zeolite at 50 °C dropped from 2.5 to 0.1 mmol/g when water vapour was loaded from 0.8 to 16.1 wt% [65]. They explained this phenomenon to be a result of competitive adsorption of water molecules resulting in blocking the available sites for CO₂ adsorption. In addition, water condensation can result in the formation of carbonic acid which destroys the adsorption beds [66]. Through the vacuum swing process, water can

be removed in 13X. However, the problem is the reduction of CO₂ desorption and purity and the requirements of additional equipment for vacuum pumping.

On the other hand, Hauchhum and Mahanta showed inefficiency in zeolite 13X and zeolite 4A due to the partial regeneration of the adsorbent [67]. The requirement of high temperature for regenerating zeolite at 300 °C is a challenge. Furthermore, zeolites showed low CO₂/N₂ selectivity due to the similarity of the kinetic diameters of CO₂ and N₂ and that the selectivity may depend on increasing temperature [15].

2.5.2 Metal-organic frameworks MOFs

The class of metal organic frameworks (MOFs) were mostly known around 1995 as structural three-dimensional (3D) porous complexes [68]. Nowadays MOFs are industrially produced by BASF and sold by Sigma Aldrich under the tradename Basolite™ [26]. The emerging MOFs have been applied in gas sorption [35,70], heavy metal sorption, storage [70], and catalysis [71]. These properties are the motivation to further develop research on these compounds for potent application.

These compounds are formed by metal cations or metal clusters bridged by anion ligands that allow spacing between cations or clusters [68]. MOFs are porous crystalline materials with a network of two or three dimensional structures that can be tuned for high porosity and a geometrically well-defined structural framework [73,74]. The most advanced MOFs are three dimensional (3D) structures with porosities and capacity to adsorb or desorb materials such as guest molecules [75–77]. The network is formed by connectivity of metal-organic hybrids that can have one of the following structures Modes A, B or C illustrated in Figure 2.3 [77] where a 3D structure can be achieved. The metal centre binds on functional groups such as oxygen or nitrogen from the organic linker in different modes forming layers which are connected to each other through organic linkers [78]. This connectivity leads to

frameworks characterised by stable building blocks resulting from the synthetic conditions allowing them to retain their structure [32,80]. These substances are known to be reticular because pore size and functionalities can be modified through organic linkers or MOFs post synthesis by keeping the same basic architecture [74].

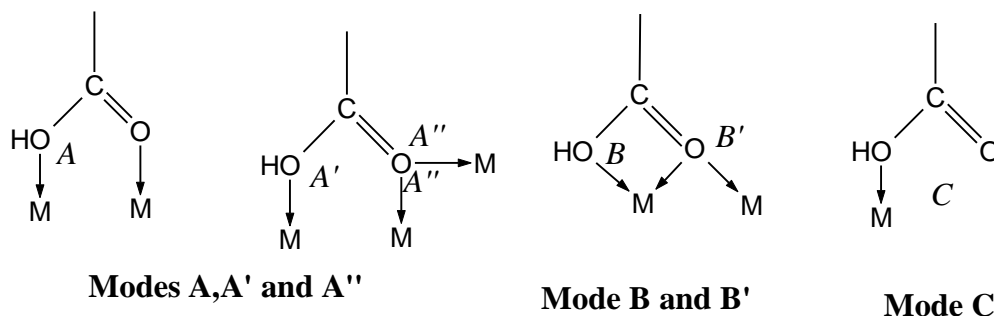


Figure 0.3: Coordination modes showing carboxylates linked to metal center or node [78]

Connectivity in the framework depends on the nature of the metal ion (Figure 5.2) that contributes to the structural dimension of the framework [80]. Apart from the metal ion connectivity, bridging ligands also contribute to different coordination modes (dimension) in network formation multidentate functionalities [80]. The metal ion can have one of the coordination modes as shown in Figure 2.4A) and the ligand can have multidentate sites (Figure 2.4B). There are three kinds of networks formed by hybrid metal and organic compounds. The first is one-dimensional (**1D**) which are compounds made of a metal centre and an organic moiety considered as having a tube like or chain (Figure 2.4C) architecture [69,82,83]. The second are two-dimensional (**2D**) structures which are sheets or polycatenated honeycombs (Figure 2.4D), [69,83] with no channel volume, whereas the third are three-dimensional (**3D**) frameworks that contain pore volumes or open channels (Figure 2.4 E) [69,73,84]. Therefore, formation of the various dimensional structures depends on the possible available bridging sites from the metal ion and the ligands. It had been shown that

3D frameworks are formed by pillared linkers (ligands) which bridge 2D sheets of metal organic building blocks in which channels or pores can be observed [73,84].

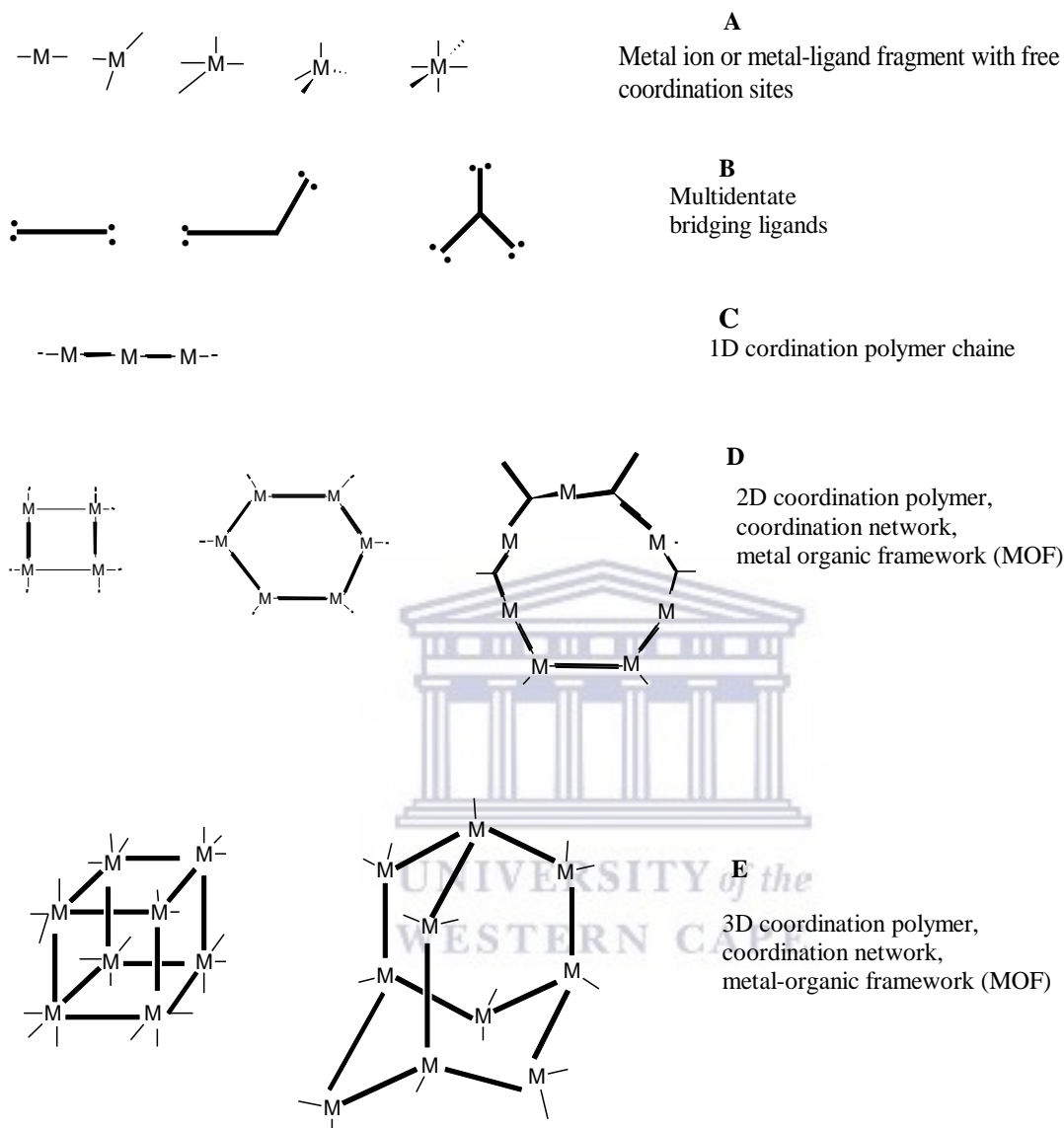


Figure 0.4: Coordination polymer MOFs with different coordination mode [67]

2.5.2.1 General synthetic strategies and features of MOFs

The synthetic method and control of reaction conditions are responsible for the features of good MOFs [18,85]. These MOFs contain pores where solvents can be hosted during synthesis with the possibility that the solvent can be removed by application of vacuum, solvent exchange using low boiling solvents or heating in order to get a high surface area

[85,86]. The paramount property is the retention of the crystalline structure of the MOF after removal of guest solvents [86–88].

The behaviour of MOFs on removal and adsorption of guest molecules can be categorized in the following groups; rigid frameworks and flexible/dynamic frameworks [89,90]. Rigid MOFs, like zeolite, are stable, robust with permanent porosity that are resistant to external stimuli. For example, during adsorption or desorption of guest molecules where pressure and temperature are applied, rigid MOFs retain their porosity [49,91]. Flexible effects in MOFs were observed in compounds containing ditopicboxylate [91]. It is found that in MOFs such as MIL-47 (VIV) (Materials of Institute Lavoisier), metal centres containing μ_2 -hydroxyl groups allow flexibility and contribute to rigidity in MIL-47 (VIV) [79]. Davies *et al.* observed that $[\text{Zn}_2(\mu_2\text{OH}_2)(\text{HBTRI})(\text{BTRI})-(\text{H}_2\text{O})_2]\cdot\text{DMA}\cdot 3\text{H}_2\text{O}$ can adsorb up to 4.5 extra water molecules with loss and restoration of crystallinity upon dehydration and rehydration [29]. Flexible property allows the adsorption and release of guest gases in pores of MOFs returning their original structure and thus are able to be used for selective adsorption [92]. On the other hand, the rigid MOFs offer a high selectivity uptake of CO_2 which depends on different interactions between adsorbent and adsorbate [17]. This was observed in Cobalt Adeninate MOFs. The selectivity and enhanced gas uptake in MOFs depends on pore size and may be enhanced by further functionalization. This process was observed in bio-MOF-11 after amino and pyridine functionalization [93]. The interaction of adsorbates and adsorbents occurs in pore channels and at the surface of the MOFs.

Pores has a feature that offers low density and increase in MOFs surface area, prompted designers or researchers in general to synthesize three-dimensional MOFs. Some parameters like; kind of metal salt, organic linker, deprotonating agent, temperature range, and reaction time are the most important to be considered in synthesis of open channel three-dimensional MOFs for gas separation and storage [18,94]. Highly porous compounds can be considered

as having the most successful application [76,95]. The MOFs can be prepared from mixtures of metal salts, ligands, solvent and deprotonating agents associated with different reaction conditions to achieve porous crystalline materials [38,96]. The templates or structural directing agent (SDA) known in zeolite synthesis to achieve desired dimension structure or increase in channels or pore capacity can also be applied in MOFs [97].

The same reaction mixture can lead to different MOFs depending on the method used or the modification of conditions [79]. For example, reduced surface area due to large particle size, occluded pores by guest molecules and catenation or interpenetration of frameworks can be caused by size or shape of ligand, high temperature and high concentration [97–99]. Moreover post-synthesis treatment may be used to enhance the quality of MOFs in enhancing gas adsorption [18,78]. Therefore optimized reaction conditions may lead to a predicted porous material.

Different methods such as, sonication, hydrothermal, and microwave assisted synthesis were used to synthesise MOFs. These methods are hydrothermal (when water is solvent) or solvothermal (solvent other than water is used) synthesis [18,100], sonication (acoustic wave generate the heating energy) [101,102] and emerging microwave assisted synthesis [41,103].

2.5.2.2 Conventional hydrothermal or solvothermal synthesis of MOFs

Reactions take place at elevated or room temperature where the solvent can be water or another organic solvent. The preparation of MOFs consists of mixing the metal salt, ligand, and water or another kind of solvent and retained at a given temperature [38,104]. Sometimes substances like deprotonating agents or structure directing agents are added to the reaction mixture allowing deprotonation of the ligand so that a porous material can be achieved [40,96].

The mixture is put in a closed vessel and heated at different temperature above the boiling point of solvent in autogenous pressure where the process is referred to as solvothermal synthesis [79]. Non-solvothermal or hydrothermal syntheses are performed at room temperature below or under reflux heating in an open vessel without auto-creation of pressure [79]. In this synthesis, there is no auto created pressure. However, a Parr reactor at high temperature is employed with auto creation of pressure [18,38,78]. Thermal synthesis of MOFs is commonly known to produce porous frameworks with the desired structure dimension [105].

2.5.2.3 *Synthesis by sonication*

Sonication is used to synthesize MOFs which offers short reaction times, high yields and crystallinity compared to conventional oven heating [41,106]. The short reaction time is due to sonication which involves the growth and collapse of bubbles in liquids known as acoustic activation [101]. This acoustic activation results in extremely high local temperature around 5000 K and pressures as well as the extraordinary heating and cooling rate [101,106].

2.5.2.4 *Microwave*

The discovery of microwave heating in 1946 by Spencer at the Raytheon Corporation heralded in the application of electromagnetic waves [40]. Microwaves are normally generated by a magnetron, consisting of an oscillator converting high-voltage direct current into high frequency radiation generating energy [40]. These radiations interact with the electrical charges of polar/ions from the solution or electrons/ions from material in the solid state [79]. Ionic liquids are potentially suitable solvents in microwave synthesis since they have the capacity to allow high ionic conductivity and polarizability throughout the bulk of the material [107]. The energy created is transmitted to the sample, and promotes dielectric

solvents like water to align with the alternating electric field of the microwaves [40]. When molecules collide with each other, heat is generated and spread out homogeneously throughout the medium [40], resulting in high speed nucleation [108]. This indicates that energy from a microwave is more efficient than that from conventional methods such as oil baths and hot plates used for chemical reactions [40]. During microwave synthesis, solvents in the mixture reach temperature above their boiling point in vessels that are pressurized [40].

Heating through Microwave is achieved through an ability to control parameters like irradiation power, time of reaction and temperature [40] which are the most important factors for chemical synthesis [109]. Advantages of this heating method are; uniform grain size, control of the mechanical and optical properties of the products and pure products compared to conventional heating [41,110]. Microwave synthesis has been developed to successfully synthesize organic and nanoporous inorganic materials [41,107,111]. The synthesis of MOFs by microwave seems to not be commonly used although being very popular in organic synthesis [41,95,107], and thus its application in the synthesis of MOFs or inorganic-organic hybrid should be expanded upon.

Microwave synthesis improves the properties such as lowering particle (Table: 2.1) size, narrow size distribution, higher crystallinity and high internal surface area in MOFs [103,111]. This allows achieving a higher internal surface area than in the other heating methods. For example, Sabouni *et al.* synthesized crystalline porous material (CPM-5) using microwave and achieved a surface area of $2187 \text{ m}^2\text{g}^{-1}$ compared to $580 \text{ m}^2\text{g}^{-1}$ from conventional thermal methods [30]. Table 2.1 illustrates that microwave syntheses achieves smaller particle size that conventional synthesis.

Table 0.1: Comparison of crystal size of MOFs synthesized from conventional and microwave synthesis

Compounds	Reaction condition	Crystal size	Reference
MOF, $Zn_2(NDC)_2(DPNI)$	Conventional: 1-C	400 μm x 150 μm	[112]
	Microwave: 1-M	150 μm x 20 μm	
MOF-5, $Zn_4(O)(BDC)_3$	Conventional	500 mm	[40]
	Microwave	20–25 mm	
MIL101: $Cr_3F(H_2O)_2O[(O_2C)-C_6H_4-(CO_2)]_3 \cdot nH_2O$	Conventional	800 mm	[113]
	Microwave	200 mm	
MIL101: $Cr_3F(H_2O)_2O[(O_2C)-C_6H_4-(CO_2)]_3 \cdot nH_2O$	Conventional	400 mm	[113]
	Microwave	200 mm	
[M3(NDC) ₃ (DMF) ₄]; M= Co, Mn	Conventional	50-200 μm	[95]
	Microwave	5-20 μm	
Cu-BTC	Conventional	20 μm	[114]
	Microwave	10 μm	
Co-MOF-74 crystals	Conventional	300 μm x 70 μm	[103]
	Microwave	50 μm x 8 μm	

The synthesis via microwave offers a short reaction time and a high yield. An example is the synthesis of $[Cu_2(oba)_2(DMF)_2] \cdot 5.25(DMF)(MCF-23)$ at 160 °C in 2 h [40]. Moreover, the small size of crystals obtained via the microwave process shows an increased in its surface area [111]. However, using conventional synthetic methods, $[Cu_2(oba)_2(DMF)_2] \cdot 5.25(DMF)(MCF-23)$ was synthesized in 72 h at the same temperature as in the microwave process [40]. Conventional synthesis also produce crystal with low surface area [113].

Microwave synthesis offers the opportunity to get good quality, and higher yield of products compared to conventional syntheses. The small size of crystals obtained via microwave process shows an increased in its surface area [111].

2.5.2.5 Temperature dependence in metal succinates and MOFs characterisation

In most cases the crystal structure formation of MOFs are influenced by temperature in the hydrothermal synthesis [115,116]. Metal-oxygen networks are arranged depending on the temperature of the synthesis [37]. This means that temperature is a factor that influences MOFs synthesis.

The network structure of metal succinates is influenced by the reaction temperature where the topology of the frameworks is sensitive to temperatures both below and above 100 °C. Forster *et al* stated that compounds synthesized below 100 °C have similar properties and ones over 100 °C have an increase in their coordination of metal cluster-sharing connectivity (rings), coordinated succinates and incorporation of hydroxyl groups [38]. For example, at room temperature $\text{Co}(\text{H}_2\text{O})_4(\text{C}_4\text{H}_4)$ was obtained whereas $\text{Co}_5(\text{OH})_2(\text{C}_4\text{H}_4\text{O}_4)_4$ was obtained hydrothermally at 180 °C [37,120]. On the other hand $\text{Co}_4(\text{OH})_2(\text{H}_2\text{O})_2(\text{C}_4\text{H}_4\text{O}_4)_3 \cdot 4\text{H}_2\text{O}$ was synthesized using the same temperature with a small noticeable change of reaction condition from the synthesis of $\text{Co}_5(\text{OH})_2(\text{C}_4\text{H}_4\text{O}_4)_4$ [117]. They noted that care should be taken for every single step in reaction conditions for hybrid metal organic synthesis. Although temperature is the most important factor, others viz., solvent, pressure and metal ions should also be considered. The latter act differently in coordinating with ligands according to the nature of transitional metal in aqueous solution to affect pH [118].

2.5.2.5.1 Influence of temperature on interpenetration control and dimensional structure

Temperature control can provide dimensional structure control of metal organic networks. A 3D metal organic hybrid can be successfully synthesized by increasing reaction temperature [38]. On the other hand, Zhang *et al.* and Janiak *et al.* showed that too high a temperature may lead in poor pore size for MOFs [69,116]. An example is the synthesis of 2D network $[\text{Cu}_3(\mu_3\text{-OH})_2(\text{H}_2\text{O})_2(\text{SIPA})(\text{OAc})]$ (SIPA: 5-sulphoisophthalate) at 125 °C while, a 3D framework $[\text{Cu}_6(\mu_3\text{-OH})_4(\text{SI-PA})_2(\text{OAc})_2]$ was formed at 180 °C [119]. Another example is the synthesis of cobalt succinate at a temperature below 100 °C resulted in 1D frameworks, and by increasing the temperature to 150 °C, a 3D framework was obtained [38]. A counter effect is that the synthesis at 190 °C causes the open window (ring) of succinates to become twisted (Figure 2.5) and resulted in very narrow windows [38].

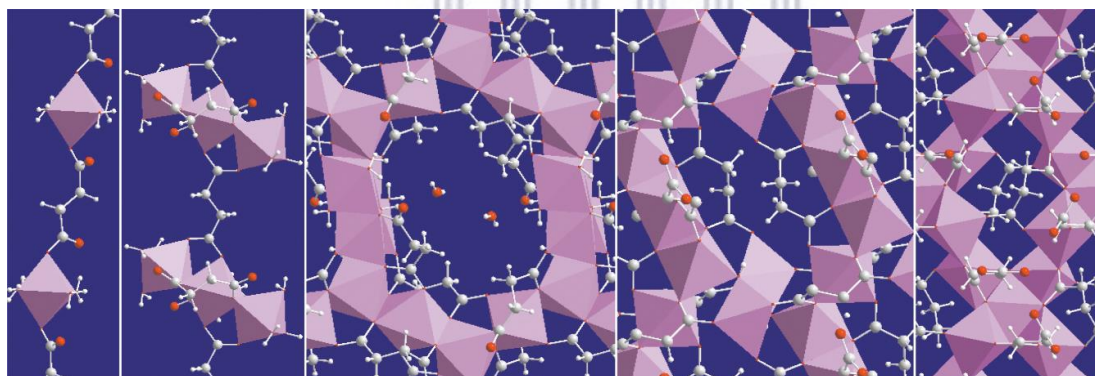


Figure 0.5: Evolution of the five phases of cobalt succinates, from low temperature (far left) to high temperature (far right)[94].

Referring to the Figure 2.4 above, the first and second phases are 1D, which are synthesized below 100 °C, the third phase illustrates the 2D synthesized at 150 °C and the fourth and fifth phases are 3D synthesized at over 150 °C [38]. Observing the two last phases, the open space in the cobalt ring network atoms is reduced with increase in reaction temperature.

To overcome this, the temperature range, dilution of starting materials were controlled to successfully get non interpenetrated framework [116]. Jiang *et al* 2010., during the synthesis of Cd(L)(bpy)(1,C2/m), Cd(L)(bpy)·4H₂O·2.5DMF (**1**), the temperature was raised to get Cd(L)(bpy)·4.5H₂O·3DMF which is an interpenetrated framework form of (**1**) with 3.4% of reduced surface area, therefore interpenetrated frameworks cause lower surface area resulting from high temperature [120].

The temperature influences structure dimension of products from the same starting materials, to produce 1D, 2D, and 3D Modes [38,115]. Their decomposition temperature or stability may also depend on the kind of metal cluster in MOFs as mentioned in the work of Kozachuk *et al* [121]. In light of the metal cluster, its combination with organic linkers provides a strong bond that influence the stability of MOFs [122].

2.5.2.6 Influences of metal source in metal organic frameworks synthesis

A metal source contributes towards the framework assembly in MOFs during their synthesis. The reaction time and features such as crystal size, surface area and pores can be different [115,126,127]. The use of copper acetate as a metal source leads to anchoring a preformed secondary building unit with a continuation of MOFs growth while the copper nitrate metal source is characterised with a delayed growth [128,129]. The precursor metal source can have a solubility that allows the self-formation of layers in MOFs [126]. The framework of Cu-BTC (benzene tricarboxylate) prepared from copper acetate contains Cu₂(COO)₄ paddle wheels with copper dimers as four connectors and benzene-1,3,5-tricarboxylate as three connectors, resulting in a cubic, wide-open framework [123]. However, Cu-BTC prepared from copper nitrate, the unit Cu₂(COO)₄ does not exist [127]. Different frameworks from different metal source can be also observed in [Ni₇(C₄H₄O₄)₄(OH)₆(H₂O)₃]·7H₂O and [Ni₇(C₄O₄)(OH)₂(H₂O)₂]·2H₂O. The two MOFs were prepared from NiCl₂·6H₂O, C₄H₆O₄

(1:1.5) and $\text{Ni}(\text{acetate})_2 \cdot 6\text{H}_2\text{O}$, $\text{C}_4\text{H}_6\text{O}_4$ (1:2), respectively [115,131]. The metal source, solvent as well as temperature are the main parameters in connecting networks during MOFs synthesis. Table 2.2 summarize the effect of reaction conditions on the formation of metal organic complexes.

2.5.2.7 Use of structure directing agents (SDA)

Structure directing agents (SDAs) are defined as substances introduced in a chemical synthesis to achieve porous materials such as MOFs with desired structures [24]. SDAs are widely known for increasing pore size in Zeolites [129]. The same idea was applied in the synthesis of MOFs where aromatic compounds such as benzene and salicylic acid were used to achieve 3D structures with wide channels of $[\text{Ho}_2(\text{C}_4\text{H}_4\text{O}_4)_3(\text{H}_2\text{O})_2]$ [97]. Cetyltrimethylammonium bromide (CTAB) as a surfactant in combination with hydrophobic organic compounds, such as 1,3,5-trimethylbenzene (TMB) was used to increase the porosity of the mesostructured $[\text{Cu}_3(\text{btc})_2(\text{H}_2\text{O})_3]$ MOFs [68]. This shows that SDA can be incorporated in MOFs synthesis to increase porous structure as well as surface area in order to improve the adsorption capacity.

Table 0.2: List of synthesized metal organic complexes with their metal sources and reaction conditions

Compounds and formulae	Mixtures ratio of metal salt : ligand	KOH molar ratio/ (pH)	Solvents/physical conditions	Ref
$\text{CoC}_4\text{H}_4\text{O}_4 \cdot 4\text{H}_2\text{O}$	$\text{CoCl}_2 \cdot 6\text{H}_2\text{O}$, $\text{C}_4\text{H}_6\text{O}_4$ (1:1.5)	1	H_2O 5ml, rt	[37]
$\text{Co}_5(\text{OH})_2(\text{C}_4\text{H}_4\text{O}_4)_4$	$\text{CoCl}_2 \cdot \text{H}_2\text{O}$, $\text{C}_4\text{H}_6\text{O}_4$ (1:1.5)	4	Autogenous, 180 °C	[41,122]
$\text{Co}[(\text{C}_4\text{H}_4\text{O}_4)]_n$	$\text{CoSO}_4 \cdot 7\text{H}_2\text{O}$, $\text{ZnSO}_4 \cdot 7\text{H}_2\text{O}$, $\text{C}_4\text{H}_6\text{O}_4$ (1:1: 0.5)	0	2-propanol, H_2O & DMF, 140 °C	[81]
$\text{Co}_2(\text{C}_8\text{H}_2\text{O}_6)(\text{H}_2\text{O})_2 \cdot 8\text{H}_2\text{O}$	$\text{Co}(\text{C}_2\text{H}_2\text{O}_4)$, $\text{C}_8\text{H}_4\text{O}_6$ (1:1.5)	0	H_2O & THF	[130]
$[\text{Ni}_7(\text{C}_4\text{H}_4\text{O}_4)_4(\text{OH})_6(\text{H}_2\text{O})_3] \cdot 7\text{H}_2\text{O}$	$\text{NiCl}_2 \cdot 6\text{H}_2\text{O}$, $\text{C}_4\text{H}_6\text{O}_4$ (1:1.5)	4.1	H_2O 5ml, Autogenous, 170 °C	[128]
$[\text{Ni}_7(\text{C}_4\text{HO}_4)_6(\text{OH})_2(\text{H}_2\text{O})_2] \cdot 2\text{H}_2\text{O}$	$\text{Ni}(\text{acetate})_2 \cdot 6\text{H}_2\text{O}$, $\text{C}_4\text{H}_6\text{O}_4$ (1:2)	0	Autogenous, 150 °C	[115]
$\text{Co}(\text{H}_2\text{O})_2(\text{C}_4\text{H}_4\text{O}_4)$	$\text{Co}(\text{OH})_2$, $\text{C}_4\text{H}_6\text{O}_4$ (1:1)	0	H_2O , 60 °C	[38]
$\text{Co}_7(\text{OH})_6(\text{H}_2\text{O})_3(\text{C}_4\text{H}_4\text{O}_4)_4 \cdot 7\text{H}_2\text{O}$	$\text{Co}(\text{OH})_2$, $\text{C}_4\text{H}_6\text{O}_4$ (4:1)	0	H_2O 5ml, Hydrothermally, 150 °C	[104]
$\text{Co}_4(\text{OH})_2(\text{H}_2\text{O})_2(\text{C}_4\text{H}_4\text{O}_4)_3 \cdot 2\text{H}_2\text{O}$	$\text{CoCl}_2 \cdot 6\text{H}_2\text{O}$, $\text{C}_4\text{H}_6\text{O}_4$ (1:1.5)	4	H_2O 5ml, Autogenous, 180 °C	[117]
$\text{Co}_3(\text{OH})_2(\text{C}_4\text{H}_4\text{O}_4)_2 \cdot 10\text{H}_2\text{O}$	$\text{Co}(\text{NO}_3)_2$, $\text{C}_4\text{H}_6\text{O}_4$ (1:0.5)	0	$\text{CH}_3\text{OH}/\text{H}_2\text{O}$ and in Na_2CO_3 , r.t	[131]
$\text{CoC}_4\text{H}_4\text{O}_4 \cdot 3\text{H}_2\text{O}$	CoCO_3 (Excess), $\text{C}_4\text{H}_6\text{O}_4$	0	H_2O near ebullition	[132]
$\text{Nd}_2(\text{C}_4\text{H}_4\text{O}_4)_3$	NdCl_3 , $\text{C}_4\text{H}_6\text{O}_4$ (1:1.6)	pH (4.5-5) py	Aqu. solution of metal salt and alcoholic solution of acid, rt	[133]
$\text{Er}_2(\text{C}_4\text{H}_4\text{O}_4)_3$	ErCl_3 , $\text{C}_4\text{H}_6\text{O}_4$ (1:1.6)	pH (4.5-5) py	Aqu. solution of metal salt and alcoholic solution of acid, rt	[133]
$\text{Ho}_2(\text{C}_4\text{H}_4\text{O}_4)_3(\text{H}_2\text{O})_4 \cdot 6\text{H}_2\text{O}$	$\text{HoCl}_3 \cdot 6\text{H}_2\text{O}$, $\text{C}_4\text{H}_6\text{O}_4$ (1:1.5)	pH (4.5) NaOH	H_2O , r.t	[134]
$\text{Ho}_2(\text{C}_4\text{H}_4\text{O}_4)_3(\text{H}_2\text{O})_2 \cdot \text{H}_2\text{O}$	$\text{HoCl}_3 \cdot 6\text{H}_2\text{O}$, $\text{C}_4\text{H}_6\text{O}_4$ (1:1.5)	pH (4.5) NaOH	H_2O , 180 °C	[134]
$[\text{Ho}_2(\text{C}_4\text{H}_4\text{O}_4)_3(\text{H}_2\text{O})_2]_3 \cdot 0.5(\text{C}_6\text{H}_6)$	$\text{Ho}(\text{NO}_3)_3 \cdot 3.5\text{H}_2\text{O}$, $\text{C}_4\text{H}_6\text{O}_4$ (0.5:0.75)	pH (5.5) TEA	H_2O 5.5 mL, benzene 4.5 mL, 160 °C	[97]

Several solvents such as dimethylformamide (DMF), dimethylacetamide (DMA), diethylformamide (DEF), N-methylpyrrolidone (NMP) and tetramethylammonium bromide were additionally identified as structure directing agents, which can be used to form one or other type of MOF [135]. It was also noted that hydrophobic molecules are able to occupy void spaces and when evacuated leave large pore size or channels [35]. These pores can perform an opening and closing process described as a breathing property which imparts important flexibility to the framework [45]. This property allows gas adsorption and removal without damaging the adsorbent materials. However, some hydrophobic molecules used as templates failed to free interpenetration but changed the MOFs structure by increasing the pore volume [35]. This depends on the nature of the framework. Some pores can contain non-deprotonated ligands [102]. Therefore, deprotonating agents are needed.

2.5.2.8 Use of deprotonating agents

Inorganic viz., KOH or NaOH and organic compounds viz., TEA (triethylamine) or pyridine are used to liberate hydrogen ions from ligands or to dissociate ligands into ions for the preparation of complexes [37,96]. These substances are referred to as deprotonating agents in synthesis of metal organic frameworks [97]. During the synthesis of MOFs, a carboxylic ligand in general can remain in the pores as guest molecules due to non-complete deprotonation [136]. The FTIR characterisation of the synthesized MOCP-H without any deprotonating agent showed the free acid (ligand) absorption band but on using TEA in the synthesis of MOCP-L and MOCP-H the absence of free acid absorption band was confirmed [136].

The use of TEA in synthesis of Zn-BTC proves the successful preparation of a 3D (dimension) structure with rigid and stable porous architecture [96]. This is compared to the synthesis of Metal-BTC using acetate and water as polar solvent which lead to a 1-D

structure while using ethanol (poor coordinating solvent) and weak base, it formed 2-D structure [96]. As the pH of the reaction medium increases, the structure dimension changes from 1-D through 2-D to 3D [129]. However, this effect is clearly demonstrated on using KOH in the synthesis of cobalt succinate at room temperature. It gives a 1-D mode at room temperature but at high temperature it gives a 3-D mode [37,38]. The KOH deprotonates the ligand becoming polydentate ligand and thus facilitating the existence of pores in the framework [137]. This process depends to the polarity of the solvent used [96]. It is noted that the deprotonating agents and SDA may play a role in structure determination of MOFs networks with free pores. The resulting porous MOFs can contribute to the high adsorption capacity of CO₂.

2.5.2.9 *Activation of MOFs*

After reaction, the MOFs products contain guest molecules or solvents in channels or porous structure. The surface area of these materials is relatively small due to the obstruction of pores or channels by guests molecules [86]. It is important to remove the guest molecules in order to increase the surface area or to make it accessible and this process is known as the activation [33,87]. The activation is performed by conventional methods which consists of heating the MOFs in vacuum [18,87]. However, this method causes partial or full loss of porosity in MOFs and it was suggested that activation using solvent exchange with low boiling solvents with is preferable [18,87]. Activations are commonly done to achieve a high surface area even though other methods such as supercritical carbon dioxide can be also used [33].

2.5.3 Adsorption capacity

Adsorption capacity is one of the ways to evaluate the amount of CO₂ that can be adsorbed by materials. This depends on different conditions such as temperature, pressure and moisture [78,140]. The adsorption capacity of CO₂ is measured by adsorption equilibria where gravimetric and volumetric equilibria are investigated [94]. The gravimetric CO₂ adsorption refers to the quantity in mass of adsorbed CO₂ per quantity in mass of adsorbents, while volumetric CO₂ uptake measures the quantity of CO₂ to be stored on volume of adsorbent [21]. The two techniques determine the heat efficiency of MOFs in order to evaluate the energy required for regeneration of adsorbent [94]. The interaction between CO₂ and adsorbent should not be strong otherwise high energy will be required to break the CO₂-framework [138]. The presence of metal ion sites in MOFs channels is a feature that plays an important role in CO₂ adsorption. For example, interaction between coordinatively unsaturated nickel sites of Ni₂(dhtp) (H₄dhtp: 2,5-dihydroxyterephthalic acid), gives rise to a high CO₂ adsorption capacity [94,140].

2.5.3.1 Interaction of absorbed gas in MOFS

The properties of solid adsorbents especially MOFs in gas adsorption and/or storage is explained by interactions found in some sites in the channels of pores or at the surface area of these porous materials [57]. Getzschmann *et al.*, in their findings showed that the gas methane (CH₄) can adsorbed at the metal site [139]. Not only CH₄ but also carbon dioxide (CO₂) was identified to be adsorbed at the metal sites i.e. Ni and Cu of MOFs such as Ni/DOBDC and CuBTC [138]. Interactions were found in Cu₃(btc)₂ MOFs where the metal centre acts as a Lewis acid [58,142] to accommodate electrons from host molecules. On the other hand, the sites of interaction of CO₂ in the framework can be other than metal centre.

Even though selectivity can be determined by pore size or kinetic separation, metal site can induce selectivity by polarizing the adsorbates, referred to as electronic polarizability. MOFs possess a high surface area with open sites which can lead to high adsorption capacity but with poor selectivity [138]. The gases possess different quadrupolar or polarizability moments that results in high enthalpy of adsorption. For example, for the CO₂/N₂ separation relevant to post-combustion for CO₂ capture, the higher polarizability (CO₂, 29.1x10⁻²⁵ cm⁻³; N₂, 17.4 x10⁻²⁵ cm⁻³) and quadrupole moment (CO₂, 13.4 x10⁻⁴⁰ C.m²; N₂, 4.7 x10⁻⁴⁰ C.m²) of CO₂ compared with N₂ results in a higher affinity of the surface of the material for CO₂ [94,140]. This means the surface of MOFs induce polarity in gases which results in a high interaction between CO₂ and the surface area of MOFs than other gases. Charged organic groups and metal cation sites in metal organic frameworks enhance selectivity due to polarizability [138].

The result found from interaction of CO₂ and MOFs typically MIL-53 [Cr^{III}(OH)(OOC-C₆H₄-COO)] showed that the site that attracts CO₂ is oxygen from hydroxyl group in the framework [45]. The role of oxygen from hydroxyl group is to provide electrons (as electron donor) to carbon dioxide for attractions [45]. It is noted that this interaction occurs in frameworks that contain coordinated hydroxyl groups. The oxygen from the carboxylate in the framework also acts as an adsorption site for CO₂, which has been computed in M(OH)(O₂C-C₆H₄-CO₂) where M stands for Al [57]. Serna-guerrero *et al.*, in their work, also identified interactions between amines and CO₂ in functionalized compounds [140].

This can help to evaluate the effect of high density of metal clusters in MOFs. The effect of the hydroxyl groups is also observed in the synthesis of cobalt succinates by increasing the temperature in presence of KOH [37] which evaluated CO₂ adsorption. All these features can have an enhancing impact on CO₂ adsorption but still also depends on the size of the pores [46,58,143].

2.5.3.2 *Enhancement of adsorption capacity*

Porous metal organic frameworks contain structures that are responsible for CO₂ adsorption. These structures are basic sites including a number of saturated metal ions and functional groups such as amino, pyridine, hydroxyl, and carboxylates groups that attract CO₂ [94,140]. In the light of these features, the arrangement or density of these structures in the framework may increase the capacity for CO₂ adsorption. A report on functionalization of MIL-53(Al³⁺) MOF based on OH-, COOH-, NH₂-, and CH₃ functional groups showed that the hydroxyl group OH- increased both adsorption capacity and adsorption selectivity than the other functional groups [51]. In some MOFs i.e. Cu-BTC an increase in the adsorption capacity via the presence of water molecules coordinated to open-metal sites of the hydrated framework [142]. It was also observed that hydrated Cu-BTC adsorbed CO₂ 71% more than the non-hydrated Cu-BTC at 0.1 bar [142]. However, this capacity was reduced to 45% at 1 bar. This shows that the pressure parameter also affects the adsorption process. In their findings they showed that water molecules create electric fields which interact with the quadrupolar moment of CO₂ for increased adsorption.

2.6 Chapter summary

Literature shows that CO₂ capture processes using sorption technique involve adsorption and desorption which has a cost implication on production of energy. In the desorption process, temperature swing adsorption (TSA) is considered as a better technique to reduce energy costs than pressure swing adsorption (PSA). Application of TSA for post-combustion techniques result in a minimum of equipment needed and allows for a continuous power plant lay out without interruption. Post-combustion techniques should be applied with materials that can adsorb CO₂.

Various materials to absorb CO₂ viz., amines and ionic liquids were developed. Among all materials, physical adsorbents require lower energy for regeneration than amines or ionic liquids. According to the findings, MOFs offer more advantages by being tunable to achieve a high adsorption and selective capacity for CO₂. Different methods to synthesize MOFs have been developed where temperature, metal source, structural directing agents and deprotonating agents are able help achieve the desired MOFs. Highly porous 3D MOFs with high surface area are more attractive for application. The variation of parameters that contribute to high surface area, porosity, and three dimensional (structure) are mostly temperature, time, and the kind of metal source. These parameters should be taken into account during conventional thermal synthesis or microwave synthesis.

In MOFs, conventional hydrothermal or solvothermal and microwave synthesis are compared where it was found that microwave synthesis can produce better adsorbents for CO₂. Microwave synthesis produces MOFs with small crystal size as materials with increased surface area compared to conventional syntheses. Short reaction times, lower energy consumption, and high yield also make this technology economically feasible.

The synthesized products can have their adsorption capacity and selectivity enhanced at lower cost by post-treatment. Different activation methods viz., solvents exchange, vacuum, and supercritical carbon dioxide make pores or channels accessible for application. The structure of the pores and polarity on the internal and external surface area are the main factors for consideration in CO₂ adsorption capacity and selectivity. The structure of the metal environment, presence of hydroxyl groups, amine, carboxylates functional groups are the most well-known sites of adsorption for carbon dioxide. The nature, quantity and the arrangement of these structures and functional groups leads to enhanced adsorption and selectivity of CO₂.

CHAPTER 3: EXPERIMENTAL

3.1 Introduction

This chapter gives procedures used to synthesize cobalt succinates and nickel terephthalates. The technical methods to characterize the synthesized compounds are also explained. This chapter illustrates summary of synthetic and characterization methods used in this study.

3.2 Materials

All reagents were used without further purification. Table 3.1 indicates reagents, origin and their purity.

Table 0.1: Chemical reagents

Reagents	Origin	Purity %
Cobalt chloride hexahydrate: $\text{CoCl}_2 \cdot 6\text{H}_2\text{O}$	Saarchem	98
Cobalt acetate tetrahydrate: $\text{Co}(\text{CH}_3\text{CO}_2)_2 \cdot 4\text{H}_2\text{O}$	Aldrich chemical company	N/A
Succinic acid: $\text{C}_4\text{H}_6\text{O}_4$	Saarchem	99
Sodium hydroxide: NaOH	KIMIX	98
Potassium hydroxide KOH	Sigma Aldrich	85
Nickel nitrate hexahydrate: $\text{Ni}(\text{NO}_3)_2$	Sigma Aldrich	96
Terephthalic acid: $\text{C}_8\text{H}_6\text{O}_4$	Sigma Aldrich	98
Hexane: C_6H_{14}	Sigma Aldrich	95
Ethanol: $\text{C}_2\text{H}_5\text{OH}$	KIMIX	98

3.3 Synthesis of cobalt succinates

The synthesis focuses on cobalt succinates where succinic acid and KOH are added to cobalt salts dissolved in water according to the literature [35,37]. Hexane was introduced in the mixture in an autogenous hydrothermal synthesis to evaluate its effect on the resulting

products. Table 3.2 lists the abbreviations of the compounds according to the synthetic method. Two reactions were carried out at room temperature (rt) using different metal sources i.e., cobalt (ii) chloride hexahydrate (CoS) and cobalt (ii) acetate tetrahydrate (CoS-Ac) by keeping the molar ratio of metal to ligand constant (1:1.5). The volume of water was 5 ml in all preparations. The molar ratio of KOH to metal salt in both CoS and CoS-Ac was (1:1). However, when $\text{CoCl}_2 \cdot 6\text{H}_2\text{O}$ was used as the metal salt, the molar ratio of KOH was increased from 1 to 4 for the synthesis of CoS-sn, CoS-th, CoS-pr1, CoS-pr2, CoS-pr3, CoS-mw1 and CoS-mw2. Typical synthesis for CoS-sn was carried out by adding succinic acid (0.41 g) to a solution of cobalt(II) chloride hexahydrate (0.55 g) in 5 ml of water. There followed by addition of potassium hydroxide (0.52 g) to raise the solution to pH around 4. The mixture was sonicated for 45 min and the resulting solid phase was collected by filtration. The synthesis of CoS-pr2 and CoS-pr3 was performed in a Parr reactor at 170 °C with the introduction of hexane. The synthesis via microwave (300W) at 150 °C was performed in one step for CoS-mw1 and in two steps for CoS-mw2.

Table 0.2: Abbreviations of cobalt succinate complexes and synthesis conditions

Compd code	Metal source	Synthetic conditions
CoS-Ac	$(\text{CH}_3\text{COO})_2\text{Co} \cdot 4\text{H}_2\text{O}$	rt (4 weeks/water)
CoS	$\text{CoCl}_2 \cdot 6\text{H}_2\text{O}$	rt (3 weeks/water)
CoS-sn	$\text{CoCl}_2 \cdot 6\text{H}_2\text{O}$	30 °C Sonication (30 min/water)
CoS-th	$\text{CoCl}_2 \cdot 6\text{H}_2\text{O}$	170 °C reflux (3 days/water)
CoS-pr1	$\text{CoCl}_2 \cdot 6\text{H}_2\text{O}$	170 °C Parr reactor, 3 days, water
CoS-pr2	$\text{CoCl}_2 \cdot 6\text{H}_2\text{O}$	170 °C Parr reactor, 3 days; water-1.25 ml hexane
CoS-pr3	$\text{CoCl}_2 \cdot 6\text{H}_2\text{O}$	170 °C Parr reactor, 3 days; water-2.5 ml hexane
CoS-mw1	$\text{CoCl}_2 \cdot 6\text{H}_2\text{O}$	150 °C microwave (60 min/water)
CoS-mw2	$\text{CoCl}_2 \cdot 6\text{H}_2\text{O}$	150 °C microwave, 60 min neat and 60 min /water

The molar ration of metal salts to ligand (1:1.5) in all compounds, rt: room temperature

All products were filtered, washed with a mixture of water and ethanol (1:1) and dried in vacuum oven at 60 °C.

3.4 Synthesis of Nickel hydroxy-terephthalates

The ligand, terephthalic acid was converted into the disodium terephthalate salt ($C_8H_4O_4Na_2$) in order to allow the dissolution in water and was synthesized according to the procedure reported by Park *et al.* [142]. Nickel hydroxy-terephthalate compounds were prepared by the hydrothermal synthetic method according to the procedure reported by Carton *et al.* [143] with slight modifications. After dissolving $C_8H_4O_4Na_2$ (0.82 g) in an aqueous solution of $Ni(NO_3)_2$ (0.96 g) in water (7.2 ml), the pH was adjusted to 8 by adding NaOH (1M). Two different volume ratios of hexane were used in the synthesis to evaluate their effects on the resulting products. The starting mixtures were sonicated for 10 minutes to allow homogeneous mixing. All reaction mixtures were heated at 150 °C for three days. The light green powder products were washed with a mixture of water and ethanol (1:1) and dried in a vacuum oven at 60 °C. The synthesized compounds are abbreviated in Table 3.3 according to the synthetic reactions conditions of nickel hydroxy-terephthalates.

Table 0.3: Abbreviations of the synthesized nickel terephthalates

Code name	Synthetic conditions
Nitp-1	Water, 7.2 ml
Nitp-2	Water, 7.2 ml + hexane, 1.8 ml
Nitp-3	Water, 7.2 ml + hexane, 3.6 ml

Ni(NO₃)₂ : C₈H₄O₄Na₂, Molar ratio (1:1.5), under Pr at 150 °C, 3 days

3.5 Characterization techniques

3.5.1 Fourier Transform Infrared (FTIR) Spectroscopy

FTIR analysis provides information of functional group in the complexes [30,148]. A Perkin Elmer FTIR spectrometer was used to scan a compressed disc of compound to analyse it in the range between 200 and 4000 cm^{-1} . The background was obtained using only potassium bromide (KBr) to correct the baseline. A small quantity of compound was crushed into a fine powder and compressed into a transparent disc. The spectra of compounds were measured under the same conditions as the background.

3.5.2 Ultraviolet-Visible spectroscopy (UV-Vis)

This method of analysis gives the information of intra-ligand charge transfer and the presence of metal ions in the coordination ligands [144]. The compounds were dissolved in solvents according to their solubility. Using two UV cells (2ml): one as blank and the other for the compound allowed analysis to be carried out in the range of wave length (λ) 200 - 800 nm using GBC UV-Vis 920 instrument.

3.5.3 Thermal gravimetric analysis (TGA)

Thermal gravimetric analysis (TGA) checks thermal stability and weight loss of guest molecules [30]. It is also used to characterize thermal chemical and physical properties [145]. A Perkin Elmer STA 6000 instrument was used for TGA analysis. A mass of 4-5 mg of the compound was loaded into a ceramic crucible and placed automatically in the TGA for heating. Heating was run from 40 to 700 $^{\circ}\text{C}$ at a rate of 10 $^{\circ}\text{C min}^{-1}$ under an air flow rate of 19.8 ml/min. The data were recorded using Pyris software. The results were plotted (weight

loss percentage against temperature) using origin software to evaluate guest gases removal capacity and the decomposition of the molecules.

3.5.4 X-ray powder diffraction (XRD)

The characterization using XRD provides an identifiable structure and crystallinity of the phase [30,148]. The diffraction pattern is used to identify the metal organic complexes [30]. Powdered cobalt succinates were qualitatively analysed on a BRUKER AXS D8 advance (Germany) diffractometer with PSD Vantec-1 Detectors. The instrument performed with a Cu-K α X-ray radiation tube with x-ray wave length ($\lambda_{K\alpha_1} = 1.5406\text{\AA}$) accelerating on voltage of 40 kv and current of 40 mA at iThemb lab, South Africa. The data were recorded at 2θ in range of 6° and 80° at room temperature and evaluated using EVA software from BRUKER.

3.5.5 Scanning electron microscopy and Energy dispersive X-ray spectroscopy (EDS)

The surface morphology and shape of complexes were determined using scanning electron microscopy (SEM). The images were obtained using Zeiss Auriga field emission gun (FEG) SEM. The compound particles were placed onto the holes of discs and coated by Iridium to allow the conductivity. The instrument operated at 5 keV for imaging using an in-lens secondary detector. The elemental composition and distribution was illustrated by Energy Dispersive X-ray spectroscopy (EDS). EDS spectra were collected at 20 keV using a silicon solid-state drift detector on a selected surface.

3.6 Adsorption and desorption process of carbon dioxide

The adsorption and desorption studies were investigated using a thermal gravimetric analyzer (TGA: PerkinElmer STA 6000) equipped with Pyris software. All compounds were activated under vacuum at 60 °C overnight to remove any excess moisture and other solvents before analysis. A mass of compound between 6 and 7 mg was loaded into the ceramic crucible and placed in the TGA machine. Desorption process was performed under nitrogen (50 ml/min at 4.8 bar) and heated from 33 to 120 °C. Desorption temperature was held isothermally at 120 °C for 60 min to evacuate the maximum guest molecules. The temperature was then cooled to 33 °C and the purge gas was switched from nitrogen (50 ml/min at 4.8 bar) to CO₂ (10 ml/min at 1.3 bar). The compound was held at 33 °C for 30 min to achieve adsorption equilibrium. Thereafter, the purge gas was switched from CO₂ to nitrogen (50 ml/min at 4.8 bar) for CO₂ desorption. The weight change due the CO₂ adsorption was measured using Pyris software. The organogram of the synthetic reaction conditions, characterization techniques and adsorption procedure used in this study are represented in Figure 3.1.

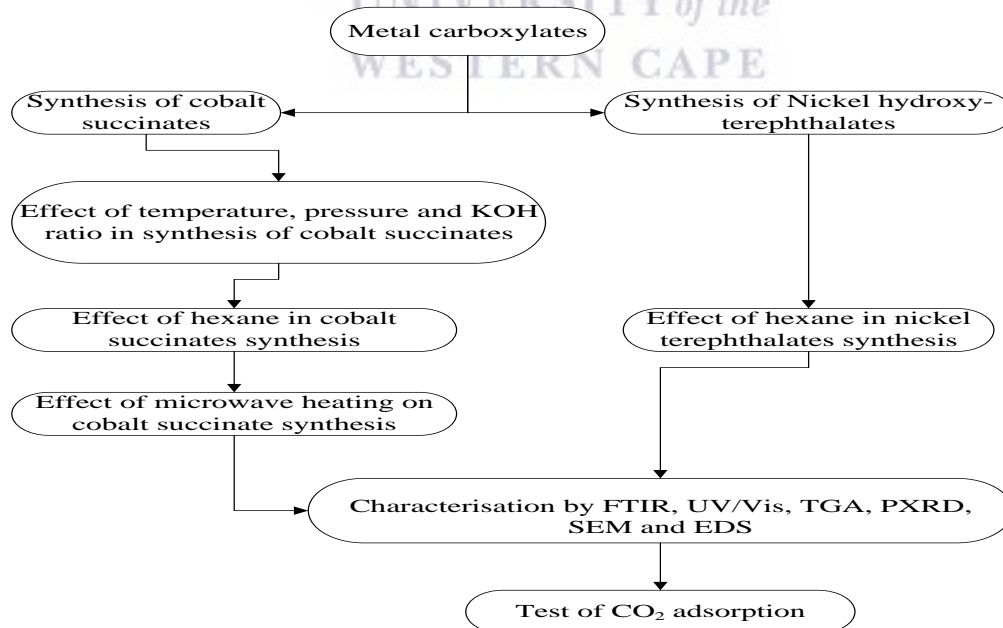
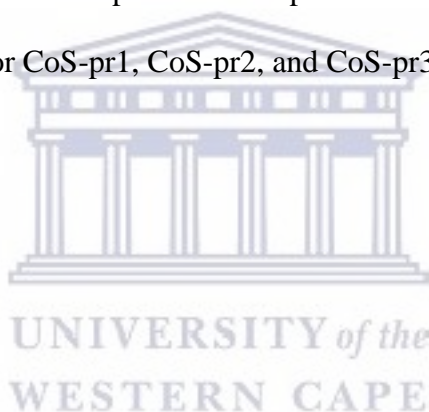


Figure 3.1: A scheme of brief experimental methods used in this study

3.7 Chapter summary

CoS and CoS-Ac were prepared from cobalt chloride hexahydrate and cobalt acetate tetrahydrate metal sources respectively at room temperature. Thermal heating at reflux of 170 °C was used to prepare CoS-th while the synthesis via sonication was used to prepare CoS-sn. Sonication for 45 mins provided a shorter reaction time. The above syntheses were carried out in open reactor vessels. Microwave heating at 150 °C was used to prepare CoS-mw1 for one hour and CoS-mw2 for two hours. The Parr reactor was used to synthesize cobalt succinates using cobalt chloride hexahydrate as a metal source to prepare CoS-pr1 using only water. Two different volumes of hexane were introduced to similar starting mixtures as in CoS-pr1 to prepare CoS-pr2 and CoS-pr3. The compounds Nitp-1, Nitp-2, and Nitp-3 were prepared in the same way as for CoS-pr1, CoS-pr2, and CoS-pr3.



CHAPTER 4: RESULTS AND DISCUSSION: COBALT SUCCINATES

4.1 Introduction

Cobalt succinates were synthesized at different temperatures (25, 150, and 170 °C) and assigned code names as shown in Table 4.1.

Table 0.1: Compound codes and their corresponding explanation

Compound code	Reaction conditions
CoS	Succinic acid and $\text{CoCl}_2 \cdot 6\text{H}_2\text{O}$ at rt.
CoS-Ac	Succinic acid and $\text{Co}(\text{CH}_3\text{COO})_2 \cdot 4\text{H}_2\text{O}$ at rt.
CoS-sn	Succinic acid and $\text{CoCl}_2 \cdot 6\text{H}_2\text{O}$ by Sonication at 30 °C.
CoS-th	Succinic acid and $\text{CoCl}_2 \cdot 6\text{H}_2\text{O}$ by thermal at 170 °C.
CoS-pr1	Succinic acid and $\text{CoCl}_2 \cdot 6\text{H}_2\text{O}$ by Parr reactor at 170 °C.
CoS-pr2	Succinic acid and $\text{CoCl}_2 \cdot 6\text{H}_2\text{O}$ by Parr reactor in hexane (1.25 ml).
CoS-pr3	Succinic acid and $\text{CoCl}_2 \cdot 6\text{H}_2\text{O}$ by Parr reactor in hexane (2.5 ml).
CoS-mw1	Succinic acid and $\text{CoCl}_2 \cdot 6\text{H}_2\text{O}$ by microwave at 150 °C
CoS-mw2	Succinic acid and $\text{CoCl}_2 \cdot 6\text{H}_2\text{O}$ by microwave 1h without water followed by 1h with water at 150 °C.

All synthesized materials were characterized using FTIR, UV-vis, XRD and TGA. Other analytical techniques such as SEM and EDS were used to characterize only CoS-pr1, CoS-pr2, CoS-pr3, and CoS-mw1.

4.2 FTIR characterisation

Analysis based on FTIR confirms the presence of different functional groups in compounds. Figures 4.1 (a, b, and c) displays the FTIR spectra of CoS-Ac, CoS, CoS-sn, CoS-th, CoS-pr1, CoS-pr2, CoS-pr3, CoS-mw1 and CoS-mw2. The spectrum of succinic acid was displayed for comparison with the synthesized compounds.

The bands at 3405, 3524 and 3632 cm^{-1} are assigned to the stretching vibrations for the O-H groups of coordinated water molecules via strong hydrogen bonding. The peak at 1700 cm^{-1} is assigned to unreacted succinic acid (ligand) [121] and is not present in all the products which confirms the complexation of the ligand to the metal centre. In addition, peaks at 1553 and 1402 cm^{-1} correspond to asymmetric and symmetric vibrations of the COO^- which supports complexation [132]. The peaks at 1327 and 1036 cm^{-1} are attributed to -O-H and -C-C- vibration mode, respectively, while the peaks at 1241 and 1176 cm^{-1} are attributed to the $-\text{CH}_2-$ group, while the peak at 803 cm^{-1} is assigned to (C-H). Small intensity peaks at 662, 559, and 520 cm^{-1} are assigned to the Co-O absorption. The IR spectra of the present compounds are essentially similar to that observed for $\text{CoC}_4\text{H}_4\text{O}_4 \cdot 4\text{H}_2\text{O}$ [146].

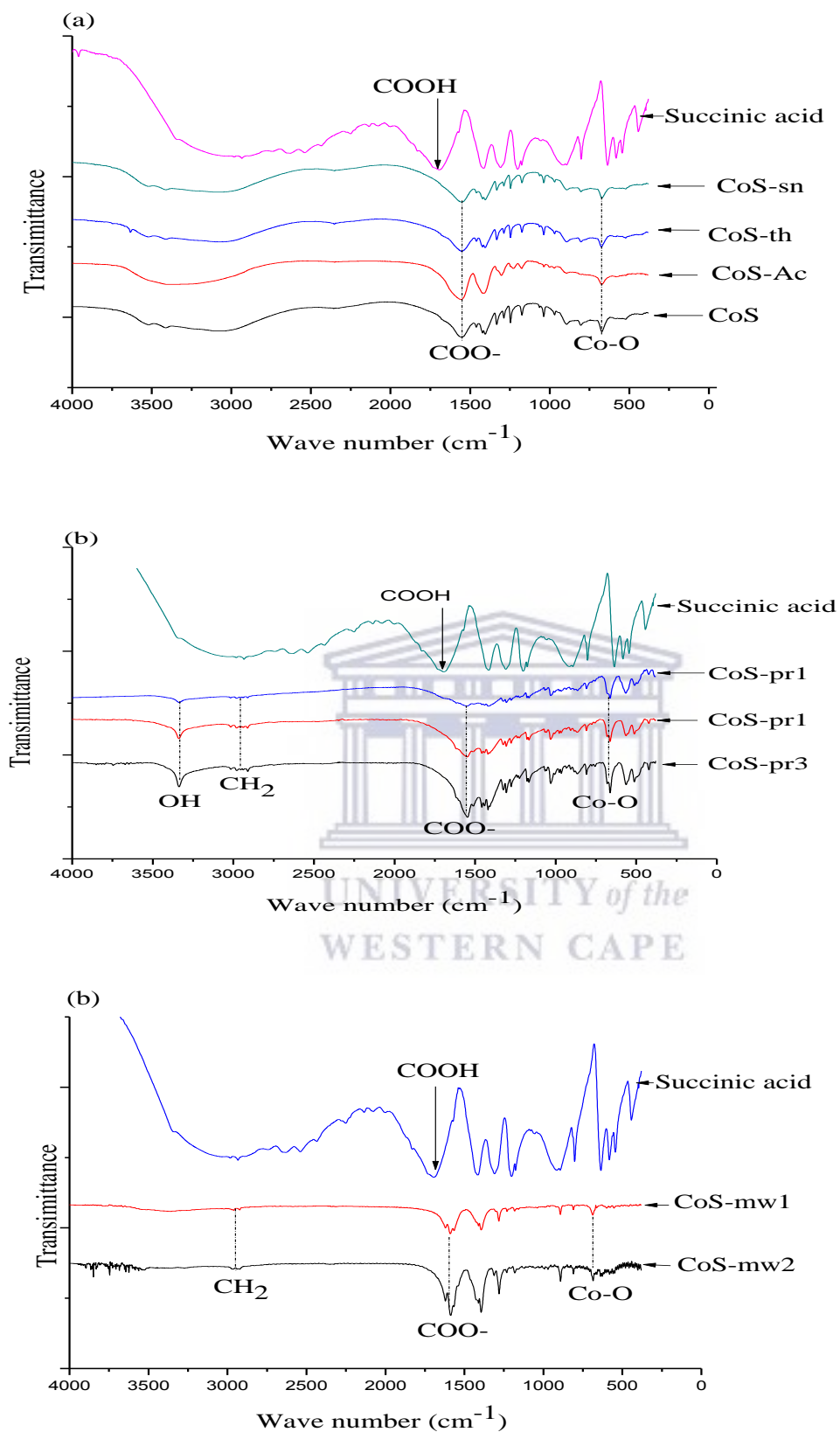


Figure 0.1: FTIR spectra of cobalt succinates a) from $\text{Co}(\text{CH}_3\text{COO})_2 \cdot 4\text{H}_2\text{O}$ or $\text{CoCl}_2 \cdot 6\text{H}_2\text{O}$ at rt, sonication & thermal reaction, b) Parr reactor and c) microwave

Figure 4.1 (b) shows sharp peak at 3337 cm^{-1} attributed to the presence of $\nu(\text{Co-O-H})$ as the free non-hydrogen bonded OH (hydroxyl) group. The stretching frequencies observed at 1550 and 1409 cm^{-1} correspond to asymmetric and symmetric vibrations of the COO^- which indicate bond formation of Co with the acetate oxygen. The other identified peaks are assigned as follow, 1316 cm^{-1} to $-\text{O-H}$, 1116 cm^{-1} to $-\text{CH}_2-$, 1036 cm^{-1} to $-\text{C-C-}$, 861 and 814 cm^{-1} to C-H , 674 , 569 , and 510 cm^{-1} to Co-O vibrations [37,150]. The peak at 417 cm^{-1} is ascribed to Co-OH absorption [37,151]. The IR spectra (Figure 4.1b) are similar to that of MIL-9 reported by Livage *et al.* [36]. It is worthy to mention that both CoS-pr2 and CoS-pr3 have peaks sharper than CoS-pr1 which could be associated with the effect of hexane used in the synthesis which enabled less interaction between functional groups.

The FTIR spectra of CoS-mw1 and CoS-mw2 (Figure 4.1c) showed a shoulder around 1600 cm^{-1} which corresponds to the bending mode related to occluded water molecules [148]. The peaks around 1550 cm^{-1} and 1409 cm^{-1} are attributed to asymmetric and symmetric vibrations of the COO^- respectively. The presence of these peaks confirms coordination of the ligand to the metal centre for CoS-mw1 and CoS-mw2. All the synthesized products showed the corresponding bands at 662 , and 559 cm^{-1} due to Co-O similar to that reported for $\text{K}_2\text{Co}_2(\text{C}_4\text{H}_4\text{O}_4)_2$ [146]. Both CoS-mw1 and CoS-mw2 seem to be similar. Figure 4.2 illustrates the structure as proposed by Sharrock and Theophanides which can be attributed to CoS-mw1 and CoS-mw2 [146].

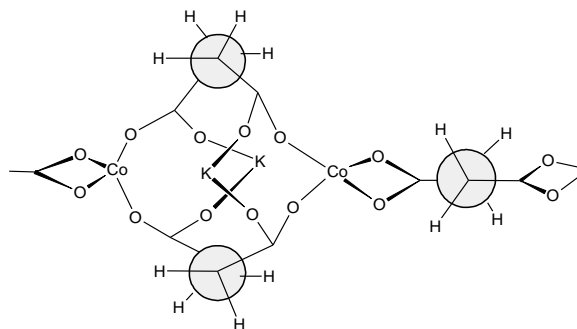


Figure 0.2: Proposed structure for the compound CoS-mw1 and CoS-mw2 [152]

Figure 4.2 shows the gauche conformation of the double bridges in the compound which results in a cage-like structure, at the point where the two COO^- groups form two bridges between cobalt and potassium. In this cage, four COO^- groups form four bridges between two identical metals. In the centre of the cage, two potassium ions (K^+) are also bridged by four oxygens from the COO^- groups. The Cl^- ions observed in the EDS analysis (Figure 4.9d) act on K^+ as counter ions [149]. This structure allows cobalt centres to adopt a tetrahedral geometry as explained by Sharrock and Theophanides [146].

The FTIR results show that the compounds CoS-Ac, CoS, CoS-sn, and CoS-th contain water molecules in the frameworks as shown by the broad peak between 3688 cm^{-1} and 2650 cm^{-1} . Compounds CoS-pr1, CoS-pr2, and CoS-pr3 synthesized at $170\text{ }^\circ\text{C}$ in the Parr reactor (pr) contain coordinating hydroxyl groups indicated by the peak around 3337 cm^{-1} instead of water molecules. The increase in the reaction temperature to above $100\text{ }^\circ\text{C}$ results in replacement of water molecules by hydroxyl groups and an increase in the number of coordinated carboxylates on the metal centre as reported by Livage *et al.* and Forster *et al.* [37,38]. However, CoS-th synthesized under reflux at $170\text{ }^\circ\text{C}$ contains water molecules without additional hydroxyl groups which could arise by the absence of pressure in preparation of CoS-th. Sun and Sun explain the effect of temperature to be associated with other parameters

such as pressure to influence the assembly of the framework, structural modulation and transformation of MOFs [150]. The effects of such combined or separated parameters could influence the presence or absence of coordinated water molecules and hydroxyl groups in MOFs. In CoS-mw1 and CoS-mw2 structures, there is no incorporation of hydroxyl groups. Even though the product was synthesized at 150 °C there was no pressure involvement as indicated by the microwave instrument. The absence of sharp peaks at 3337 and 417 cm^{-1} in CoS-mw1 and CoS-mw2 indicates that there are no coordinated hydroxyl groups or water molecules. This could be caused by removal of water at the beginning of the reaction thereby preventing creation of pressure during microwave heating.

4.3 Ultraviolet and Visible (UV-Vis) characterization

All the synthesized compounds were dissolved in different solvents according to the extent of the compound's solubility. The UV-Vis spectra presented in Figures 4.3a, b and c illustrate the intra-ligand charge transfer transition and the presence of metal ions in coordination with the ligand. The peak values corresponding to their assigned states are presented in Table 4.2.

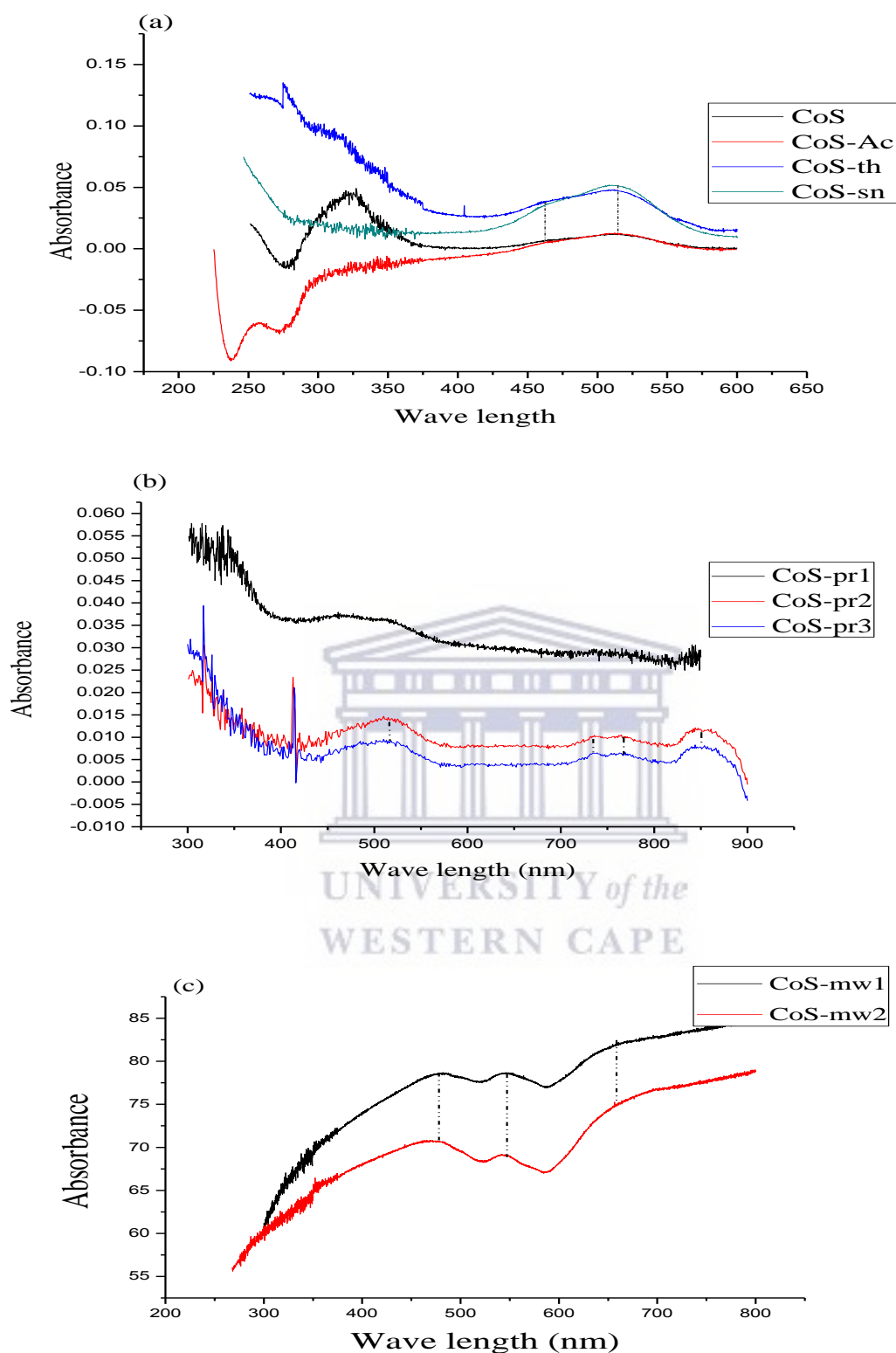


Figure 0.3: UV-Vis spectra of cobalt succinates a) from $\text{Co}(\text{CH}_3\text{COO})_2 \cdot 4\text{H}_2\text{O}$ or $\text{CoCl}_2 \cdot 6\text{H}_2\text{O}$ at rt, sonication & thermal reaction, b) Parr reactor and c) microwave.

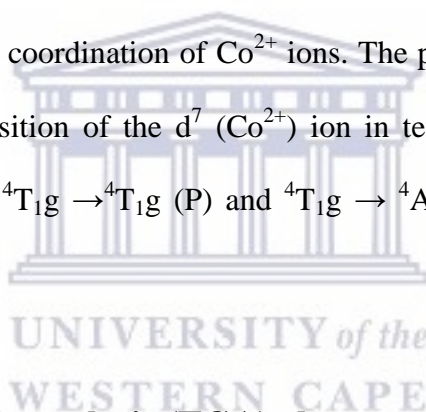
Table 0.2: UV-Vis spectra observed for cobalt succinates

Compound	UV-Vis absorption bands (nm)			
	Intra-ligand charge transfer	${}^4T_{1g}(P) \leftarrow {}^4T_{1g}(F)$	${}^4T_{1g} \rightarrow {}^4A_{2g}(F)$	${}^4A_{2'}(F) \rightarrow {}^4A_{2'}(P)$
CoS	225	466 and 514	-	-
CoS-Ac	255 and 297	466 and 514	-	-
CoS-th	275	466 and 514	-	-
CoS-sn	-	466 and 514	-	-
CoS-pr1	-	466 and 516	767	-
CoS-pr2	-	516	731 and 767	850
CoS-pr3	-	516	731 and 767	850
CoS-mw1	-	477 and 543	650	-
CoS-mw2	-	477 and 543	650	-

Figure 4.3 (a) shows a shoulder around 466 and a peak at 514 nm attributed to the absorbance of Co-O which also indicates the presence of Co^{2+} ions. These peaks are assigned to the ${}^4T_{1g}(P) \leftarrow {}^4T_{1g}(F)$ transition, with octahedral coordination. Similarly, the transition state of cobalt ions in octahedral coordination has been reported by Poul *et al.* and Bordbar *et al.* [155,156]. This state indicates the transfer of charge from the d orbital of the metal ion to a void orbital of the ligand. Sharrock and Theophanides observed similar absorption peaks at 511 and 470 nm for cobalt succinate tetrahydrate (511 and 470 nm) in the form of octahedral and tetrahedral geometry respectively [146]. The absorption bands between 200 and 347 nm are assigned to intra-ligand charge transfer [144].

UV-Vis spectra of CoS-pr1, CoS-pr2, and CoS-pr3 (Figure 4.3b) provide information on coordination of the succinate ligand to cobalt centre. The observed peak at 516 nm in all three compounds is attributed to the ${}^4T_{1g}(P) \leftarrow {}^4T_{1g}(F)$ transition for octahedral coordination to the Co^{2+} ion. Peaks at 731 and 767 nm are associated with ${}^4T_{1g} \rightarrow {}^4A_{2g}(F)$ transition for octahedral coordination of Co^{2+} with succinate ligand. The absorption band at 850 nm could be due to the ${}^4A_2'(F) \rightarrow {}^4A_2'(P)$ transition of the square pyramidal d^7 (Co^{2+}) ion. Similarly, these absorption bands are found in cobalt compounds synthesized by Sarma *et al.* [144] and Poul *et al.* [151].

UV-Vis absorption spectra (Figure 4.3c) of CoS-mw1 and CoS-mw2 are similar. The absorption band around 477 nm is assigned to the ${}^4T_{1g}(F) \rightarrow {}^4T_{1g}(P)$ transition and is associated with the octahedral coordination of Co^{2+} ions. The peaks around 543 and 650 nm are attributed to the d-d transition of the d^7 (Co^{2+}) ion in tetrahedral coordination. These bands have been assigned to ${}^4T_{1g} \rightarrow {}^4T_{1g}(P)$ and ${}^4T_{1g} \rightarrow {}^4A_{2g}(F)$ transitions respectively [144].



4.4 Thermal gravimetric analysis (TGA) characterisation

The weight loss percentages and stability of the porous metal frameworks were investigated by thermal gravimetric analysis (TGA). The thermal gravimetric data of cobalt succinates shown by the percentages mass loss and their probable attributions are presented in Table 4.3 and displayed in Figures 4.4a, b, and c).

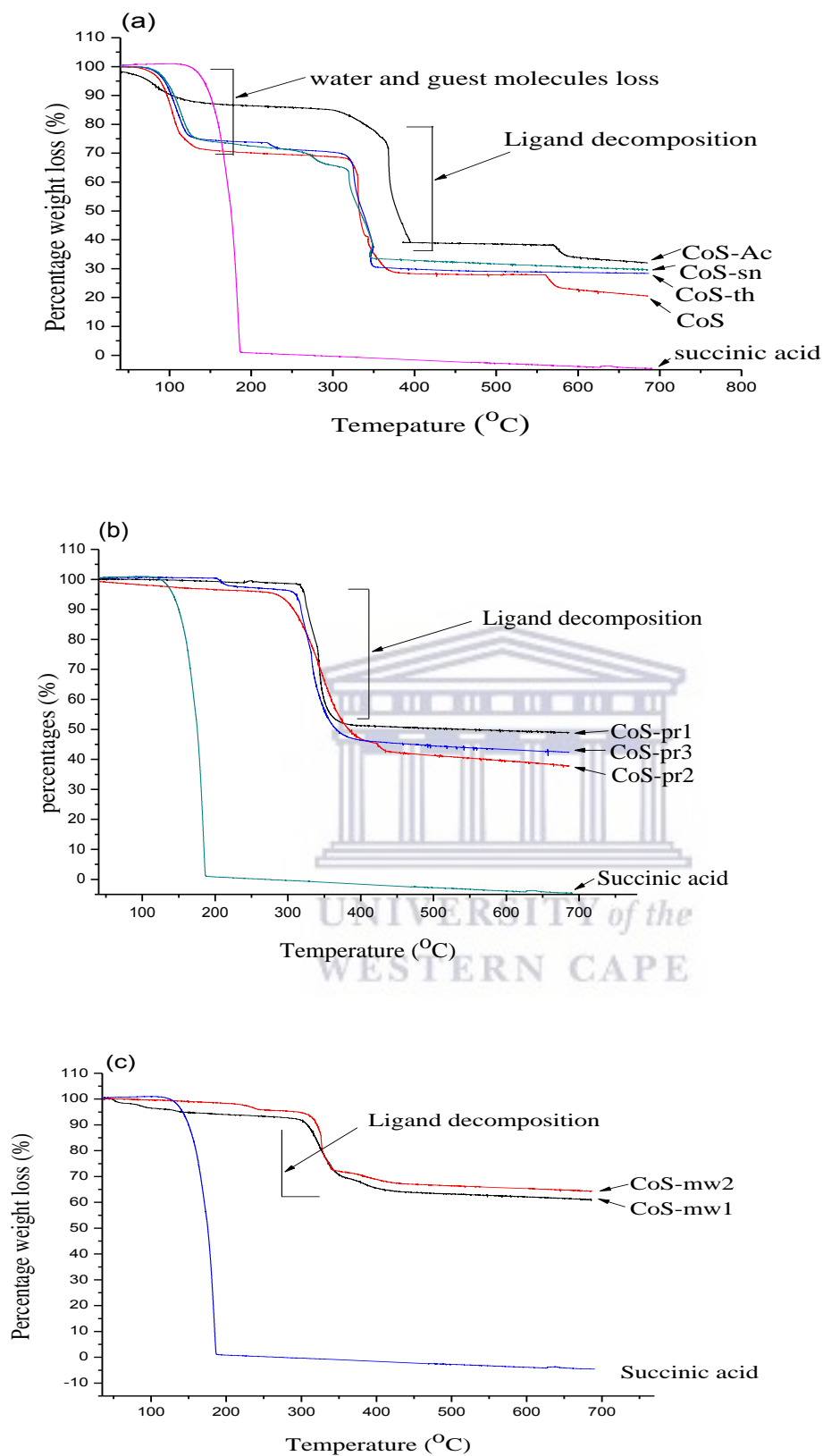


Figure 0.4: Thermal behaviour of cobalt succinates compounds under air a) at rt, sonication & thermal conditions, b) Parr reactor, and c) microwave.

Table 0.3: Weight loss analysis for cobalt succinates

Compound	Temperature range (°C)	Weight loss (%)	Group lost
CoS-Ac	40 - 139	10.6	H ₂ O (coordinate)+ Ethanol
	300 - 393	46	Ligand decomposition
CoS-th	40 - 134	25	H ₂ O (coordinate) + Ethanol
	308 - 352	40	Ligand decomposition
CoS-sn	40 - 134	24.6	H ₂ O (coordinate) + Ethanol
	260 - 346	40	Ligand decomposition
CoS	40 - 135	29.9	H ₂ O (coordinate) + Ethanol
	314 - 376	40	Ligand decomposition
CoS-pr1	40 - 313	1.9	Guest H ₂ O + Ethanol
	314 - 389	47.6	Ligand decomposition
CoS-pr2	40 - 277	3.6	Guest H ₂ O + Ethanol
	277 - 401	54	Ligand decomposition
CoS-pr3	40 - 297	4	Guest H ₂ O + Ethanol
	305 - 391	52	Ligand decomposition
CoS-mw1	293 - 417	7.2	Guest H ₂ O + Ethanol
	293 - 417	28	Ligand decomposition
CoS-mw2	293 - 417	7.2	Guest H ₂ O + Ethanol
	293 - 417	28	Ligand decomposition

The coordinated water and other guest molecules are removed during the first stage and the ligand was decomposed at the second step (Figure 4.4a, b, and c). The % weight loss is far different from that of starting material (succinic acid). Figure 4.4 (a) illustrates two main

steps in weight loss. The first weight loss of 25 and 24.6% (calculated 23.6%) respectively, for CoS-th and CoS-sn was noted between 40 and 134 °C. These weight losses are attributed to the removal of three water molecules similar to Caires *et al's*. findings [132]. The weight loss of 29.9% in CoS, from 40 to 135 °C could be associated to four water and one ethanol molecule. The theoretical weight loss percentage corresponds to 29.12%. Similarly, Randhawa and Gandotra [153] observed the same weight loss in $\text{Co}(\text{C}_4\text{H}_4\text{O}_4)\cdot 4\text{H}_2\text{O}$ using TGA analysis. The first stage of the weight loss of 10.6% (calculated 10.3%) in CoS-Ac was observed from 40 to 139 °C which corresponds to the removal of one water and ethanol molecule.

The second stage of weight loss defines the stability of the synthesized compounds. The compound CoS-sn collapses from 260 to 346 °C with weight loss of 40%, while CoS-th collapses from 308 to 352 °C with a similar weight loss of 40%. CoS collapses from 314 to 376 °C with a weight loss of 40%, and CoS-Ac collapses from 300 to 393 °C with weight loss of 46% of the organic moiety. This indicates that over these temperatures, the synthesized compounds start to decompose by loss of the organic molecule resulting to cobalt oxide. However, among these four synthesized compounds, CoS-sn is the least stable. The percentages noted for the resulting cobalt oxides are 43.4 for CoS-Ac, 35 for CoS-th, 35.4 for CoS-sn, and 30.1 for CoS. Figure 4.4 (b) illustrates a slight weight loss of 1.9% from 40 to 313 °C in CoS-pr1 and corresponds to removal of the guest water and ethanol molecules [80,84]. Also, the 3.6% weight lost from 40 to 277 °C of CoS-pr2 resulted from the removal of guest molecules including hexane [35,80,84]. The weight loss of 4% observed from 40 to 297 °C in CoS-pr3 is attributed to removal of guest and hexane molecules from the structural channels of the synthesized product. In CoS-pr3 the weight loss of 2.7% observed in the range 198 - 220 °C which could be related to the trapped molecules in the pore wall's structure [154].

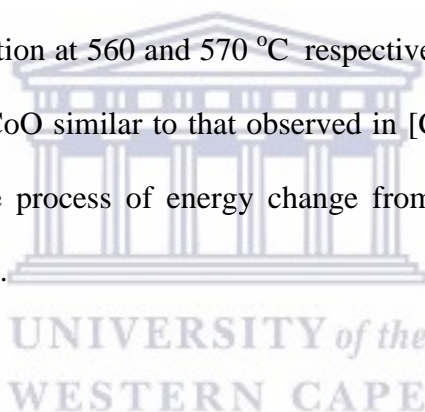
Considering compounds synthesized in the Parr reactor, the removal of water, ethanol, and hexane guest molecules increased from compound CoS-pr1 to CoS-pr3. This increase can be attributed to the effect of hexane which can change the size or create the pores allowing the accessibility by the guest molecules [35]. The hydrophobicity of the hexane template can allow formation of pores around it. The hexane template can also influence the flexibility of the succinate bridges by influencing the pore size. A similar effect was reported for $[\text{Co}_2(\text{ndc})_2(\text{bi-pyren})] \cdot \text{C}_6\text{H}_6 \cdot \text{H}_2\text{O}$, where benzene increased the capacity of the host-guest gases in the compound [35].

Combustion of the organic moiety in CoS-pr1 was noticed between 314 and 389 °C with a corresponding weight loss of 47.6 %. At a temperature between 277 and 401 °C, compound CoS-pr2 underwent a 54.0% weight loss, while between 305 and 391 °C a 52% weight loss in CoS-pr3 was noted. Similarly, Livage *et al.* observed a 53.0% weight loss due to combustion of the organic moiety in $\text{Co}_5(\text{OH})_2(\text{C}_4\text{H}_4\text{O}_4)_4$ [36]. The compound, CoS-pr1 showed a higher thermal stability (314 °C) than CoS-pr2 and CoS-pr3. The percentages of resulting cobalt oxides are 50.5 for CoS-pr1, 42.5 for CoS-pr2, and 44.0 for CoS-pr3.

The observed weight loss from 40 to 293 °C in CoS-mw1 and CoS-mw2 (Figure 4.4c) corresponds to 7.2% for both compounds. The two compounds showed the same % in the weight for the same temperature range. These weight losses are related to the removal of occluded guest water and ethanol molecules.

The decomposition of CoS-mw1, and CoS-mw2 occurred between 293 and 417 °C with 28% weight loss. From the TGA results for CoS-mw1 and CoS-mw2, it is concluded that both compounds are similar and confirmed by FTIR analysis (Figure 4.1b) and XRD diffractograms (Figure 4.7 section 4.6). The percentage of residue (cobalt oxide) after decomposition in the two compounds is 64.8.

The TGA analysis showed possible guest molecules accessibility in the synthesized metal organic frameworks using hexane. According to the TGA results, removal of guest molecules corresponded to the capacity of guest molecules that had been hosted in the framework. As hexane was used in the synthesis of CoS-pr2 and CoS-pr3, the percentage of weight loss before ligand decomposition was higher than that of CoS-pr1. It has been reported that the hydrophobic molecules which occupy pores are able to increase the size of pores [35]. The adsorption capacity for CO₂ could be higher in the compounds where higher amounts of the guest molecules have been removed [155]. TGA also provides the maximum temperature of activation at which the porous compounds is stable before decomposition [83,160]. The final residue in all the compounds after complete decomposition is CoO. However, CoS and CoS-Ac showed further decomposition at 560 and 570 °C respectively which can probably be the decomposition of Co₃O₄ to CoO similar to that observed in [Co(HCOO)₂·2H₂O] [81]. This difference may be due to the process of energy change from the transitional state to the formation of the final products.



4.5 Scanning electron microscopy (SEM) and energy dispersive X-ray spectroscopy (EDS)

The surface morphology, and pore structures of the synthesized products were investigated by scanning electron microscopy (SEM) techniques (Figures 4.5 - 4.8). The elemental composition was identified using energy dispersive x-ray spectroscopy (EDS) (Figure 4.9a-d). CoS-pr1, CoS-pr2, CoS-pr3 and CoS-mw1 were selected for SEM and EDS analysis.

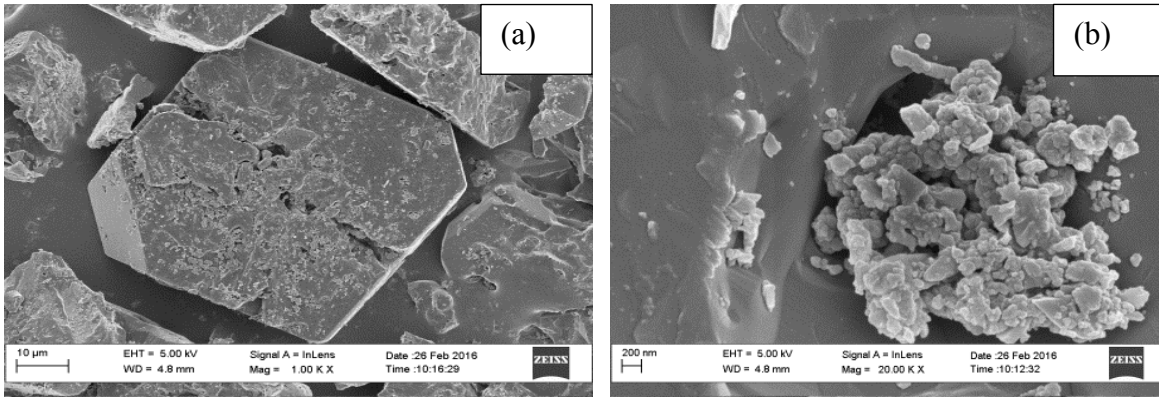


Figure 0.5: SEM images of CoS-pr1 synthesized using only water, showing a) the surface morphology b) the aggregate particles filled in pores

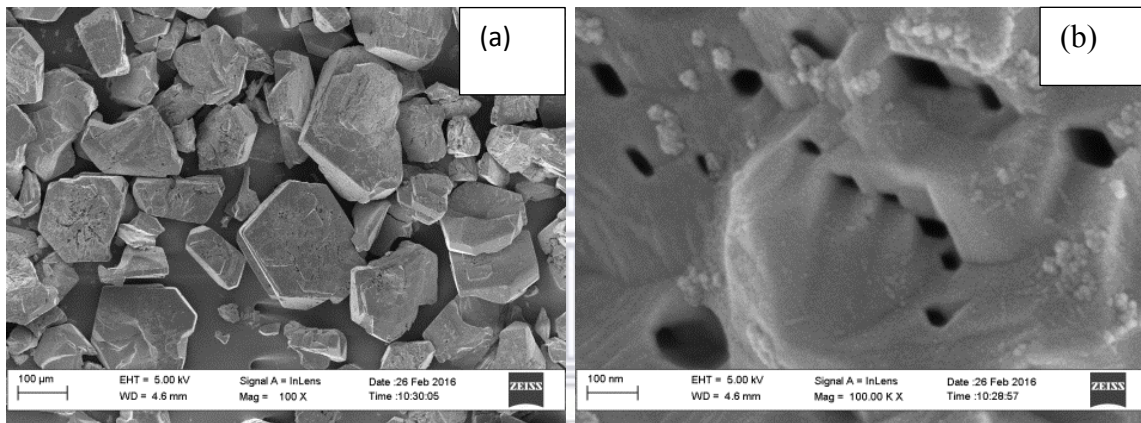


Figure 0.6: SEM images of CoS-pr2 synthesized using water and 1.25 ml of hexane a) surface morphology and shape and b) free pores and very few aggregate particles at the surface.

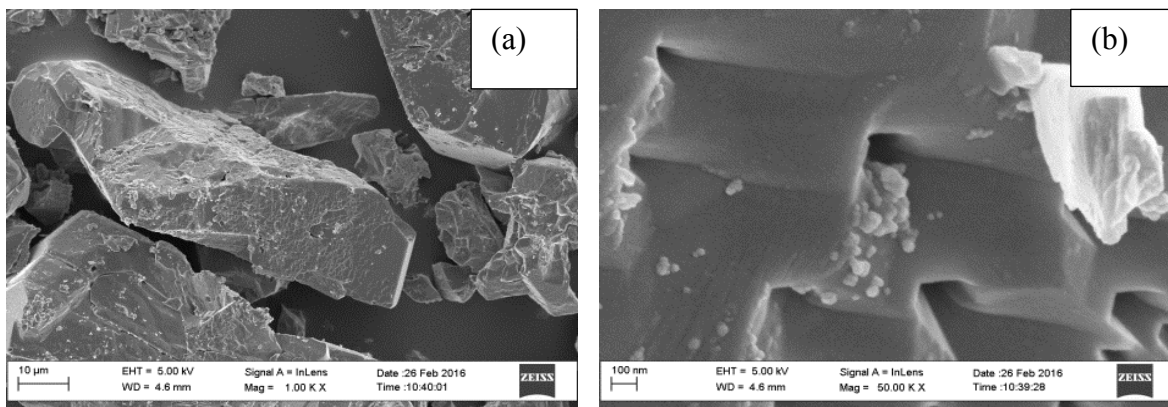


Figure 0.7: SEM image of CoS-pr3 synthesized using water and 2.5 ml of hexane a) Surface morphology and shape and b) free pores and aggregate particles at the surface

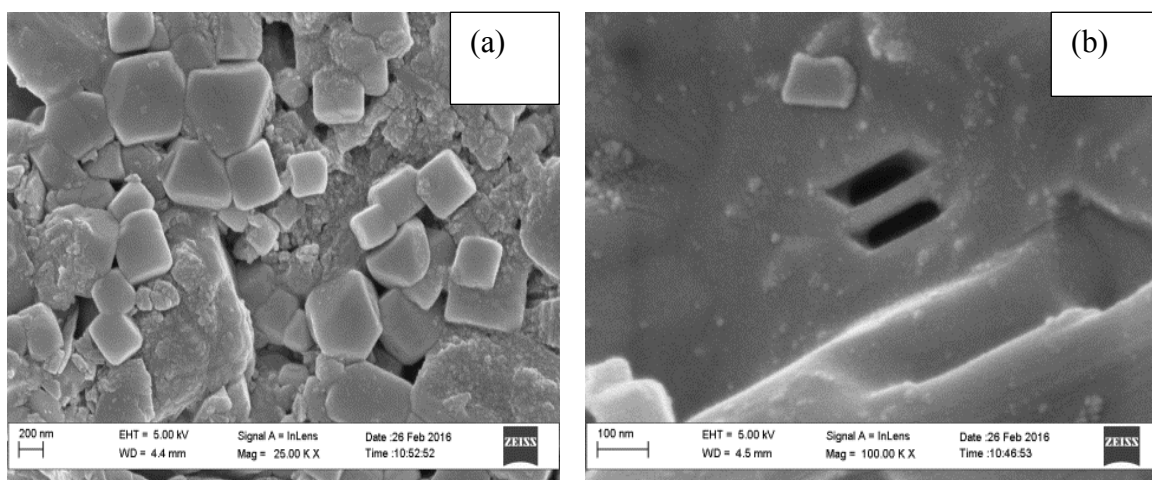


Figure 0.8: SEM image of CoS-mw1 showing a) surface morphology b) open pore structures.

The micrograph images of CoS-pr1, CoS-pr2, and CoS-pr3 (Figures 4.5a, 4.6a, and 4.7a) show polycrystalline structures with a rough surface. There are some particles at the surface of CoS-p1 (Figure 4.5b) which can limit the pores accessibility. This might be caused by the ionic interaction of guest particles to the surface [35]. Figure 4.6b shows open pores without particle blockage in CoS-pr2 which is different from CoS-pr1. Figure 4.7b also shows some pores at the surface of CoS-pr3.

The polycrystalline materials with irregular shape could be due to the versatility of Co^{2+} coordination which can be found in tetrahedral or octahedral forms [157]. In addition, there could be a combination of both octahedral, tetrahedral, and square pyramidal lattices [157] of cobalt succinates as discussed within UV-Vis data. Both the octahedral and tetrahedral forms are observed in cobalt succinates as reported by Poul *et al* [151], Guillou *et al* [158], and Sharrock and Theophanides [146]. The accessible open pores in CoS-pr2 and in CoS-pr3 is related to the hydrophobicity of hexane and the pressure generated during heating the reaction that removes the occluded particles at the surface and pores.

Figure 4.8a displays a cubic like structure of CoS-mw1 synthesized using the microwave method. Figure 4.8b shows that the synthesized materials possess some pore structures as supported by Sharrock and Theophanides [146]. The surface area in CoS-mw1 was uniform compared to all products synthesized from conventional hydrothermal methods. Therefore the microwave heating provided homogeneous nucleation. The elemental composition was also investigated for these compounds. Figures 4.9 (a-d) and Table 4.3 show the EDS analysis and illustrates the percentage compositions for CoS-pr1, CoS-pr2, CoS-pr3 and CoS-mw1 where five spots were selected for the analysis.

Table 0.4: EDS states quantitative elemental analysis of compounds CoS-pr1, CoS-pr2, CoS-pr3, and CoS-mw1

Element	CoS-pr1	CoS-pr2	CoS-pr3	CoS-mw1
	Atomic (%)	Atomic (%)	Atomic (%)	Atomic (%)
C	46.256	44.836	47.396	43.402
O	38.954	40.854	38.714	46.77
Co	14.776	14.312	13.862	5.622
Cl	-	-	-	1.704
K	-	-	-	2.04

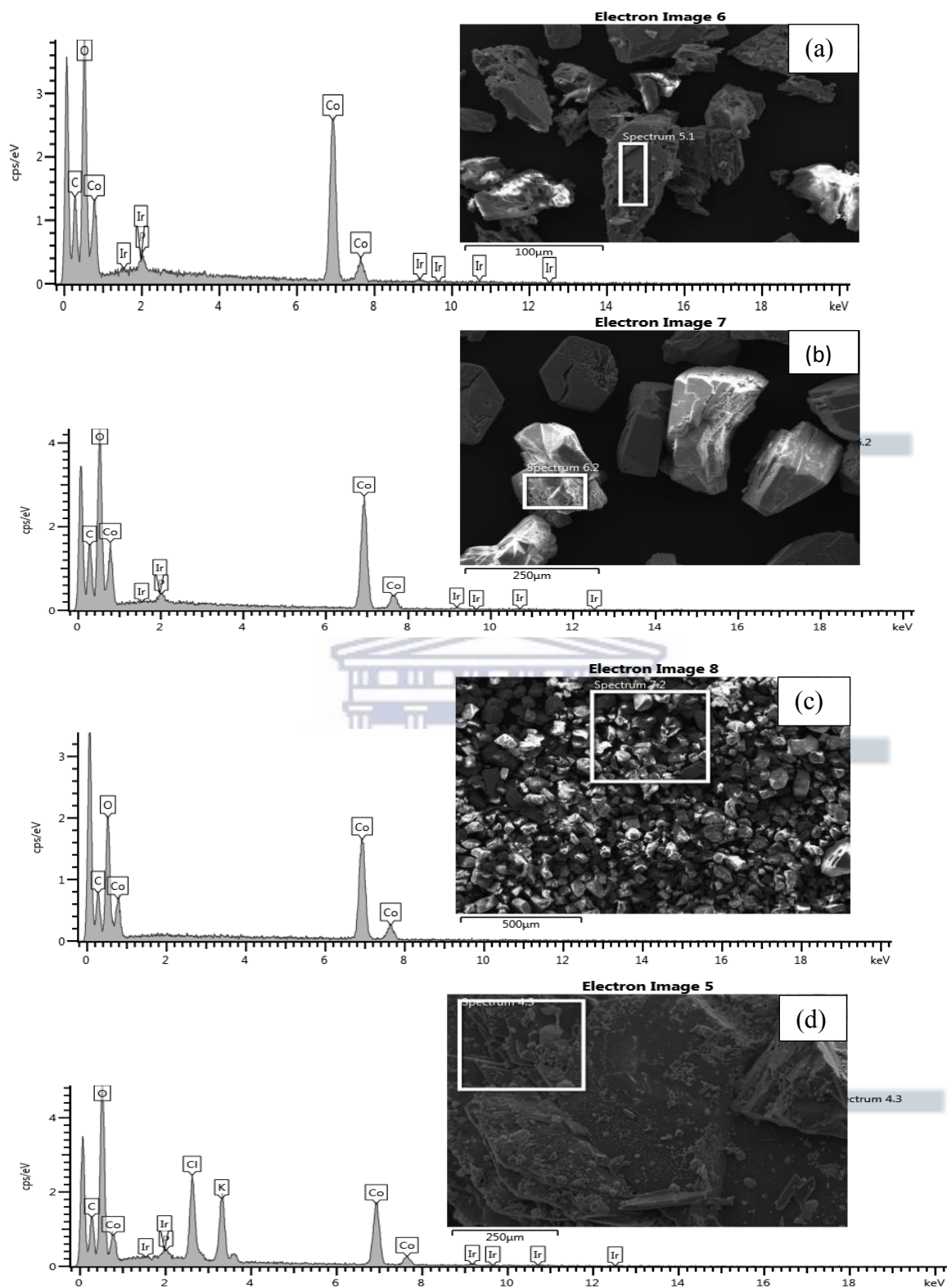


Figure 0.9: EDS spectra of cobalt succinates a) Parr reactor b) Parr reactor, 1.25 ml hexane, and c) Parr reactor, 2.5 ml of hexane, and d) by microwave.

In general, EDS showed that cobalt (Co), carbon (C), and oxygen (O), are present in the synthesized products. Compounds CoS-pr1, CoS-pr2, and CoS-pr3 have similar averages in elemental composition (C, O and Co). In addition, Co, C, and O were also found in the compounds synthesized from pr. Furthermore, potassium (K) and chlorine (Cl) elements were identified in CoS-mw1 (Figure 4.9d). In fact, the two elements (K and Cl) were unexpected and their presence might be associated to the forcing out of water molecules from the mixture at the beginning of the reaction during microwave heating. Solvent and pressure did not play their roles to solubilize both K and Cl ions during microwave heating and could account for this observation. The arrangement of these elements in the crystal structure could possibly block or reduce accessibility of the pore structures [159].

The minor presence of iridium and phosphorus originated from the coating process. The percentages of Ir and P were subtracted from compound results. Table 4.3 presents percentages of elements from the cobalt succinate spectra and helps to confirm the elements found in the compounds of cobalt succinate as characterized by FTIR and TGA. Thus the EDS technique complements the above characterisation techniques.

4.6 X-ray diffraction (XRD) characterisation

The XRD measurements were carried out from 2Θ (2theta) = 6 to 80°. Figures 4.10 (a, b, and c) illustrate the spectra for the synthesized Co-Succinates. It was noted that the synthesized products are all crystallines with high and sharp peak intensities pattern. The XRD patterns, Figure 4.10a match the standard cobalt succinate results from JCPDS (Joint Committee on Powder Diffraction Standards data) with formula $\text{Co}(\text{C}_4\text{H}_4\text{O}_4)\cdot 4\text{H}_2\text{O}$ (appendix 1 and 2). The difference in intensity of some peaks might be due to the water content as discussed in the TGA analysis (see Figure 4.4a). Therefore, it is concluded that

the chemical formula for CoS is $\text{Co}(\text{C}_4\text{H}_4\text{O}_4)\cdot 4\text{H}_2\text{O}$ and for CoS-th and CoS-sn is $\text{Co}(\text{C}_4\text{H}_4\text{O}_4)\cdot 3\text{H}_2\text{O}$ while CoS-Ac is $\text{Co}(\text{C}_4\text{H}_4\text{O}_4)\cdot \text{H}_2\text{O}$.

Presence of the peak at $2\theta = 9.3^\circ$ (Figure 4.10b) is observed in the data of a typical crystalline anhydrous cobalt succinate, $\text{Co}(\text{C}_4\text{H}_4\text{O}_4)$ from JCPDS (appendix 3). The more intense and sharpness of this peak is attributed to the presence of hydroxyl groups coordinated on the cobalt centres in the absence of water molecules [160]. The very small peak at $2\theta = 12^\circ$ is found in cobalt succinates in general [117] and matches with JCPDS (appendix1). Furthermore, this peak ($2\theta = 12^\circ$) is also present as the main peak in $\text{Co}_4(\text{OH})_2(\text{H}_2\text{O})_2(\text{C}_4\text{H}_4\text{O}_4)_3\cdot 2\text{H}_2\text{O}$ which differs in water content of the products.

The cobalt succinates prepared under high pressure viz. CoS-pr1, CoS-pr2, and CoS-pr3 show a similarity in their XRD patterns with slight change. CoS-pr2 showed a higher peak intensity which corresponds to its higher crystallinity. Their FTIR spectra (Figure 4.1b) and the percentage of elements from EDS (Figures 4.9a, b, and c) are also very similar with little differences. The small difference could be attributed to the difference in synthetic conditions [30,130].

The XRD patterns for CoS-mw1 and CoS-mw2 (Figure 4.10c) are also similar. They have some peaks around $2\theta = 13, 24, 28$ and 40° in common which correlate with data of cobalt succinates from the JCDS (appendix 2). However, they show new peaks which are different from the other synthesized cobalt succinates. The new peaks and shift could be associated with the presence of K and Cl elements (shown by EDS Figure 4.9d and table 4.3).

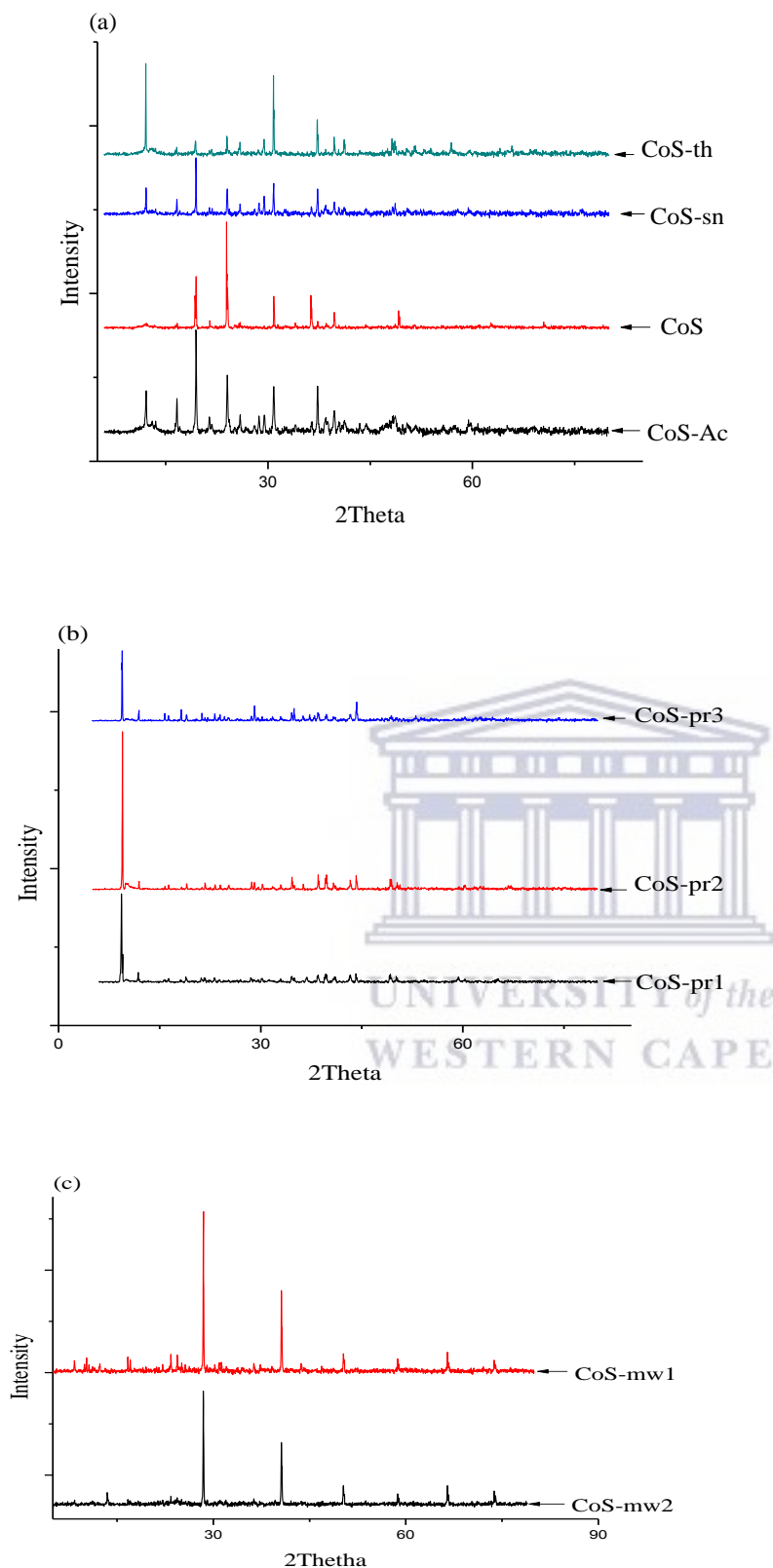


Figure 0.10: XRD spectra of cobalt succinates a) from $(\text{CH}_3\text{COO})_2\text{Co}\cdot 4\text{H}_2\text{O}$ and $\text{CoCl}_2\cdot 6\text{H}_2\text{O}$ at rt, using sonication and thermal reaction, b) using Parr reactor and c) using microwave.

4.7 Chapter summary

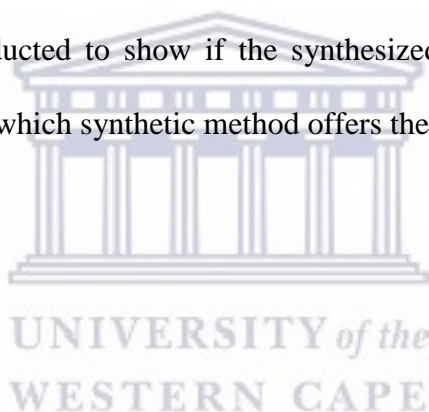
Structures of the cobalt succinates synthesized using various methods are interpreted from various techniques. FTIR spectroscopy indicates the presence of COO⁻ functional group along with Co-O, and H₂O molecule in the vibrations of CoS, CoS-sn, CoS-Ac, and CoS-th. The XRD data confirm the synthesized compounds to be cobalt succinates. Their TGA analysis indicated that the contents in coordinated water molecules are different depending on the synthetic methods used. These porous metal compounds showed a thermal stability to around 300 °C except CoS-sn which started decomposing at around 260 °C. The possible formula of CoS is Co(C₄H₄O₄)·(H₂O)₄, whereas the formula of CoS-sn and CoS-th is Co(C₄H₄O₄)·(H₂O)₃ and CoS-Ac is Co(C₄H₄O₄)·(H₂O). For the first time sonication was used to synthesize CoS-sn which was obtained in 45 min. Results from FTIR, XRD, TGA all identified CoS-th. CoS-Ac was synthesized for the first time from cobalt acetate tetrahydrate. The difference between the latter CoS-Ac and that synthesized from other cobalt succinates is the fact that the source of metal ion influences the coordination. These cobalt succinates including CoS-Ac are referred to as possessing a one dimension (1D) structure according to the literature [38]. The one dimension in these compounds might be caused by the synthesis at low temperature and the absence of pressure.

FTIR as well as TGA analysis also demonstrated the presence of functional groups viz., OH, COO⁻, and Co-O for CoS-pr that match with those in MIL-9 [Co₅(OH)₂(C₄H₄O₄)] which has a 3-D dimensional structure [36]. The pore structures were observed in these compounds using SEM techniques. The elemental composition from EDS confirmed the presence of Co, O, and C elements in these compounds. The effect of hexane in the preparation process showed an increase in the capacity to host guest molecules due to the pores accessibility as shown by TGA. They were decomposed at temperature around 300 °C in the range of MOFs

except CoS-pr2 which decomposed at 277 °C. The range of stability between 300 and 500 °C characterize them as having MOF structures [137].

The proposed structure of compounds CoS-mw1 and CoS-mw2 could be illustrated as $K_2Co_2(C_4H_4O_4)_2Cl_n$. The EDS analysis confirmed the presence of Co, C, O, K, and Cl elements. The absence of coordinated water molecules was also supported by TGA analysis. These compounds may have a polymeric structure [146].

The variation of synthetic methods led to the formation of different frameworks as revealed by characterization. They showed different weight loss as well as stability as demonstrated by TGA analysis due to the different synthetic methods. Therefore, TGA analysis provides the temperature range where the sample is stable and suitable for CO₂ adsorption [161]. The test for CO₂ adsorption was conducted to show if the synthesized cobalt succinates have any adsorption property and if so, which synthetic method offers the higher adsorption capacity.



CHAPTER 5: RESULTS AND DISCUSSION: NICKEL HYDROXY-TEREPHTHALATES

5.1 Introduction

Terephthalic acid (TPA) was used as the organic linker to synthesize these nickel compounds abbreviated as Nitp-1, Nitp-2 and Nitp-3. Nitp-1 was prepared using water as solvent while Nitp-2 and Nitp-3 were synthesized with the introduction of 1.8 ml and 3.6 ml of hexane, respectively, (Table 5.1). The following techniques: FTIR (Fourier Transform Infrared), UV-Vis (Ultraviolet and Visible), TGA (Thermal gravimetric analysis), SEM (Scanning electron microscopy), EDS (Energy dispersive X-ray spectroscopy) and XRD (X-ray diffraction) were used to characterize the synthesized compounds.

Table 0.1: Table of abbreviations of nickel terephthalates according to the synthetic conditions

Compound Code	Name and synthetic conditions
TPA	Terephthalic acid
Na ₂ tp	Disodium terephthalate
Nitp-1	Pr (water)
Nitp-2	Pr (water +1.8 ml hexane)
Nitp-3	Pr (water + 3.6 ml hexane)

Pr: Parr reactor

5.2 Fourier transform infrared (FTIR)

The FTIR spectroscopy indicates functional groups present in the products. Figure 5.1 displays the spectra of synthesized nickel terephthalates along with the free ligand (TPA).

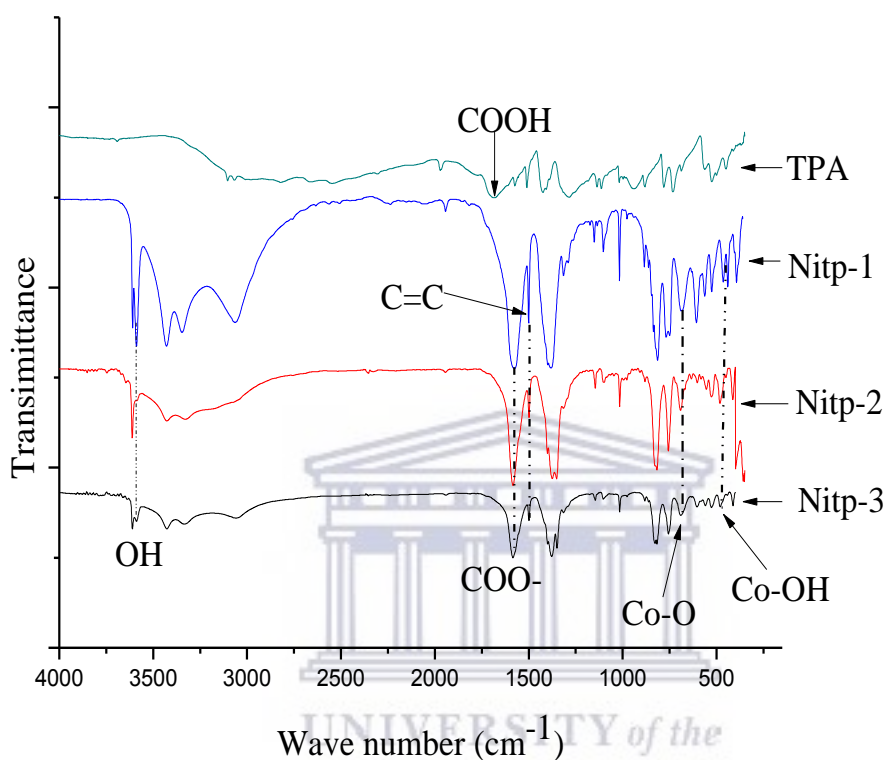


Figure 0.1: FTIR spectra of nickel hydroxy-terephthalates and TPA

Peaks at 3600, 3427, and 3345 cm^{-1} in all the synthesized compounds are assigned to the vibration of non-hydrogen bonded OH coordinated to Ni [40,147]. These peaks extend over a broad range between 3100 and 3700 cm^{-1} , attributed to the vibration of water molecules. The broader peaks observed for Nitp-2 and Nitp-3 could be caused by hexane acting as a template and occupying channels which could cause the bending of OH groups and in turn, OH groups could have weak interactions between themselves together with π bonding of the bridging ligand within the pores [49,97,165]. The weak vibration peak around 3060 cm^{-1} is assigned to an aromatic C-H stretching vibration [31]. The band at 1947 cm^{-1} is attributed to the out-of-

plane C-H vibration in the aromatic ring [163]. Peaks observed at 1700 and 1437 cm^{-1} in the free ligand (terephthalic acid) are shifted to 1573 and 1381 cm^{-1} for the synthesized compounds. The latter peaks correspond to asymmetric and symmetric COO group vibration, respectively [162]. This illustrates that the ligand is coordinated to the metal (nickel). The stretching vibration peak observed at 1500 cm^{-1} is due to the presence of C=C of the p-disubstituted aromatic ring. Peaks around 1108 and 1016 cm^{-1} were assigned to C-C bonds, and peaks 743, 679 and 606 cm^{-1} represent C-H deformation vibrations within the aromatic ring [164]. Bands at 570, 533, 470, 433, and 397 cm^{-1} were attributed to Ni-O bonding [151,167].

It was noted that the intensities of peaks in the FTIR spectra became weak as hexane was introduced in the starting mixture of the synthesized compounds. The effect of hydrophobicity was reported by Mukherje *et al.*, to tune the geometry of compounds [166] which can have an impact on the chemical bonds with possibility of distortion [167]. FTIR spectra of the synthesized compounds show similarities to $[\text{Ni}_3(\text{OH})_2(\text{C}_8\text{H}_4\text{O}_4)_2(\text{H}_2\text{O})_4] \cdot 2\text{H}_2\text{O}$ synthesized by Carton *et al.* [162] with slight changes.

5.3 Ultraviolet and visible (UV-VIS)

Figures 5.2a and b show the UV-Vis spectra of Nitp-1, Nitp-2, and Nitp-3 along with the parent starting material TPA. It is noteworthy that Nitp-1, Nitp-2, and Nitp-3 dissolved in a mixture of water and ethanol whereas TPA dissolved in DMF due to its insolubility in the same mixture mentioned above.

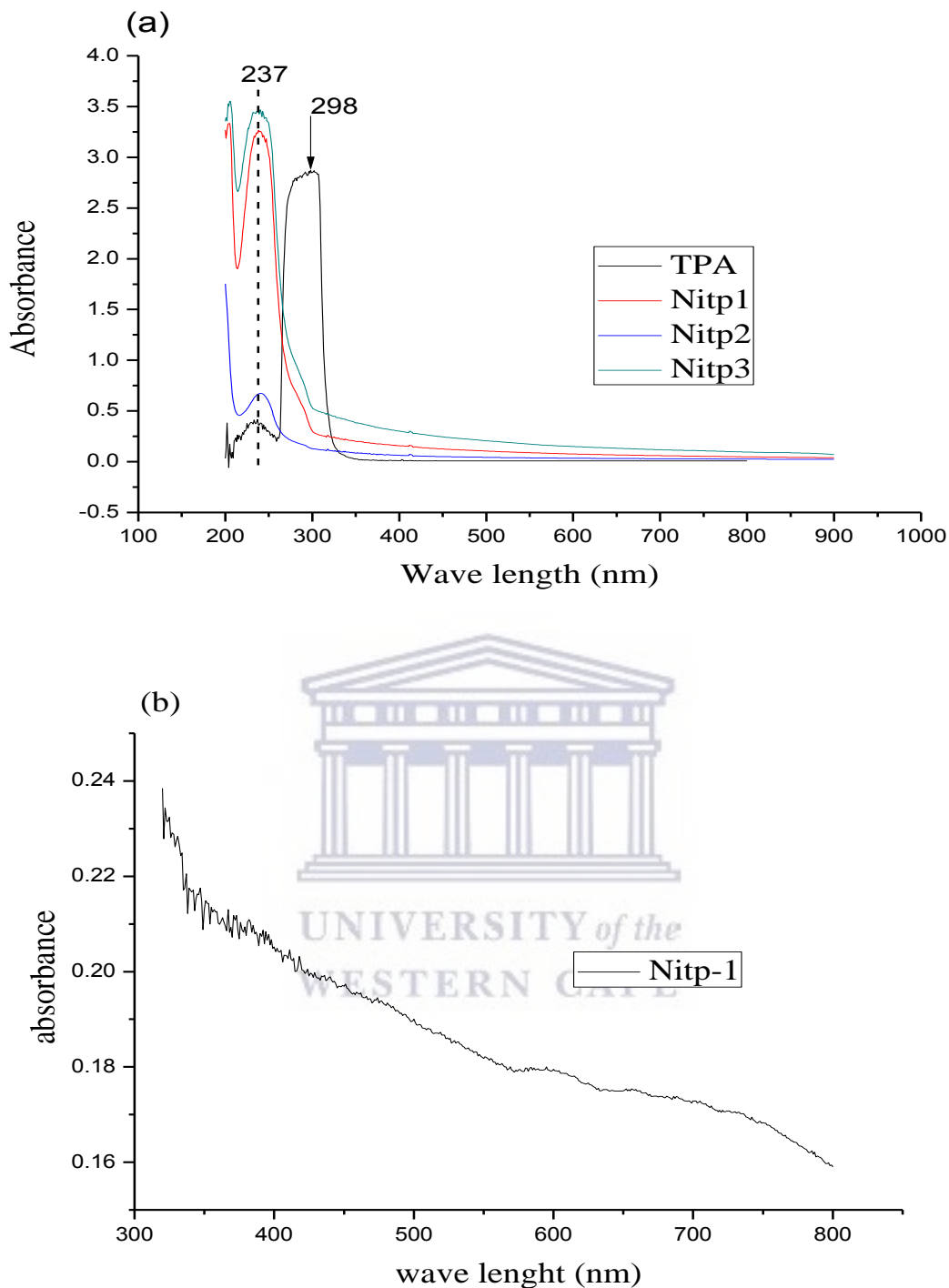


Figure 0.2: UV-Vis spectra of a) nickel hydroxy-terephthalates synthesized along with parent compound TPA, b) Peaks of NiTPA-1 between 300 and 800 nm wavelengths.

From the UV-Vis spectra it is observed that the absorption peak at 298 nm in free terephthalic acid (TPA) was shifted to 237 nm in all the synthesized compounds. The peak at 237 nm is assigned to intra-ligand charge transfer [144]. The peaks at around 597 and 710 nm

(Figure 5.2b) correspond to ${}^3T_{2g} \leftarrow {}^3A_{2g}$ and ${}^3T_{1g}(F) \leftarrow {}^3A_{2g}(F)$ electronic transitions respectively from the fundamental state to the excited state, where nickel ions are in the octahedral coordination state [155,170].

5.4 Thermal gravimetric analysis (TGA)

The results of TGA analysis for Ni-terephthalates are illustrated in the Figure 5.3 and Table 5.2.

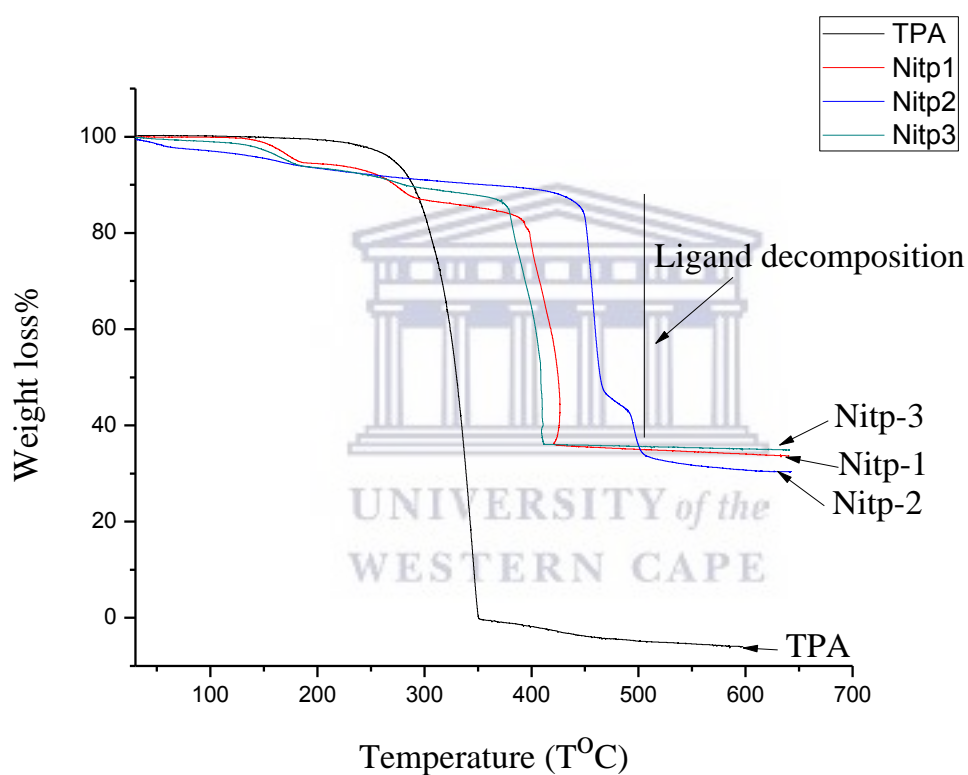


Figure 0.3: TGA of nickel hydroxy-terephthalates.

Table 0.2: TGA results of nickel hydroxy-terephthalates

Compounds	Temperature range (°C)	Weight loss (%)	Group lost
Nitp-1	30 - 183	5.5	H ₂ O (coordinated and solvated)+ ethanol
	218 - 293	20.5	Unreacted ligand
	373 - 424	49.3	Ligand decomposition
Nitp-2	30 - 180	6	H ₂ O + ethanol + hexane
	180 - 420	5.4	Unreacted ligand
	420 - 524	56	Ligand decomposition
Nitp-3	30 - 180	6	H ₂ O + ethanol + hexane
	180 - 365	8	unreacted ligand
	365 - 410	51.5	Ligand decomposition

Figure 5.3 and Table 5.2 show the weight loss of Nitp-1, Nitp-2, and Nitp-3. The TGA patterns for these compounds show similar steps as in nickel hydroxy-terephthalate reported [162]. The TGA results of Nitp-1 showed a weight loss of 5.5% at 183 °C which corresponds to the removal of water and ethanol [147,157]. The weight loss of 20.5% between 218 and 293 °C could be attributed to removal of coordinated water, occluded ligand and other guest molecules. Similar weight loss of unreacted ligand was observed in Ni(BDC)(1,10-phen)(H₂O)·0.5H₂BDC (H₂BDC: benzene dicarboxylic acid and bipy: 2,2'-bipyridine) where H₂BDC is removed as guest molecule at temperature more than 210 °C [154]. Nitp-2 and Nitp-3 showed 6% weight loss between 30 and 180 °C. This weight loss corresponds to removal of water, ethanol, and hexane molecules. From 180 to 420 °C Nitp-2 lost 5.4% while, Nitp-3 showed a weight loss of 8% from 180 to 365 °C which could be attributed to the removal of the occluded ligand and the remaining water, ethanol, and hexane molecules [154]. It is noted that the weight loss in Nitp-1 differs from that of Nitp-2 and Nitp-3. This difference may be attributed to the amount of hexane introduced into the reaction mixture in

Nitp-2 and Nitp-3 synthesis by removing the free ligand in the channels of the framework to increase the pores accessibility. A similar effect was reported for $[\text{Co}_2(\text{ndc})_2(\text{bi-pyren})]\cdot\text{C}_6\text{H}_6\cdot\text{H}_2\text{O}$ by Choi *et al.*, [35], where benzene increased the capacity of the host-guest gases in the compound. Moreover, the results from TGA show that use of hexane contributed to the formation of Nitp-2 and Nitp-3 with very little unreacted ligand remaining in the framework. FTIR data (Figure 5.1) supported the effect of the presence of hexane by reduction in the sharpness of the peak for the OH group compared to Nitp-1.

It was noted that Nitp-1 collapses between 373 and 424 °C with 49.3% weight loss while Nitp-2 collapses between 420 and 524 °C with weight loss of 56% and Nitp-3 decomposes between 365 and 410 °C with weight of 51.5%. These weight losses correspond to complete combustion of the ligand [153] and formation of nickel oxide NiO [162]. The percentages of the resulting NiO correspond to 36 for Nitp-1, 32.5 for Nitp-2, and 36 to Nitp-3. It was noticed that Nitp-2 is more stable while Nitp-3 is less stable among these three compounds.

5.5 Scanning electron microscopy spectroscopy (SEM) and energy dispersive X-ray spectroscopy (EDS)

The technique of scanning electron microscopy (SEM) was used to investigate the surface morphology and shape of nickel terephthalates (Figures 5.4a, b, and c). Figure 5.4a represents Nitp-1 synthesized without the use of hexane and Figures 5.4b and c represents Nitp-2 and Nitp-3 synthesized with the introduction of hexane (1.8 ml and 3.6 ml respectively). The presence of the elements in the products was identified using energy dispersive X-ray spectroscopy (EDS). The SEM images show diamond like shapes of Nitp-1, Nitp-2, and Nitp-3. The surface morphology of the compounds showed a slight change which can be attributed to the effect of hexane. The EDS results, Figure 5.5a-c are representative of an average of 5 spots.

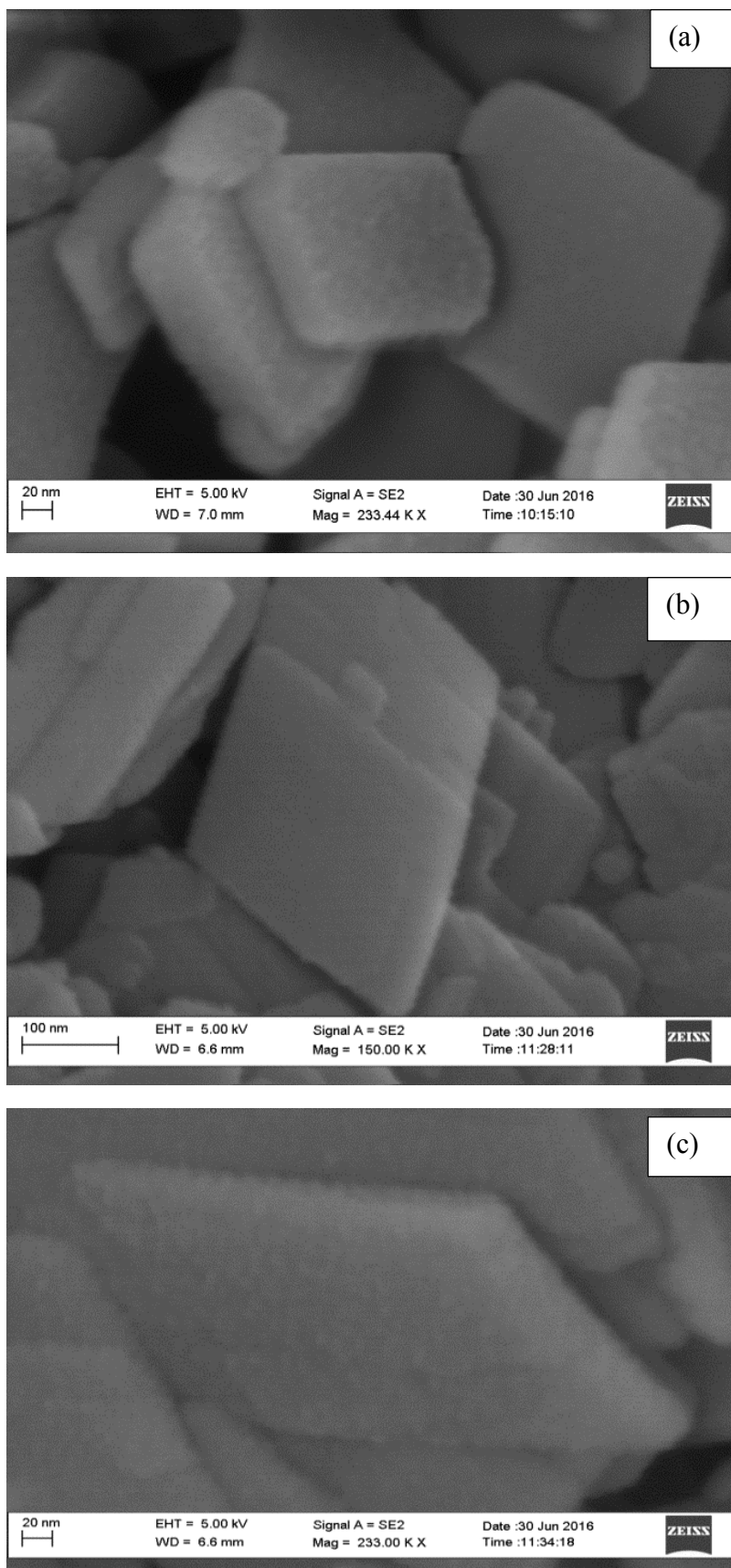


Figure 0.4: SEM images of nickel hydroxy-terephthalates synthesized a) Nitp-1, b) (Nitp-2, and c) Nitp-3.

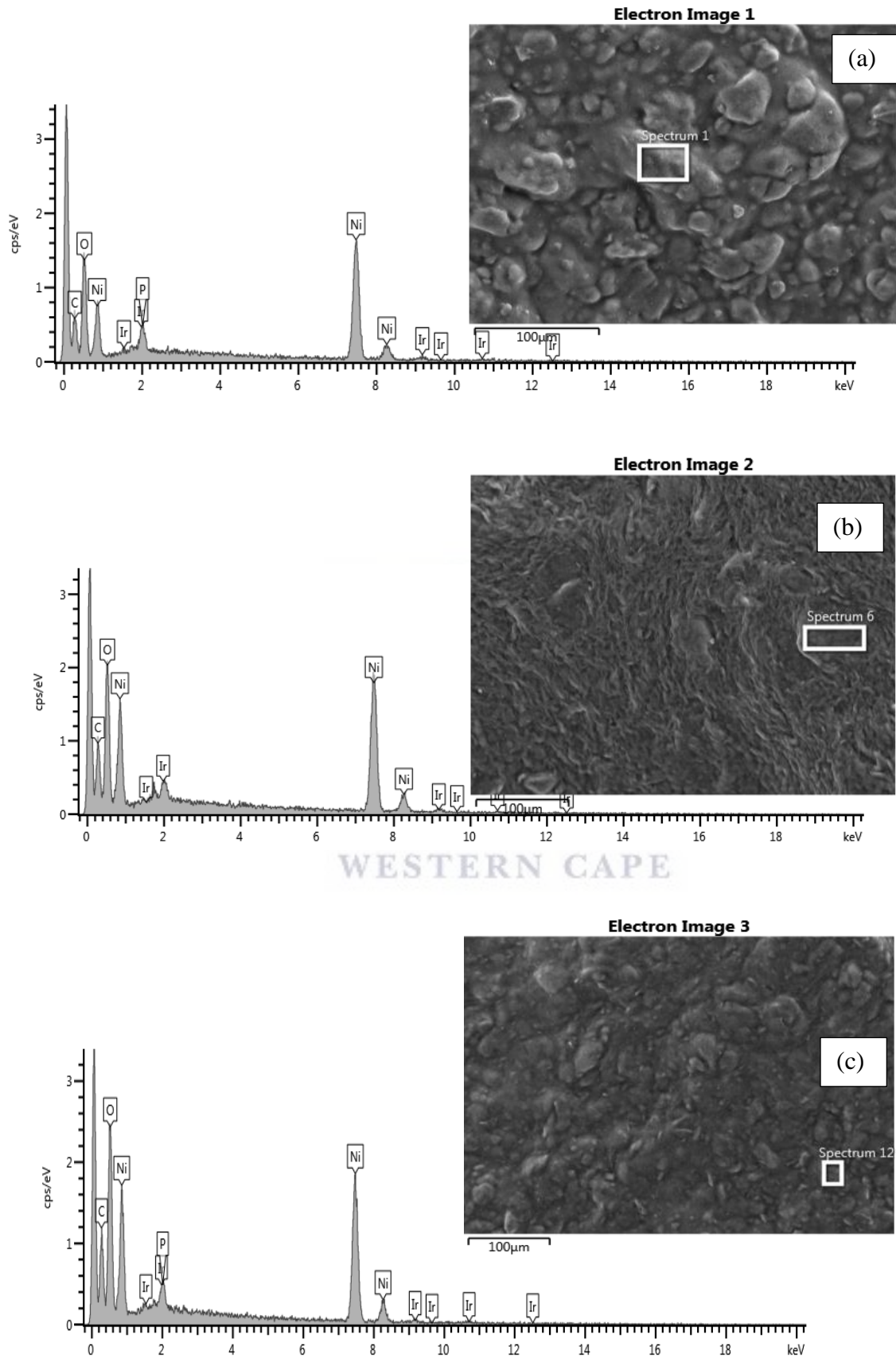


Figure 0.5: EDS spectra of nickel hydroxy-terephthalates a) Nitp-1, b) Nitp-2 and c) Nitp-3.

Table 0.3: The elemental composition of Nitp-1, Nitp-2, and Nitp-3 from EDS analysis

Element	Nitp-1 Atomic %	Nitp-2 Atomic %	Nitp-3 Atomic %
C	50.906	51.598	51.112
O	32.728	34.742	37.56
Ni	16.366	13.66	11.326
Total	100	100	100

Figure 5.5a, b, and c show the EDS spectra of the detected elements for the synthesized compounds. The observed elements Ni, C, O, Ir, and P in the spectra were detected from both compounds and coating materials. The chemical composition of Ni, C, and O originated from the synthesized compounds. However, Ir and P elements originated from coating materials. The percentages of these elements for the compounds are shown in Table 5.3. The results presented are an average of five spots from each compound. The very minor percentage from Ir and P coating materials were subtracted for calculation purposes. From the above results, it can be concluded that the synthesized products have similar structures.

5.6 X-ray diffraction analysis (XRD)

The Figure 5.6 illustrates the XRD diffractograms used to analyze the formed phases in Nitp-1, Nitp-2, and Nitp-3 compounds.

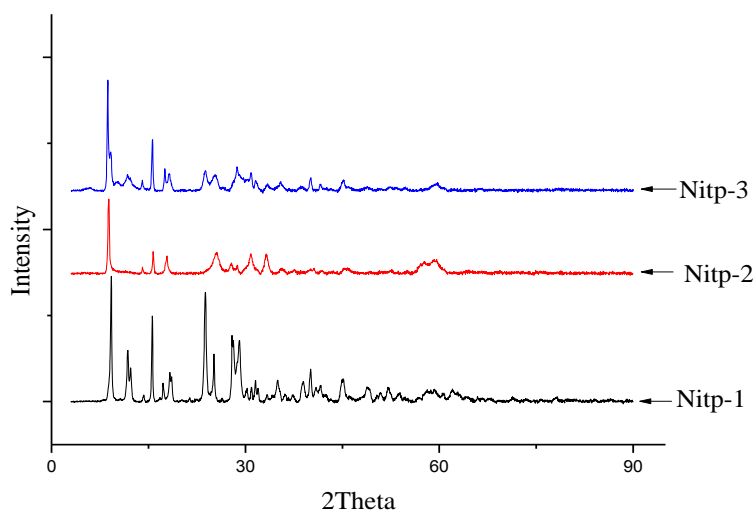


Figure 0.6: XRD diffractograms of nickel hydroxy-terephthalates.

Figure 5.6 showed that the XRD diffraction patterns for the synthesized Nitp-1 are in good agreement with reported XRD data for $[\text{Ni}_3(\text{OH})_2(\text{tp})_2(\text{H}_2\text{O})_4] \cdot 2\text{H}_2\text{O}$ [162]. The presence of the main peaks at $2\theta = 9^\circ$, 12° , 15.6° , 18° , and around 25° confirm the synthesis of these Nickel hydroxy-terephthalates. However, Nitp-2 and Nitp-3 showed some anomalies. Only the peak at 9° is clearly identifiable while the peak at 12° disappeared. The intensity of the peak at 15.6° has been reduced but is also different in both Nitp-2 and Nitp-3. The remaining peaks in Nitp-1 tend also to disappear in both Nitp-2 and Nitp-3. The noted difference in XRD pattern for the synthesized compounds could be due to the changes in the pore structures or to inherent difference in compounds [35]. The presence of some peaks in Nitp-1 might be due to the free carboxylic acid and other guest molecules in the pores which could result in some additional peaks with different intensity [35]. The presence of occluded free carboxylic acid and other guest molecules was supported by TGA and FTIR results. The synthesized Nitp-1, Nitp-2, and Nitp-3 are crystalline materials.

5.7 Chapter summary

The results from FTIR identify the functional groups viz., OH, COO-, aromatic CH-, and aromatic C=C were identified. The UV-Vis absorption bands show intra-ligand charge transfer in these three compounds. The EDS data proved that all compounds contain Ni, C, and O. The SEM analysis showed a slight change in surface morphology of these compounds. According to TGA results, the weight loss of water, ethanol, hexane, and unreacted ligand was lower for Nitp-2 and Nitp-3 than that for Nitp-1. The difference in the hosted-guest molecules in these compounds could be attributed to the effect of hexane during their syntheses. Similarly, Benzene was used as a template in the synthesis of $[\text{Co}_2(\text{ndc})_2(\text{bipyen})] \cdot \text{C}_6\text{H}_6 \cdot \text{H}_2\text{O}$ from $[\text{Co}_3(\text{ndc})_3(\text{bipyen})_{1.5}] \cdot \text{H}_2\text{O}$ where the resulting different weight losses at different temperatures were noted [35]. Moreover, modification of the solvent composition can lead to two different MOFs [35]. The XRD patterns of Nitp-2 and Nitp-3 are different and clearly different from that of Nitp-1. These different peaks could be attributed to the differences in the structure of the synthesized compounds and the amount of guest molecules viz., solvate water molecules, hexane and unreacted ligand [35,137]. The synthesized nickel hydroxy-terephthalates are thus thought to possess three different crystalline structures or forms which can provide potential for CO₂ adsorption [161].

CHAPTER 6: CARBON DIOXIDE (CO₂) ADSORPTION

6.1 Introduction

This chapter reports on the CO₂ adsorption study of cobalt succinates and nickel terephthalates using TGA. The trend of CO₂ adsorption capacity on cobalt succinates and nickel hydroxy-terephthalates synthesized via different methods is presented. The effect of hexane was considered in studying the adsorption capacity. Experimental conditions for CO₂ adsorption for all the cobalt succinates and the nickel hydroxy-terephthalates are presented in Table 6.1. The adsorption-desorption recycling process was also carried out for three cycles a representative of the abilities of all compounds in order to investigate the effectiveness of regeneration and recycling of the adsorbents. The adsorption capacity for CO₂ is compared to the reported ones to evaluate whether any of these adsorbents have potential.

Table 0.1: Experimental condition for CO₂ adsorption

Step	Purge gas	Temperature (°C)	Period (min)	Gas flow (ml/min)	Pressure (bar)
1	Nitrogen	33 to 120	11		
2	Nitrogen	120 (isothermal)	60	50	4.8
3	Nitrogen	120 to 33	11		
4	CO ₂	33 (isothermal)	30	10	1.3
5	Nitrogen	33 to 120	11	50	4.8

The adsorption capacity was calculated according to the equations 1 and 2:

$$\text{CO}_2 \text{ adsorption capacity in mg/g} = \frac{W_e(\text{mg}) - W_i(\text{mg})}{W_i(\text{g})} \quad \text{or} \quad \frac{W_{\text{after}} - W_{\text{before}}}{W_{\text{before}}} \quad (1)$$

$$\text{CO}_2 \text{ adsorption capacity in mmol/g} = \frac{W_e(\text{mg}) - W_i(\text{mg})}{W_i(\text{g}) M_{\text{mCO}_2}} \quad (2)$$

Where W_e and W_i are the amounts of adsorbent before and after adsorption respectively, and M_m is the molar weight (g/mol) of the CO₂ molecule.

6.2 Adsorption capacity of CO₂ for the cobalt succinates

Figures 6.1a and b show the CO₂ adsorption processes on the cobalt succinate compounds. The thermogram displays the results from 130 min. The compounds CoS-mw1 was not tested for CO₂ because it is the same as CoS-mw2 as shown by the different characterization techniques. Table 6.2 displays the summary of the adsorption capacity found for these compounds.

Table 0.2: Adsorption capacity of CO₂ in cobalt succinates

N ^o	Compounds	CO ₂ adsorption capacity (mg/g)	CO ₂ adsorption capacity (mmol/g)
1	CoS-Ac	1.8	0.041
2	CoS	3.16	0.072
3	CoS-sn	2.99	0.068
4	CoS-th	2.5	0.057
5	CoS-pr1	2.24	0.045
6	CoS-pr2	2.58	0.061
7	CoS-pr3	1.9	0.051
8	CoS-mw2	3.26	0.074

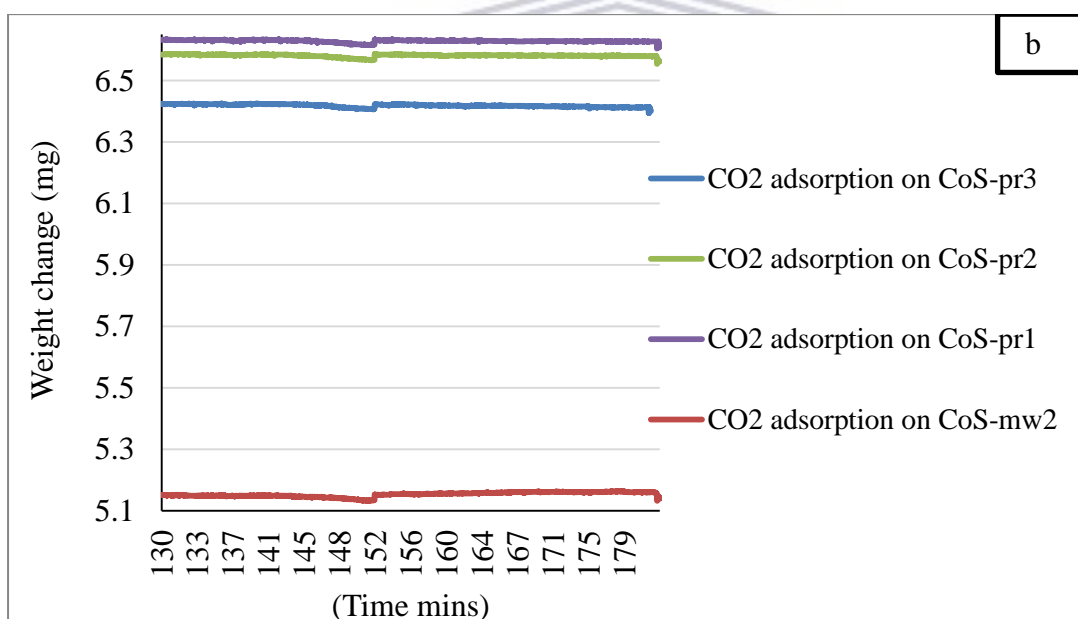
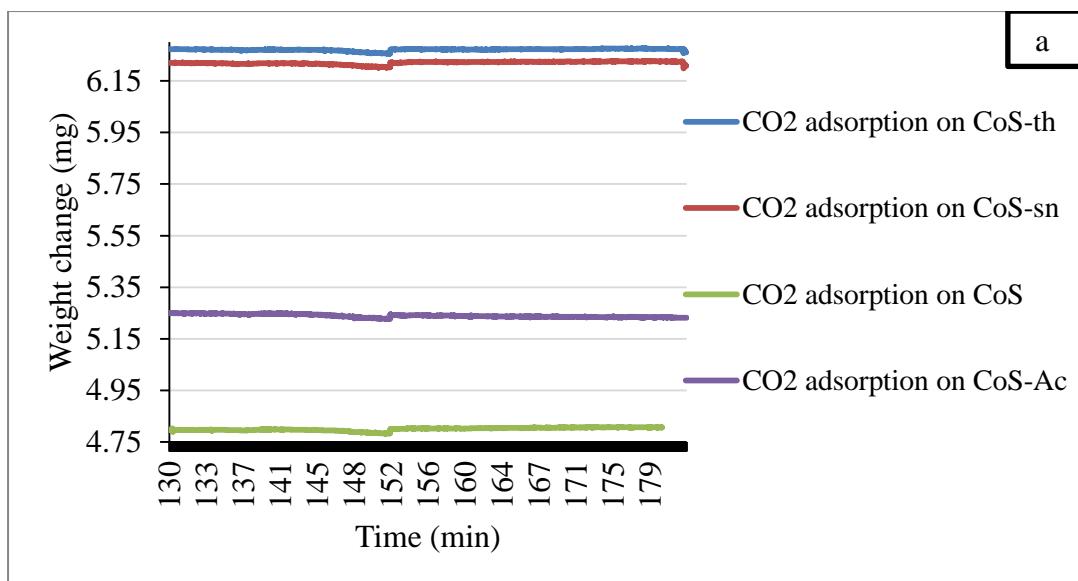


Figure 0.1: CO₂ Adsorption of cobalt succinates at 33 °C a) at rt, sonication, and thermal reaction and b): by Parr reactor and microwave.

Figures 6.1 (a) shows that the cobalt succinates viz. CoS, CoS-Ac, CoS-sn, and CoS-th adsorbed CO₂ at different extents. Table 6.2 shows the higher adsorption capacity of 0.074 mmol/g CO₂/g achieved by CoS-mw2 compared to CoS, CoS-Ac, CoS-sn, and CoS-th. The

difference in adsorption capacity could be due to the differences in the structures of these complexes [169].

Figure 6.1 (b) presents CoS-mw2 with adsorption capacity of 0.074 mmol of CO₂/g (Table 6.2). In the library of cobalt succinates synthesized autogenously, CoS-pr1 showed a lower adsorption capacity than CoS-pr2 and CoS-pr3 (Table 6.2). Compound CoS-pr2 has the highest adsorption capacity among these three and could be associated with the role of hexane used in the autogenous synthesis of these cobalt succinates. However, the adsorption capacity for CoS-pr3 was less than that for CoS-pr2 while the volume of hexane used in its synthesis was double that of the synthesis of CoS-pr2. Therefore, this effect could be associated with the volume ratio of hexane used in the synthesis. The adsorption capacity for CoS-pr2 which is considered to have a 3D structure was less than that for CoS considered to have a 1D structure. However, the 3D structure was supposed to contribute to the higher adsorption capacity due to the pores with channels [17].

The adsorption of CO₂ in these materials was sharp and quick and was followed by a quick desorption by the high flow rate of nitrogen (50 ml/min). Furthermore, CO₂ could interact with available adsorption sites of cobalt succinates without involving the sorption in pores or the channels. In light of the easy sorption of CO₂ in these cobalt succinates, it could be concluded that these are weak adsorbents.

6.3 Adsorption capacity of CO₂ for the nickel hydroxyl-terephthalates

Figure 6.3 shows the adsorption capacity of CO₂ for Nitp-1, Nitp-2, and Nitp-3 compounds. Nitp-1 was synthesized with only water as a solvent while Nitp-2 and Nitp-3 were synthesized with the introduction of hexane. Table 6.3 displays adsorption capacity from these compounds.

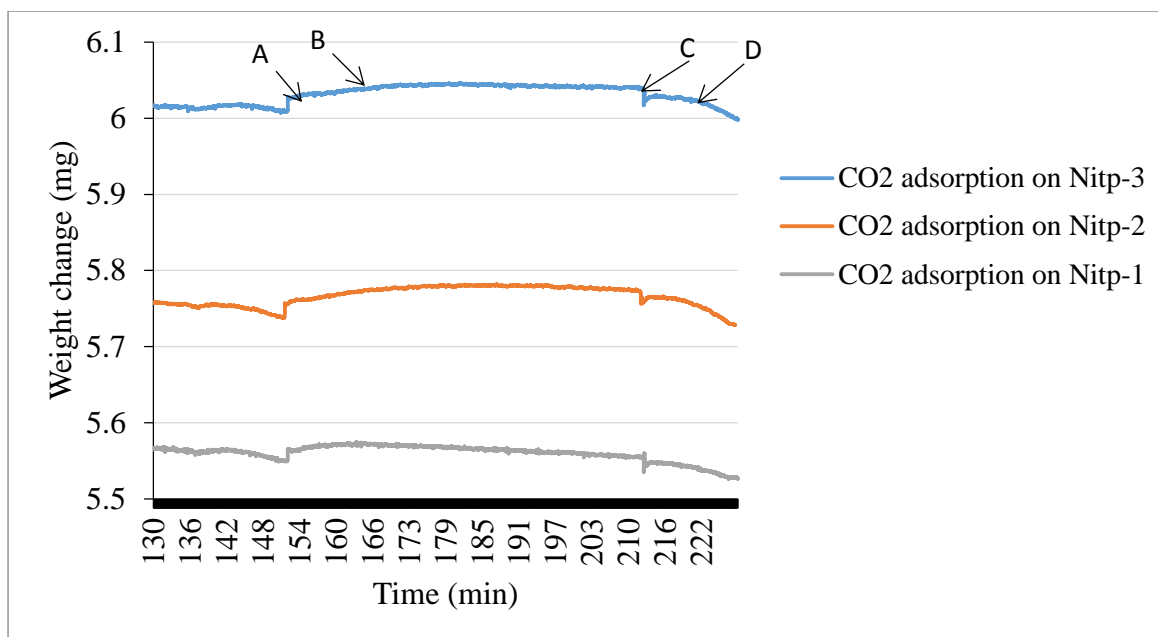


Figure 0.2: Adsorption process of CO₂ at 33 °C for nickel hydroxy-terephthalates.

Table 0.3: Adsorption capacity of CO₂ for nickel hydroxy-terephthalates

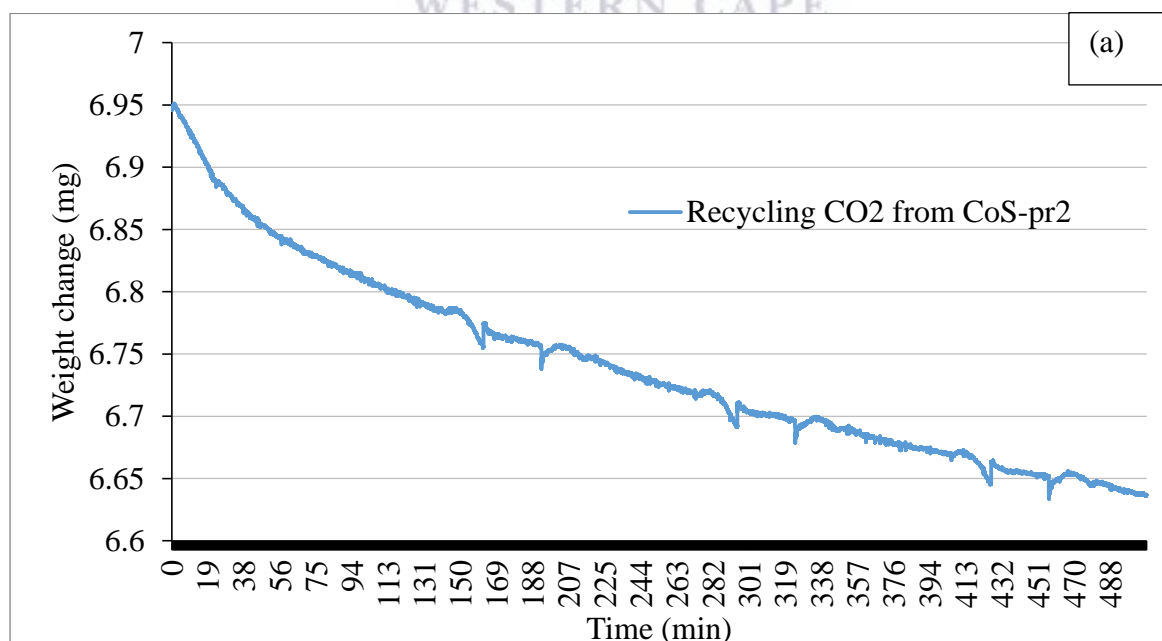
Compounds	CO ₂ adsorption capacity (mg/g)	CO ₂ adsorption capacity (mmol/g)
Nitp-1	3.4	0.08
Nitp-2	7.5	0.16
Nitp-3	4.8	0.12

Figure 6.2 shows that the behaviour of the CO₂ adsorption process was similar in all three prepared nickel hydroxy-terephthalates. At the start of flushing the sample with CO₂ there was a steep CO₂ adsorption (step A) which could correspond to CO₂ adsorption onto Nitp [109,172]. Step B continue with adsorption which was not steep leading to the equilibrium adsorption of CO₂. After complete adsorption, a sharp desorption of CO₂ started on switching the gas to N₂ while heating-up (step C) to complete the desorption of CO₂ at higher temperature (Step D).

Table 6.3 shows the adsorption capacity of nickel terephthalates. The measurements showed that the highest adsorption capacity was 0.16 mmol of CO₂/g for Nitp-2. The adsorption capacity was increased in nickel terephthalates synthesized with the introduction of hexane which clearly indicates the role of the introduction of hexane to increase adsorption capacity of CO₂ in the synthesis of Nickel hydroxy-terephthalates. However, the adsorption capacity in Nitp-3 (using a greater volume of hexane) was lower than that for Nitp-2. It has been shown that that the solvent system can result in MOFs with different sorption characteristic by providing open pores [35].

6.4 Recycling CO₂ from adsorbent

The test of the operational stability of adsorbent was investigated using CoS-pr2 and Nitp-2 as representative materials. The recycling process (CO₂ adsorption-desorption) was studied for three cycles (Figure 6.3a and b) demonstrated that the adsorbent can be reused many times for the adsorption-desorption process.



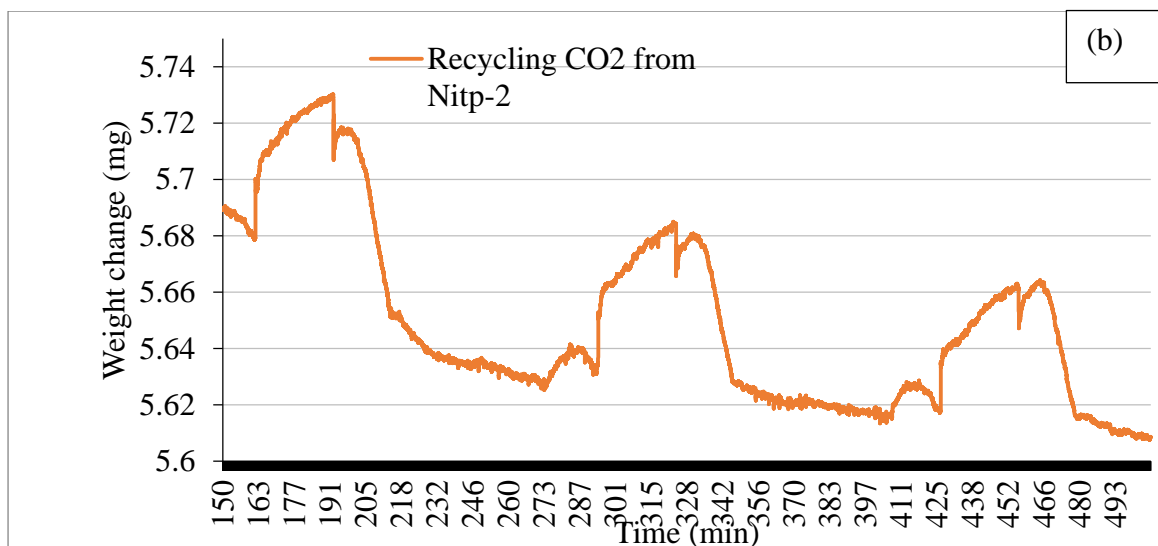


Figure 0.3: cyclic adsorption-desorption of CO₂ a by CoS-pr2 and b) Nitp-2.

Figure 6.3 (a) shows the cyclical adsorption-desorption measurement for CO₂ observed by CoS-pr2. It shows CoS-pr2 can adsorb and desorb the gas. This explains the stability of the adsorbent to perform adsorption and desorption during long-term cyclical operation.

Figure 6.3 (b) shows the cyclical adsorption-desorption process for Nitp-2. Due to the time limitation, only three adsorption cycles are presented here. The first cycle showed that the adsorption is less than the desorption cycle. This could be due to the limited time used for the first desorption. However, the two next cycles showed complete adsorption-desorption process similar to what observed in MOF-5 [84]. The higher desorption capacity than adsorption capacity for the first cycle could be associated with the removal of both CO₂ and other occluded molecules. The observed decrease of adsorbed CO₂ from the cycle to cycle could be due to the short time used to degas the sample as compared to literature where it took 12 h to degas [30]. Thus, the first desorption process should require longer times for the complete desorption of occluded molecules before CO₂ adsorption. Furthermore, the advanced activation process such as supercritical carbon dioxide (SCD) could be used for the complete removal of occluded molecules [33].

6.5 Summary of the chapter

The adsorption of CO₂ was observed for both the synthesized cobalt succinates and nickel hydroxy-terephthalates. CoS-mw2 showed a higher adsorption capacity of 0.074 mmol of CO₂/g among the synthesized cobalt succinates. The higher CO₂ adsorption uptake for CoS-mw2 is in agreement with the other compounds synthesized by microwave [30,85]. Also the cobalt succinates synthesized using Parr reactor viz. CoS-pr1, CoS-pr2, and CoS-p3 showed a relatively lower adsorption capacity. Among these, CoS-pr2 however, showed a higher adsorption capacity of 0.061 mmol of CO₂/g.

The highest adsorption capacity for nickel hydroxy-terephthalates viz. Nitp-1, Nitp-2, and Nitp-3 was 0.16 mmol of CO₂/g for Nitp-2. The trend for adsorption capacity in Nitp-1, Nitp-2, and Nitp-3 correlates with the one for CoS-pr1, CoS-pr2, and CoS-pr3 which illustrates the role played by the use of hexane to increase adsorption capacity. The adsorption capacity for the synthesized nickel hydroxy-terephthalates was higher than that for cobalt succinates which could be attributed to factors viz., the kind of metal cluster and ligand used for synthesis [138]. Particularly, the terephthalate linker could provide the pores accessible by CO₂ that could not be found in succinates linker [171]. Furthermore, the aromatic ring of the terephthalate linker would provide the intermolecular interactions with CO₂ bonding which could enhance the adsorption capacity [171].

All synthesized cobalt succinates showed low adsorption capacity for CO₂ (Figure 6.1a and b) compared to that observed for Co₂(ad)₂(CO₂CH₃)₂·2DMF·0.5H₂O (bio-MOF-11) with 4.1 mmol/g at 25 °C and 1 bar [172]. The low CO₂ adsorption capacity in similar Co-3D complexes could be attributed to non-accessible pores [173] and incomplete removal of the guest molecules from its framework [174]. Another reason could be due to the nature of the ligand of the framework [52,93,173]. The synthesized nickel hydroxy-terephthalates showed lower adsorption capacity (Figure 6.2 and Table 6.3) than other reported MOFs, it is still

lower than 1 mmol of CO₂/g at 303 K and 1 bar observed for Sc₂(O₂CC₆H₄CO₂)₃ [171]. The difference could be attributed to the nature of the metal centre in MOFs [138]. The low adsorption capacity for CO₂ in the synthesized nickel hydroxy-terephthalates could also be due to the vacuum activation method which might not offer enough pore accessibility.

The cyclical adsorption-desorption process in CoS-pr2 and Nitp-2 showed that the cobalt succinates and nickel hydroxyl-terephthalates can be regenerated after CO₂ adsorption. There was a clear cyclical adsorption-desorption for Nitp-2. The cyclic adsorption for CoS-pr2 was not stable because it showed a continuous desorption even during CO₂ adsorption stage.



CHAPTER 7: CONCLUSION AND RECOMMENDATIONS

7.1 Conclusion

In this study, porous cobalt succinates and porous nickel hydroxy-terephthalates designed for carbon capture were successfully synthesized using different synthetic routes and methodologies. Use of cobalt acetate as metal source was used to prepare new cobalt succinates (CoS-Ac) for the first time at room temperature. Sonication was used to synthesize the compound (CoS-sn). The short reaction time of the latter could be attributed to the fast and high cavitation energy and pressure created to allow fast nucleation [106]. Different synthetic methods were adopted, namely thermal, reflux, autogenous pressure in a Parr reactor, using different solvent mixtures and ratios and different metal sources in order to prepare different structural compounds despite using the same starting materials. Thermal or reflux and autogenous pressure in a Parr reactor produced CoS-th and CoS-pr respectively. Microwave was also used to prepare CoS-mw. The proposed structure for CoS-mw was $K_2Co_2(C_4H_4O_4)_2Cl_n$ (n: numeric number of counter chloride anions).

Use of hexane during synthesis was interrogated to see whether its presence could have influence on the formation of new phases as characterized. The weight loss from TGA i.e CoS-pr1 synthesized without hexane was lower (1.9%) than, CoS-pr2 which synthesized with 1.25 ml of hexane (3.6 %), and CoS-pr3 which were synthesized with 2.5 ml of hexane (4%). These can show that the adsorption capacity in these compounds could be different. Furthermore, XRD analysis showed changes in their spectra.

Similarly, nickel hydroxy-terephthalates viz. Nitp-1, Nitp-2, and Nitp-3 were synthesized in a solvent system containing hexane in different ratios. According to XRD, TGA, and FTIR results, Nitp-1, Nitp-2, and Nitp-3 are different compounds. Nitp-1 showed a higher content of unreacted ligand and was different from Nitp-2 and Nitp-3. The synthesis of the purer

nickel hydroxy-terephthalates was attributed to the effect of hexane. All these compounds are crystalline with thermal stability between 365 - 420 °C in the same range of many MOFs suitable for gas adsorption application. Nitp-1 is thermally more stable than Nitp-3 while Nitp-2 has the highest stability at 420 °C among these three compounds.

All synthesized compounds showed potential gas adsorption property to different extents. The lower adsorption capacity among cobalt succinates was observed for CoS-Ac with a value of 0.04 mmol of CO₂/g. The best one was 0.074 mmol of CO₂/g for CoS-mw2. Use of hexane cobalt succinates showed increased adsorption capacity in CoS-pr2. However, the adsorption capacity for cobalt succinates was far lower compared to 4.1 mmol/g at 25 °C and 1 bar for Co₂(ad)₂(CO₂CH₃)₂·2DMF·0.5H₂O [172]. The higher adsorption capacity in the synthesized nickel hydroxy-terephthalates was 0.16 mmol of CO₂/g for Nitp-2. The adsorption capacity for CO₂ in hydroxy-terephthalates was also relatively low compared to the ones reported for MOFs such as Sc₂(O₂CC₆H₄CO₂)₃ [171].

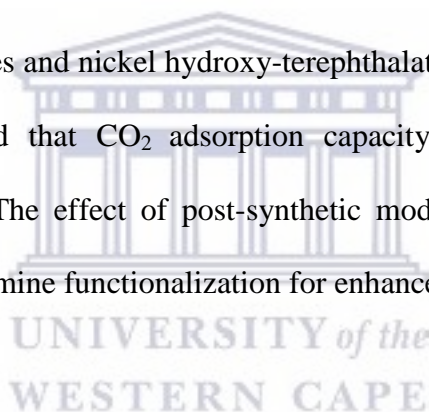
Both cobalt succinates and nickel hydroxy-terephthalates showed a successful regeneration after CO₂ adsorption. Nickel terephthalates were more potent than cobalt succinates. However, the adsorption capacity of cobalt succinates is lower than that of nickel terephthalates.

Despite several studies reported on cobalt succinates and nickel terephthalates, no study has been carried out on CO₂ sorption properties on these materials.

Hexane was used as solvent for the first time in the synthesis of the title compounds to investigate the effect of hexane on synthesized MOF structures, which might affect CO₂ adsorption capacity. From the results obtained it was observed that hexane play a role in the synthesis of MOFs.

7.2 Recommendations and future work

Different synthetic methods should be adopted for the synthesis of cobalt succinates based on cobalt acetate as a metal source. Also, variation of the synthetic parameters is needed to establish the optimal condition for the synthetic process. The synthesis by sonication was done only at 30 °C. Syntheses at different temperature should be evaluated. Microwave heating to synthesize cobalt succinates was to 150 °C for one hour. However, the effect of reaction time and temperature using the microwave method should be fully investigated. Use of hexane in the compounds synthesized in this work influences the CO₂ adsorption capacity which can also be applied for the synthesis of other metal-organic complexes. The supercritical carbon dioxide activation method as well the measurement of surface area and pores for both cobalt succinates and nickel hydroxy-terephthalates should be done to improve CO₂ uptake. We recommend that CO₂ adsorption capacity can be tested at different temperatures and pressures. The effect of post-synthetic modification in nickel hydroxy-terephthalates by ethylene-diamine functionalization for enhancement of CO₂ adsorption must be investigated.



REFERENCES

- [1] R. K. Pachauri, M. R. Allen, V. R. Barros, J. Broome, W. Cramer, and R. Christ, *Climate Change 2014 Synthesis Report*. 2014.
- [2] T. L. Chew, A. L. Ahmad, and S. Bhatia, "Ordered mesoporous silica (OMS) as an adsorbent and membrane for separation of carbon dioxide (CO₂)," *Adv. Colloid Interface Sci.*, vol. 153, no. 1–2, pp. 43–57, 2010.
- [3] A. D. Owen, "Renewable energy: Externality costs as market barriers," *Energy Policy*, vol. 34, no. 5, pp. 632–642, 2006.
- [4] K. Menyah and Y. Wolde-Rufael, "Energy consumption, pollutant emissions and economic growth in South Africa," *Energy Econ.*, vol. 32, no. 6, pp. 1374–1382, 2010.
- [5] J. G. J. Olivier, G. Janssens-Maenhout, M. Muntean, and J. A. H. W. Peters, "Trends in global CO₂ emissions. 2016 Report," *PBL Netherlands Environ. Assess. Agency; Ispra*, no. 2315, pp. 1–82, 2016.
- [6] S. Rahmstorf, "Projecting Future Sea-Level Rise," no. January, pp. 368–370, 2007.
- [7] C. H. Yu, C. H. Huang, and C. S. Tan, "A review of CO₂ capture by absorption and adsorption," *Aerosol Air Qual. Res.*, vol. 12, no. 5, pp. 745–769, 2012.
- [8] D. Camper, J. E. Bara, D. L. Gin, and R. D. Noble, "Room-temperature ionic liquid-amine solutions: Tunable solvents for efficient and reversible capture of CO₂," *Ind. Eng. Chem. Res.*, vol. 47, no. 21, pp. 8496–8498, 2008.
- [9] D. Britt, H. Furukawa, B. Wang, T. G. Glover, and O. M. Yaghi, "Highly efficient separation of carbon dioxide by a metal-organic framework replete with open metal sites," *Proc. Natl. Acad. Sci. U. S. A.*, vol. 106, no. 49, pp. 20637–20640, 2009.
- [10] M. R. M. Abu-Zahra, L. H. J. Schneiders, J. P. M. Niederer, P. H. M. Feron, and G. F. Versteeg, "CO₂ capture from power plants. Part I. A parametric study of the technical performance based on monoethanolamine," *Int. J. Greenh. Gas Control*, vol. 1, no. 1, pp. 37–46, 2007.
- [11] E. Blomen, C. Hendriks, and F. Neele, "Capture technologies: Improvements and promising developments," *Energy Procedia*, vol. 1, no. 1, pp. 1505–1512, 2009.
- [12] Z. Zhao, Z. Li, and Y. S. Lin, "Adsorption and diffusion of carbon dioxide on metal-organic framework (MOF-5)," *Ind. Eng. Chem. Res.*, vol. 48, no. 22, pp. 10015–10020, 2009.
- [13] T. C. Merkel, H. Lin, X. Wei, and R. Baker, "Power plant post-combustion carbon dioxide capture: An opportunity for membranes," *J. Memb. Sci.*, vol. 359, no. 1–2, pp. 126–139, 2010.
- [14] S. R. Venna and M. A. Carreon, "Highly permeable zeolite imidazolate framework-8 membranes for CO₂/CH₄ separation," *J. Am. Chem. Soc.*, vol. 132, no. 1, pp. 76–78, 2010.
- [15] R. V. Siriwardane, M. S. Shen, E. P. Fisher, and J. Losch, "Adsorption of CO₂ on zeolites at moderate temperatures," *Energy and Fuels*, vol. 19, no. 3, pp. 1153–1159, 2005.

References

- [16] P. Aprea, D. Caputo, N. Gargiulo, F. Iucolano, and F. Pepe, "Modeling carbon dioxide adsorption on microporous substrates: Comparison between Cu-BTC metal-organic framework and 13X zeolitic molecular sieve," *J. Chem. Eng. Data*, vol. 55, no. 9, pp. 3655–3661, 2010.
- [17] N. L. Rosi, J. An, and S. J. Geib, "High and Selective CO₂ Uptake in a Cobalt Adeninate Metal-Organic Framework Exhibiting Pyrimidine- and Amino-Decorated Pores," *J. Am. Chem. Soc.*, vol. 132, no. 1, pp. 38–39, 2010.
- [18] Y.-B. Zhang, H. Furukawa, N. Ko, W. Nie, H. J. Park, S. Okajima, K. E. Cordova, H. Deng, J. Kim, and O. M. Yaghi, "Introduction of Functionality, Selection of Topology, and Enhancement of Gas Adsorption in Multivariate Metal–Organic Framework-177," *J. Am. Chem. Soc.*, vol. 147, no. 7, pp. 2641–2650, 2015.
- [19] J. D. Figueroa, T. Fout, S. Plasynski, H. McIlvried, and R. D. Srivastava, "Advances in CO₂ capture technology-The U.S. Department of Energy's Carbon Sequestration Program," *Int. J. Greenh. Gas Control*, vol. 2, no. 1, pp. 9–20, 2008.
- [20] M. E. Boot-Handford, J. C. Abanades, E. J. Anthony, M. J. Blunt, S. Brandani, N. Mac Dowell, J. R. Fernández, M.-C. M.-C. Ferrari, R. Gross, J. P. Hallett, R. S. Haszeldine, P. Heptonstall, A. Lyngfelt, Z. Makuch, E. Mangano, R. T. J. Porter, M. Pourkashanian, G. T. Rochelle, N. Shah, J. G. Yao, and P. S. Fennell, "Carbon capture and storage update," *Energy Environ. Sci.*, vol. 7, no. 1, p. 130, 2014.
- [21] A. MacKenzie, D. L. Granatstein, E. J. Anthony, and J. C. Abanades, "Economics of CO₂ Capture Using the Calcium Cycle with a Pressurized Fluidized Bed Combustor," *Energy & Fuels*, vol. 21, no. 2, pp. 920–926, 2007.
- [22] J. Kittel, R. Idem, D. Gelowitz, P. Tontiwachwuthikul, G. Parrain, and A. Bonneau, "Corrosion in MEA units for CO₂ capture: Pilot plant studies," *Energy Procedia*, vol. 1, no. 1, pp. 791–797, 2009.
- [23] Y. C. Park, S.-H. Jo, C. K. Ryu, and C.-K. Yi, "Long-term operation of carbon dioxide capture system from a real coal-fired flue gas using dry regenerable potassium-based sorbents," *Energy Procedia*, vol. 1, no. 1, pp. 1235–1239, 2009.
- [24] R. Banerjee, H. Furukawa, D. Britt, C. Knobler, M. O'Keeffe, and O. M. Yaghi, "Control of pore size and functionality in isorecticular zeolitic imidazolate frameworks and their carbon dioxide selective capture properties," *J. Am. Chem. Soc.*, vol. 131, no. 11, pp. 3875–3877, 2009.
- [25] G.-P. Hao, W.-C. Li, D. Qian, G.-H. Wang, W.-P. Zhang, T. Zhang, A.-Q. Wang, F. Schüth, H.-J. Bongard, and A.-H. Lu, "Structurally Designed Synthesis of Mechanically Stable Poly(benzoxazine-co-resol)-Based Porous Carbon Monoliths and Their Application as High-Performance CO₂ Capture Sorbents," *J. Am. Chem. Soc.*, vol. 133, no. 29, pp. 11378–11388, 2011.
- [26] J. Nakhla, "Metal Organic Frameworks (MOFs)," *Sigmaaldrich.Com*, vol. 9, no. 2, pp. 9–10, 2012.
- [27] K. Osman, C. Coquelet, and D. Ramjugernat, "Review of carbon dioxide capture and storage with relevance to the South African power sector," *S. Afr. J. Sci.*, vol. 110, no. 5, pp. 1–12, 2014.
- [28] J. Ren, H. W. Langmi, B. C. North, M. Mathe, and D. Bessarabov, "Modulated

References

- synthesis of zirconium-metal organic framework (Zr-MOF) for hydrogen storage applications,” *Int. J. Hydrogen Energy*, vol. 39, no. 2, pp. 890–895, 2014.
- [29] K. Davies, S. a Bourne, and C. L. Oliver, “Solvent- and Vapor-Mediated Solid-State Transformations in 1,3,5- Benzenetricarboxylate Metal – Organic Frameworks,” *Cryst. Growth Des.*, vol. 12, pp. 1999–2003, 2012.
- [30] R. Sabouni, H. Kazemian, and S. Rohani, “Microwave Synthesis of the CPM-5 Metal Organic Framework,” *Chem. Eng. Technol.*, vol. 35, no. 6, pp. 1085–1092, 2012.
- [31] E. Biemmi, T. Bein, and N. Stock, “Synthesis and characterization of a new metal organic framework structure with a 2D porous system: (H₂NEt₂)₂[Zn₃(BDC)₄]-3DEF,” *Solid State Sci.*, vol. 8, no. 3–4, pp. 363–370, 2006.
- [32] H. L. Jiang, D. Feng, T. F. Liu, J. R. Li, and H. C. Zhou, “Pore surface engineering with controlled loadings of functional groups via click chemistry in highly stable metal-organic frameworks,” *J. Am. Chem. Soc.*, vol. 134, no. 36, pp. 14690–14693, 2012.
- [33] O. K. Farha, I. Eryazici, N. C. Jeong, B. G. Hauser, C. E. Wilmer, A. a. Sarjeant, R. Q. Snurr, S. T. Nguyen, a. Ö. Yazaydin, and J. T. Hupp, “Metal-organic framework materials with ultrahigh surface areas: Is the sky the limit?,” *J. Am. Chem. Soc.*, vol. 134, no. 36, pp. 15016–15021, 2012.
- [34] E. Biemmi, S. Christian, N. Stock, and T. Bein, “High-throughput screening of synthesis parameters in the formation of the metal-organic frameworks MOF-5 and HKUST-1,” *Microporous Mesoporous Mater.*, vol. 117, no. 1–2, pp. 111–117, 2009.
- [35] E. Y. Choi, K. Park, C. M. Yang, H. Kim, J. H. Son, S. W. Lee, Y. H. Lee, D. Min, and Y. U. Kwon, “Benzene-templated hydrothermal synthesis of metal-organic frameworks with selective sorption properties,” *Chem. - A Eur. J.*, vol. 10, no. 21, pp. 5535–5540, 2004.
- [36] C. Livage, C. Egger, and M. Nogues, “Hybrid open frameworks (MIL-n). Part 5† Synthesis and crystal structure of MIL-9: a new three-dimensional ferrimagnetic cobalt(II) carboxylate with a two-dimensional array of edge-sharing Co octahedra with 12-membered rings,” *J. Mater. Chem.*, vol. 8, no. 12, pp. 2743–2747, 1998.
- [37] C. Livage, Egger, T. A. Chem, I. Ed, and G. C. R. A. S. Paris, “Hydrothermal versus Nonhydrothermal Synthesis for the Preparation of Organic - Inorganic Solids : The Example of Cobalt (II) Succinate,” *Chem. Mater.*, vol. 13, no. 2, pp. 410–414, 2001.
- [38] P. M. Forster, A. R. Burbank, C. Livage, G. Férey, and A. K. Cheetham, “The role of temperature in the synthesis of hybrid inorganic-organic materials: the example of cobalt succinates,” *Chem. Commun. (Camb)*, vol. 5, no. 4, pp. 368–369, 2004.
- [39] Z. Zhang, S. Xian, Q. Xia, H. Wang, and Z. L. Li, “Enhancement of CO₂ Adsorption and CO₂/N₂ Selectivity on ZIF-8 via Postsynthetic Modification,” *IFAC Proc. Vol.*, vol. 59, no. 6, pp. 405–410, 2009.
- [40] J. Klinowski, F. A. Almeida Paz, P. Silva, and J. Rocha, “Microwave-Assisted Synthesis of Metal–Organic Frameworks,” *Dalt. Trans.*, vol. 40, no. 2, pp. 321–330, 2011.
- [41] R. Heede, “Tracing anthropogenic carbon dioxide and methane emissions to fossil fuel

References

- and cement producers, 1854-2010,” *Clim. Change*, vol. 122, no. 1–2, pp. 229–241, 2014.
- [42] Y. Tan, E. Croiset, M. A. Douglas, and K. V. Thambimuthu, “Combustion characteristics of coal in a mixture of oxygen and recycled flue gas,” *Fuel*, vol. 85, no. 4, pp. 507–512, 2006.
- [43] M. J. B. Kioko, “Who stole the rain? The case of recent severe droughts in Kenya,” *Eur. Sci. J.*, vol. 9, no. 5, pp. 29–40, 2013.
- [44] A. B. Rao and E. S. Rubin, “A Technical, Economic, and Environmental Assessment of Amine-Based CO₂ Capture Technology for Power Plant Greenhouse Gas Control,” *Environ. Sci. Technol.*, vol. 36, no. 20, pp. 4467–4475, 2002.
- [45] C. Serre, S. Bourrelly, A. Vimont, N. A. Ramsahye, G. Maurin, P. L. Llewellyn, M. Daturi, Y. Filinchuk, O. Leynaud, P. Barnes, and G. Férey, “An explanation for the very large breathing effect of a metal-organic framework during CO₂ adsorption,” *Adv. Mater.*, vol. 19, no. 17, pp. 2246–2251, 2007.
- [46] S. Himeno, T. Tomita, K. Suzuki, and S. Yoshida, “Characterization and selectivity for methane and carbon dioxide adsorption on the all-silica DD3R zeolite,” *Microporous Mesoporous Mater.*, vol. 98, no. 1–3, pp. 62–69, 2007.
- [47] M. S. Jassim, G. T. Rochelle, M. S. Jassim, and G. T. Rochelle, “Innovative Absorber / Stripper Configurations for CO Capture by Aqueous Monoethanolamine Innovative Absorber / Stripper Configurations for CO₂ Capture by Aqueous Monoethanolamine,” *Ind. Eng. Chem. Res.*, vol. 45, no. 8, pp. 2465–2472, 2006.
- [48] H. R. Abid, J. Shang, H.-M. Ang, and S. Wang, “Amino-functionalized Zr-MOF nanoparticles for adsorption of CO₂ and CH₄,” *Int. J. Smart Nano Mater.*, vol. 4, no. 1, pp. 72–82, 2013.
- [49] C. H. Yu, C. H. Huang, and C. S. Tan, “A review of CO₂ capture by absorption and adsorption,” *Aerosol Air Qual. Res.*, vol. 12, no. 5, pp. 745–769, 2012.
- [50] J. Merel, M. Clause, and F. Meunier, “Experimental investigation on CO₂ post-combustion capture by indirect thermal swing adsorption using 13X and 5A zeolites,” *Ind. Eng. Chem. Res.*, vol. 47, no. 1, pp. 209–215, 2008.
- [51] A. Torrisi, R. G. Bell, and C. Mellot-Draznieks, “Functionalized MOFs for enhanced CO₂ capture,” *Cryst. Growth Des.*, vol. 10, no. 7, pp. 2839–2841, 2010.
- [52] B. Arstad, H. Fjellvåg, K. O. Kongshaug, O. Swang, and R. Blom, “Amine functionalised metal organic frameworks (MOFs) as adsorbents for carbon dioxide,” *Adsorption*, vol. 14, no. 6, pp. 755–762, 2008.
- [53] D. V. Quang, N. El Hadri, and M. R. M. Abu-zahra, “Reduction in the regeneration energy of CO₂ capture process by impregnating amine solvent onto precipitated silica,” *Esj*, vol. 9, no. 30, pp. 82–102, 2013.
- [54] Z.-Z. Yang, Y.-N. Zhao, and L.-N. He, “CO₂ chemistry: task-specific ionic liquids for CO₂ capture/activation and subsequent conversion,” *Rsc Adv.*, vol. 1, no. 4, pp. 545–567, 2011.
- [55] B. E. Gurkan, J. C. de la Fuente, E. M. Mindrup, L. E. Ficke, B. F. Goodrich, E. A. Price, W. F. Schneider, and J. F. Brennecke, “Equimolar CO₂ absorption by

References

- Functionalized Ionic Liquids,” *J. Am. Chem. Soc.*, vol. 132, no. 7, pp. 2116–2117, 2010.
- [56] C. W. Jones, “CO₂ Capture from Dilute Gases as a Component of Modern Global Carbon Management,” *Annu. Rev. Chem. Biomol. Eng.*, vol. 2, no. 1, pp. 31–52, 2011.
- [57] N. A. Ramsahye, G. Maurin, S. Bourrelly, P. L. Llewellyn, T. Devic, C. Serre, T. Loiseau, and G. Ferey, “Adsorption of CO₂ in metal organic frameworks of different metal centres: Grand Canonical Monte Carlo simulations compared to experiments,” *Adsorption*, vol. 13, no. 5–6, pp. 461–467, 2007.
- [58] J. Thompson, N. Brunelli, R. P. Lively, J. R. Johnson, C. W. Jones, and S. Nair, “Tunable CO₂ Adsorbents by Mixed-Linker Synthesis and Postsynthetic Modification of Zeolitic Imidazolate Frameworks,” *J. Phys. Chem. C*, vol. 117, pp. 8198–8207, 2013.
- [59] K. Kusakabe, T. Kuroda, A. Murata, and S. Morooka, “Formation of a Y-Type Zeolite Membrane on a Porous α -Alumina Tube for Gas Separation,” *Ind. Eng. Chem. Res.*, vol. 36, no. 3, pp. 649–655, 1997.
- [60] B. Zornoza, C. Tellez, J. Coronas, J. Gascon, and F. Kapteijn, “Metal organic framework based mixed matrix membranes: An increasingly important field of research with a large application potential,” *Microporous Mesoporous Mater.*, vol. 166, pp. 67–78, 2013.
- [61] J. Kim, L. Lin, J. a Swisher, M. Haranczyk, B. Smit, and J. Swisher, “Predicting Large CO Adsorption in Aluminosilicate Zeolites for Post-combustion Carbon Dioxide Capture Predicting Large CO₂ Adsorption in Aluminosilicate Zeolites for Post-combustion Carbon Dioxide Capture,” *J. Am. Chem. Soc.*, vol. 134, pp. 18940–18943, 2012.
- [62] M. Zaarour, B. Dong, I. Naydenova, R. Retoux, and S. Mintova, “Progress in zeolite synthesis promotes advanced applications,” *Microporous Mesoporous Mater.*, vol. 189, pp. 11–21, 2014.
- [63] K. S. Park and others, “Exceptional chemical and thermal stability of zeolitic imidazolate frameworks,” *Proc. Natl. Acad. Sci. USA*, vol. 103, p. 10186, 2006.
- [64] F. Su and C. Lu, “CO₂ capture from gas stream by zeolite 13X using a dual-column temperature/vacuum swing adsorption,” *Energy Environ. Sci.*, vol. 5, no. 10, p. 9021, 2012.
- [65] F. Brandani and D. M. Ruthven, “The Effect of Water on the Adsorption of CO₂ and C₃H₈ on Type X Zeolites,” *Ind. Eng. Chem. Res. engineering*, vol. 43, no. 26, pp. 8339–8344, 2004.
- [66] G. Li, P. Xiao, P. Webley, J. Zhang, R. Singh, and M. Marshall, “Capture of CO₂ from high humidity flue gas by vacuum swing adsorption with zeolite 13X,” *Adsorption*, vol. 14, no. 2–3, pp. 415–422, 2008.
- [67] L. Hauchhum and P. Mahanta, “Carbon dioxide adsorption on zeolites and activated carbon by pressure swing adsorption in a fixed bed,” *Int. J. Energy Environ. Eng.*, vol. 5, no. 4, pp. 349–356, 2014.
- [68] C. Janiak and J. K. Vieth, “MOFs, MILs and more: concepts, properties and

References

- applications for porous coordination networks (PCNs),” *New J. Chem.*, vol. 34, no. 11, p. 2366, 2010.
- [69] Z. Xiang, Z. Hu, W. Yang, and D. Cao, “Lithium doping on metal-organic frameworks for enhancing H₂ Storage,” *Int. J. Hydrogen Energy*, vol. 37, no. 1, pp. 946–950, 2012.
- [70] Y. Wu, G. Xu, W. Liu, J. Yang, F. Wei, L. Li, W. Zhang, and Q. Hu, “Postsynthetic modification of copper terephthalate metal-organic frameworks and their new application in preparation of samples containing heavy metal ions,” *Microporous Mesoporous Mater.*, vol. 210, pp. 110–115, 2015.
- [71] Y. K. Hwang, D. Y. Hong, J. S. Chang, S. H. Jung, Y. K. Seo, J. Kim, A. Vimont, M. Daturi, C. Serre, and G. Férey, “Amine grafting on coordinatively unsaturated metal centers of MOFs: Consequences for catalysis and metal encapsulation,” *Angew. Chemie - Int. Ed.*, vol. 47, no. 22, pp. 4144–4148, 2008.
- [72] Z. Chen, S. Xiang, H. D. Arman, J. U. Mondal, P. Li, D. Zhao, and B. Chen, “Three-Dimensional Pillar-Layered Copper(II) Metal-Organic Framework with Immobilized Functional OH Groups on Pore Surfaces for Highly Selective CO₂/CH₄ and C₂H₂/CH₄ Gas Sorption at Room Temperature,” *Inorg. Chem.*, vol. 50, pp. 3442–3446, 2011.
- [73] Y. Wang, B. Bredenkötter, B. Rieger, and D. Volkmer, “Two-dimensional metal-organic frameworks (MOFs) constructed from heterotrimeric coordination units and 4,4'-biphenyldicarboxylate ligands,” *Dalt. Trans.*, no. 6, pp. 689–696, 2007.
- [74] M. Eddaoudi, J. Kim, N. Rosi, D. Vodak, J. Wachter, M. O’Keeffe, and O. M. Yaghi, “Systematic design of pore size and functionality in isoreticular MOFs and their application in methane storage,” *Science*, vol. 295, no. 5554, pp. 469–472, 2002.
- [75] C. Wu, A. Hu, L. Zhang, and W. Lin, “Communication A Homochiral Porous Metal – Organic Framework for Highly Enantioselective Heterogeneous Asymmetric Catalysis A Homochiral Porous Metal-Organic Framework for Highly Enantioselective,” *J. Am. Chem. Soc.*, vol. 127, no. 25, pp. 8940–8941, 2005.
- [76] G. Mehlana, G. Ramon, and S. A. Bourne, “A 4-fold interpenetrated diamondoid metal-organic framework with large channels exhibiting solvent sorption properties and high iodine capture,” *Microporous Mesoporous Mater.*, vol. 231, pp. 21–30, 2016.
- [77] N. L. Rosi, J. Kim, M. Eddaoudi, B. Chen, M. O. Keffe, and O. M. Yaghi, “Article Rod Packings and Metal – Organic Frameworks Constructed from Rod-Shaped Secondary Building Units Rod Packings and Metal - Organic Frameworks Constructed from Rod-Shaped Secondary Building Units,” *Am. Chem. Soc.*, vol. 127, no. 5, pp. 1504–1518, 2005.
- [78] H. Li, M. Eddaoudi, T. L. Groy, and O. M. Yaghi, “Establishing microporosity in open metal-organic frameworks: Gas sorption isotherms for Zn (BDC)(BDC= 1, 4-benzenedicarboxylate),” *J. Am. Chem. Soc.*, vol. 120, no. 9, pp. 8571–8572, 1998.
- [79] S. Biswas, D. E. P. Vanpoucke, T. Verstraelen, M. Vandichel, S. Couck, K. Leus, Y. Liu, M. Waroquier, V. Van Speybroeck, J. F. M. Denayer, and P. Van Der Voort, “New Functionalized Metal – Organic Frameworks MIL-47 - X (X = - Cl), Adsorption Properties,” *Inorg. Chem.*, vol. 53, no. 1, pp. 113–120, 2013.
- [80] O. M. Yaghi, H. L. Li, C. Davis, D. Richardson, and T. L. Groy, “Synthetic strategies,

References

- structure patterns, and emerging properties in the chemistry of modular porous solids,” *Acc. Chem. Res.*, vol. 31, pp. 474–484, 1998.
- [81] S. Demir, G. K. Kantar, Y. Topcu, and Q. Li, “Solvothermal synthesis and characterization of coordination polymers of cobalt(II) and zinc(II) with succinic acid,” *Transit. Met. Chem.*, vol. 37, no. 3, pp. 257–263, 2012.
- [82] J. Fan, H. Zhu, T. Okamura, W. Sun, W. Tang, and N. Ueyama, “Novel One-Dimensional Tubelike and Two-Dimensional Polycatenated Metal – Organic Frameworks,” *Inorg. Chem.*, vol. 42, no. 1, pp. 1999–2003, 2003.
- [83] O. R. Evans and W. Lin, “Pillared, 3D metal-organic frameworks with rectangular channels. Synthesis and characterization of coordination polymers based on tricadmium carboxylates,” *Inorg. Chem.*, vol. 39, no. 10, pp. 2189–2198, 2000.
- [84] C. M. Lu, J. Liu, K. Xiao, and A. T. Harris, “Microwave enhanced synthesis of MOF-5 and its CO₂ capture ability at moderate temperatures across multiple capture and release cycles,” *Chem. Eng. J.*, vol. 156, no. 2, pp. 465–470, 2010.
- [85] A. P. Nelson, O. K. Farha, K. L. Mulfort, and J. T. Hupp, “Supercritical Processing as a Route to High Internal Surface Areas and Permanent Microporosity in Metal # Organic Framework Materials Supercritical Processing as a Route to High Internal Surface Areas and Permanent Microporosity in Metal-Organic Framework,” *Communication*, vol. 131, no. 2, pp. 458–460, 2009.
- [86] O. K. Farha and J. T. Hupp, “Rational Design, Synthesis, Purification, and Activation of Metal-Organic Framework Materials,” *Am. Chem. Soc.*, vol. 43, no. 8, pp. 1166–1175, 2010.
- [87] F. Ke, L. G. Qiu, Y. P. Yuan, F. M. Peng, X. Jiang, A. J. Xie, Y. H. Shen, and J. F. Zhu, “Thiol-functionalization of metal-organic framework by a facile coordination-based postsynthetic strategy and enhanced removal of Hg²⁺ from water,” *J. Hazard. Mater.*, vol. 196, pp. 36–43, 2011.
- [88] D. N. Dybtsev, H. Chun, and K. Kim, “Rigid and flexible: A highly porous metal-organic framework with unusual guest-dependent dynamic behavior,” *Angew. Chem. Int. Ed.*, vol. 43, pp. 5033–5036, 2004.
- [89] H. Li, M. Eddaoudi, M. O’Keeffe, and O. M. Yaghi, “Design and synthesis of an exceptionally stable and highly porous metal-organic framework,” *Nature*, vol. 402, no. 6759, pp. 276–279, 1999.
- [90] D. N. Dybtsev, H. Chun, and K. Kim, “Rigid and Flexible: A Highly Porous Metal–Organic Framework with Unusual Guest-Dependent Dynamic Behavior,” *Angew. Chemie*, vol. 116, no. 38, pp. 5143–5146, 2004.
- [91] Y. Liu, S. Couck, M. Vandichel, M. Grzywa, K. Leus, S. Biswas, D. Volkmer, J. Gascon, F. Kapteijn, J. F. M. Denayer, M. Waroquier, V. Van Speybroeck, and P. Van Der Voort, “New VIV-Based Metal – Organic Framework Having Framework Flexibility and High CO₂ Adsorption Capacity,” *Inorg. Chem.*, vol. 52, no. 1, pp. 113–120, 2013.
- [92] Y. Liu, S. Couck, M. Vandichel, M. Grzywa, K. Leus, S. Biswas, D. Volkmer, J. Gascon, F. Kapteijn, J. F. M. Denayer, M. Waroquier, V. Van Speybroeck, and P. Van Der Voort, “New VIV-Based Metal – Organic Framework Having Framework

References

- Flexibility and High CO₂ Adsorption Capacity,” *Am. Chem. Soc.*, vol. 52, pp. 113–120, 2013.
- [93] J. An, S. J. Geib, and N. L. Rosi, “High and Selective CO₂ Uptake in a Cobalt Adeninate Metal-Organic Framework Exhibiting Pyrimidine- and Amino-Decorated Pores,” *J. Am. Chem. Soc.*, vol. 132, no. 1, pp. 38–39, 2010.
- [94] J. R. Li, Y. Ma, M. C. McCarthy, J. Sculley, J. Yu, H. K. Jeong, P. B. Balbuena, and H. C. Zhou, “Carbon dioxide capture-related gas adsorption and separation in metal-organic frameworks,” *Coord. Chem. Rev.*, vol. 255, no. 15–16, pp. 1791–1823, 2011.
- [95] N. Stock and S. Biswas, “Synthesis of Metal-Organic Frameworks (MOFs): Routes to Various MOF Topologies, Morphologies, and Composites,” *Am. Chem. Soc.*, vol. 112, pp. 933–969, 2012.
- [96] O. M. Yaghi, C. E. Davis, G. Li, and H. Li, “Selective guest binding by tailored channels in a 3-D porous zinc(II)-benzenetricarboxylate network,” *J. Am. Chem. Soc.*, vol. 119, no. 12, pp. 2861–2868, 1997.
- [97] M. C. Bernini, N. Snejko, E. Gutierrez-Puebla, E. V. Brusau, G. E. Narda, and M. Á. Monge, “Structure-directing and template roles of aromatic molecules in the self-assembly formation process of 3D holmium-succinate MOFs,” *Inorg. Chem.*, vol. 50, no. 13, pp. 5958–5968, 2011.
- [98] J. Fizovic, M. Bjørgen, U. Olsbye, P. Dh. C. Dietzel, S. Bordiiaaga, C. Prestipino, C. Lamberti, and K. P. Lillerud, “The inconsistency in adsorption properties and powder XRD data of MOF-5 is rationalized by framework interpenetration and the presence of organic and inorganic species in the nanocavities,” *J. Am. Chem. Soc.*, vol. 129, no. 12, pp. 3612–3620, 2007.
- [99] M. Kim, J. F. Cahill, H. Fei, K. A. Prather, and S. M. Cohen, “Postsynthetic Ligand and Ion Exchange in Robust Metal – Organic Frameworks,” *J. Am. Chem. Soc.*, vol. 134, no. 43, pp. 18082–18088, 2012.
- [100] S. Choi, J. H. Drese, and C. W. Jones, “Adsorbent Materials for Carbon Dioxide Capture from Large Anthropogenic Point Sources,” *ChemSusChem*, vol. 2, pp. 796–854, 2009.
- [101] K. S. Suslick, T. Hyeon, M. Fang, J. T. Ries, and A. A. Cichowlas, “Sonochemical Synthesis of Nanophase Metals, Alloys and Carbides,” *Mater. Sci. Forum*, vol. 225–227, pp. 903–912, 1996.
- [102] C. Chen, J. Kim, D. W. Park, and W. S. Ahn, “Ethylenediamine grafting on a zeolite-like metal organic framework (ZMOF) for CO₂ capture,” *Mater. Lett.*, vol. 106, pp. 344–347, 2013.
- [103] Z. Xiang, D. Cao, X. Shao, W. Wang, J. Zhang, and W. Wu, “Facile preparation of high-capacity hydrogen storage metal-organic frameworks: A combination of microwave-assisted solvothermal synthesis and supercritical activation,” *Chem. Eng. Sci.*, vol. 65, no. 10, pp. 3140–3146, 2010.
- [104] P. M. Forster, A. R. Burbank, M. C. O’Sullivan, N. Guillou, C. Livage, G. Férey, N. Stock, and A. K. Cheetham, “Single-crystal characterization of Co₇(OH)₆(H₂O)₃(C₄H₄O₄)·4·7H₂O; A new cobalt succinate identified through high-throughput synthesis,” *Solid State Sci.*, vol. 7, no. 12, pp. 1549–1555, 2005.

References

- [105] M. Eddaoudi, D. B. Moler, H. Li, B. Chen, T. M. Reineke, M. O’Keeffe, and O. M. Yaghi, “Modular chemistry: Secondary building units as a basis for the design of highly porous and robust metal-organic carboxylate frameworks,” *Acc. Chem. Res.*, vol. 34, no. 4, pp. 319–330, 2001.
- [106] W. J. Son, J. Kim, and W. S. Ahn, “Sonochemical synthesis of MOF-5,” *Chem. Commun.*, no. 47, pp. 6336–6338, 2008.
- [107] Z. Lin, D. S. Wragg, and R. E. Morris, “Microwave-assisted synthesis of anionic metal-organic frameworks under ionothermal conditions,” *Chem. Commun.*, vol. 4, no. 19, p. 2021, 2006.
- [108] N. A. Khan, E. Haque, and S. H. Jung, “Rapid syntheses of a metal-organic framework material $\text{Cu}_3(\text{BTC})_2(\text{H}_2\text{O})_3$ under microwave: a quantitative analysis of accelerated syntheses,” *Phys. Chem. Chem. Phys.*, vol. 12, no. 11, pp. 2625–2631, 2010.
- [109] H.-Y. Cho, D.-A. Yang, J. Kim, S.-Y. Jeong, and W.-S. Ahn, “CO₂ adsorption and catalytic application of Co-MOF-74 synthesized by microwave heating,” *Catal. Today*, vol. 185, no. 1, pp. 35–40, 2012.
- [110] J. Liu and A. T. Harris, “Microwave-assisted acid digestion of alumina-supported carbon nanotubes,” *Sep. Purif. Technol.*, vol. 62, no. 3, pp. 602–608, 2008.
- [111] J. S. Lee, S. B. Halligudi, N. H. Jang, D. W. Hwang, J. S. Chang, and Y. K. Hwang, “Microwave synthesis of a porous metal-organic framework, nickel(II) dihydroxyterephthalate and its catalytic properties in oxidation of cyclohexene,” *Bull. Korean Chem. Soc.*, vol. 31, no. 6, pp. 1489–1495, 2010.
- [112] Y. Bae, K. L. Mulfort, H. Frost, P. Ryan, S. Punnathanam, L. J. Broadbelt, J. T. Hupp, and R. Q. Snurr, “Separation of CO₂ from CH₄ Using Mixed-Ligand Metal - Organic Frameworks,” *Langmuir*, vol. 24, no. 16, pp. 8592–8598, 2008.
- [113] N. A. Khan, I. J. Kang, H. Y. Seok, and S. H. Jung, “Facile synthesis of nano-sized metal-organic frameworks, chromium-benzenedicarboxylate, MIL-101,” *Chem. Eng. J.*, vol. 166, no. 3, pp. 1152–1157, 2011.
- [114] Y.-K. Seo, G. Hundal, I. T. Jang, Y. K. Hwang, C.-H. Jun, and J.-S. Chang, “Microwave synthesis of hybrid inorganic-organic materials including porous $\text{Cu}_3(\text{BTC})_2$ from Cu(II)-trimesate mixture,” *Microporous Mesoporous Mater.*, vol. 119, no. 1–3, pp. 331–337, 2009.
- [115] P. M. Forster and A. Cheetham*, “Open-Framework Nickel Succinate, $[\text{Ni}_7(\text{C}_4\text{H}_4\text{O}_4)_6(\text{OH})_2(\text{H}_2\text{O})_2] \cdot 2\text{H}_2\text{O}$: A New Hybrid Material with Three-Dimensional Ni-O-Ni Connectivity*,” *Situ*, vol. 7, pp. 457–459, 2002.
- [116] J. Zhang, Lukasz, R. W. Larsen, M. Eddaoudi, and M. J. Zaworotko, “Temperature and Concentration Control over Interpenetration in a Metal - Organic Material,” *J. Am. Chem. Soc.*, vol. 131, no. 47, pp. 17040–17041, 2009.
- [117] C. Livage, C. Egger, and G. Férey, “Hybrid Open Networks (MIL-16): Synthesis, Crystal Structure, and Ferrimagnetism of $\text{Co}_4(\text{OH})_2(\text{H}_2\text{O})_2(\text{C}_4\text{H}_4\text{O}_4)_3 \cdot 2\text{H}_2\text{O}$, a New Layered Co(II) Carboxylate with 14-Membered Ring Channels,” *Chem. Mater.*, vol. 11, no. 6, pp. 1546–1550, 1999.

References

- [118] Y. Jin, D.-Y. Jung, K. Hong, G. Demazeau, and Y. J. Kim, "Solid solution of transition metal-dicarboxylates with tunable magnetic properties," *Solid State Sci.*, vol. 3, no. 8, pp. 837–846, 2001.
- [119] D. Sarma and S. Natarajan, "Usefulness of in situ single crystal to single crystal transformation (SCSC) studies in understanding the temperature-dependent dimensionality cross-over and structural reorganization in copper-containing metal-organic frameworks (MOFs)," *Cryst. Growth Des.*, vol. 11, no. 12, pp. 5415–5423, 2011.
- [120] H. L. Jiang, Y. Tatsu, Z. H. Lu, and Q. Xu, "Non-, micro-, and mesoporous metal-organic framework isomers: Reversible transformation, fluorescence sensing, and large molecule separation," *J. Am. Chem. Soc.*, vol. 132, no. 16, pp. 5586–5587, 2010.
- [121] O. Kozachuk, K. Khaletskaya, M. Halbherr, A. Bétard, M. Meilikhov, R. W. Seidel, B. Jee, A. Pöppl, and R. A. Fischer, "Microporous Mixed-Metal Layer-Pillared [Zn_{1-x}Cu_x(bdc)(dabco)_{0.5}] MOFs: Preparation and Characterization," *Eur. J. Inorg. Chem.*, vol. 2012, no. 10, pp. 1688–1695, 2012.
- [122] M. Kandiah, M. H. Nilsen, S. Usseglio, S. Jakobsen, U. Olsbye, M. Tilset, C. Larabi, E. A. Quadrelli, F. Bonino, and K. P. Lillerud, "Synthesis and stability of tagged UiO-66 Zr-MOFs," *Chem. Mater.*, vol. 22, no. 24, pp. 6632–6640, 2010.
- [123] P. D. C. Dietzel, B. Panella, M. Hirscher, R. Blom, and H. Fjellvåg, "Hydrogen adsorption in a nickel based coordination polymer with open metal sites in the cylindrical cavities of the desolvated framework," *Chem. Commun. (Camb.)*, vol. 1, no. 9, pp. 959–961, 2006.
- [124] N. Guillou, C. Livage, W. van beek, M. Nogues, and G. Férey, "A layered Nickel Succinate with Unprecedented Hexanickel Units: Structure Elucidation from Powder-Diffraction Data, and Magnetic and Sorption Properties," *Chemie*, vol. 116, no. 6, pp. 667–671, 2003.
- [125] O. Shekhah, H. Wang, D. Zacher, R. A. Fischer, and C. Wöll, "Growth mechanism of metal-organic frameworks: Insights into the nucleation by employing a step-by-step route," *Angew. Chemie - Int. Ed.*, vol. 48, no. 27, pp. 5038–5041, 2009.
- [126] R. Ameloot, F. Vermoortele, W. Vanhove, M. B. J. Roeffaers, B. F. Sels, and D. E. De Vos, "Interfacial synthesis of hollow metal-organic framework capsules demonstrating selective permeability," *Nat. Chem.*, vol. 3, no. 5, pp. 382–387, 2011.
- [127] P. Chowdhury, C. Bikkina, D. Meister, F. Dreisbach, and S. Gumma, "Comparison of adsorption isotherms on Cu-BTC metal organic frameworks synthesized from different routes," *Microporous Mesoporous Mater.*, vol. 117, no. 1–2, pp. 406–413, 2009.
- [128] N. Guillou, C. Livage, W. van beek, M. Nogues, and G. Férey, "A Layered Nickel Succinate with Unprecedented Hexanickel Units: Structure Elucidation from Powder-Diffraction Data, and Magnetic and Sorption Properties," *Angew. Chemie*, vol. 115, no. 6, pp. 667–671, 2003.
- [129] A. K. Cheetham, C. N. R. Rao, and R. K. Feller, "Structural diversity and chemical trends in hybrid inorganic-organic framework materials," *Chem. Commun.*, no. 46, p. 4780, 2006.
- [130] P. D. C. Dietzel, Y. Morita, R. Blom, and H. Fjellvåg, "An In Situ High-Temperature

References

- Single-Crystal Investigation of a Dehydrated Metal-Organic Framework Compound and Field-Induced Magnetization of One-Dimensional Metal-Oxygen Chains,” *Angew. Chemie*, vol. 117, no. 39, pp. 6512–6516, 2005.
- [131] Y.-Q. Zheng and J.-L. Lin, “Crystal structure of tricobalt dihydroxide disuccinate decahydrate,” vol. 6, pp. 139–140, 2000.
- [132] F. J. Caires, L. S. Lima, C. T. Carvalho, R. J. Giagio, and M. Ionashiro, “Thermal behaviour of malonic acid, sodium malonate and its compounds with some bivalent transition metal ions,” *Thermochim. Acta*, vol. 497, no. 1–2, pp. 35–40, 2010.
- [133] I. V. Shabanova, V. T. Panyushkin, T. P. Storozhenko, and V. I. Zelenov, “Standard Enthalpies of Formation of Neodymium (III) and Erbium (III) Succinates and Malates,” vol. 75, no. 8, pp. 1171–1172, 2005.
- [134] M. C. Bernini, E. V. Brusau, G. E. Narda, G. E. Echeverria, C. G. Pozzi, G. Punte, and C. W. Lehmann, “The effect of hydrothermal and non-hydrothermal synthesis on the formation of holmium(III) succinate hydrate frameworks,” *Eur. J. Inorg. Chem.*, no. 5, pp. 684–693, 2007.
- [135] Y. Q. Tian, Y. M. Zhao, Z. X. Chen, G. N. Zhang, L. H. Weng, and D. Y. Zhao, “Design and generation of extended zeolitic metal-organic frameworks (ZMOFs): Synthesis and crystal structures of zinc(II) imidazolate polymers with zeolitic topologies,” *Chem. - A Eur. J.*, vol. 13, no. 15, pp. 4146–4154, 2007.
- [136] L. Huang, “Synthesis, morphology control, and properties of porous metal–organic coordination polymers,” *Microporous Mesoporous Mater.*, vol. 58, no. 2, pp. 105–114, 2003.
- [137] J. L. C. Rowsell and O. M. Yaghi, “Metal-organic frameworks: A new class of porous materials,” *Microporous Mesoporous Mater.*, vol. 73, no. 1–2, pp. 3–14, 2004.
- [138] K. Sumida, D. L. Rogow, J. A. Mason, T. M. McDonald, E. D. Bloch, Z. R. Herm, T. Bae, and J. R. Long, “Carbon Dioxide Capture in Metal-Organic Frameworks,” *Am. Chem. Soc.*, vol. 112, pp. 724–781, 2012.
- [139] J. Getzschmann, I. Senkovska, D. Wallacher, M. Tovar, D. Fairen-Jimenez, T. Düren, J. M. van Baten, R. Krishna, and S. Kaskel, “Methane storage mechanism in the metal-organic framework Cu₃(btc)₂: An in situ neutron diffraction study,” *Microporous Mesoporous Mater.*, vol. 136, no. 1–3, pp. 50–58, 2010.
- [140] R. Serna-guerrero, E. Da, and A. Sayari, “New Insights into the Interactions of CO₂ with Amine-Functionalized Silica,” *Ind. Eng. Chem. Res.*, vol. 47, pp. 9406–9412, 2008.
- [141] M. Alhamami, H. Doan, and C.-H. Cheng, “A Review on Breathing Behaviors of Metal-Organic-Frameworks (MOFs) for Gas Adsorption,” *Materials (Basel)*, vol. 7, no. 4, pp. 3198–3250, 2014.
- [142] A. O. Yazaydin, A. I. Benin, S. a Faheem, P. Jakubczak, J. J. Low, R. R. Willis, and R. Q. Snurr, “Enhanced CO₂ Adsorption in Metal-Organic Frameworks via Occupation of Open-Metal ...,” *Chem. Mater.*, vol. 21, no. 13, pp. 1425–1430, 2009.
- [143] Y. Park, D. S. Shin, S. H. Woo, N. S. Choi, K. H. Shin, S. M. Oh, K. T. Lee, and S. Y. Hong, “Sodium terephthalate as an organic anode material for sodium ion batteries,”

References

- Adv. Mater.*, vol. 24, no. 26, pp. 3562–3567, 2012.
- [144] D. Sarma, K. V. Ramanujachary, S. E. Lofland, T. Magdaleno, and S. Natarajan, “Amino acid based mofs: Synthesis, structure, single crystal to single crystal transformation, Magnetic and related studies in a family of cobalt and nickel aminoisophthales,” *Inorg. Chem.*, vol. 48, no. 24, pp. 11660–11676, 2009.
- [145] X. Xu, C. Song, J. M. Andresen, B. G. Miller, and A. W. Scaroni, “Novel polyethylenimine-modified mesoporous molecular sieve of MCM-41 type as high-capacity adsorbent for CO₂ capture,” *Energy and Fuels*, vol. 16, no. 6, pp. 1463–1469, 2002.
- [146] P. Sharrock and T. Theophanides, “Etude des succinates simples et complexes de cobalt(II),” *Can. J. Chem.*, vol. 53, no. 1, pp. 98–105, 1975.
- [147] Y.-Y. Liang, L. Cao, L.-B. Kong, and H.-L. Li, “Synthesis of Co(OH)₂/USY composite and its application for electrochemical supercapacitors,” *J. Power Sources*, vol. 136, no. 1, pp. 197–200, 2004.
- [148] C. A. F. de Oliveira, F. F. da Silva, I. Malvestiti, V. R. D. Malta, J. D. L. Dutra, N. B. da Costa, R. O. Freire, and S. A. Junior, “Effect of temperature on formation of two new lanthanide metal-organic frameworks: Synthesis, characterization and theoretical studies of Tm(III)-succinate,” *J. Solid State Chem.*, vol. 197, pp. 7–13, 2013.
- [149] M. Eddaoudi, D. B. Moler, H. Li, B. Chen, T. M. Reineke, M. O. Keffe, and O. M. Yaghi, “Modular Chemistry : Secondary Building Units as a Basis for the Design of Highly Porous and Robust Metal – Organic Carboxylate Frameworks Modular Chemistry : Secondary Building Units as a Basis for the Design of Highly Porous and Robust Metal-Organic Carb,” *Acc. Chem. Res.*, vol. 34, no. 4, pp. 319–330, 2001.
- [150] Y.-X. Sun and W.-Y. Sun, “Influence of temperature on metal-organic frameworks,” *Chinese Chem. Lett.*, vol. 25, no. 6, pp. 823–828, 2014.
- [151] L. Poul, A. Jouini, Nouredine, and F. Fievet, “Layered Hydroxide Metal Acetates (Metal = Zinc, Cobalt, and Nickel): Elaboration via Hydrolysis in Polyol Medium and Comparative Study,” *Chem. Mater.*, vol. 12, no. 10, pp. 3123–3132, 2000.
- [152] M. Bordbar, M. Tabatabaee, M. Alizadeh-Nouqi, Z. Mehri-Lighvan, H. R. Khavasi, A. YeganehFaal, F. Fallahian, and M. Dolati, “Synthesis, characterization, cytotoxic activity and DNA-binding studies of cobalt (II) mixed-ligand complex containing pyridine-2,6-dicarboxylate ion and 2-aminopyrimidine,” *J. Iran. Chem. Soc.*, vol. 13, no. 6, pp. 1125–1132, 2016.
- [153] B. S. Randhawa and K. Gandotra, “A comparative study on the thermal decomposition of some transition metal carboxylates,” *J. Therm. Anal. Calorim.*, vol. 85, no. 2, pp. 417–424, 2005.
- [154] Y. Go, X. Wang, E. V. Anokhina, and A. J. Jacobson, “A chain of changes: Influence of noncovalent interactions on the one-dimensional structures of nickel(II) dicarboxylate coordination polymers with chelating aromatic amine ligands,” *Inorg. Chem.*, vol. 43, no. 17, pp. 5360–5367, 2004.
- [155] P. Chowdhury, C. Bikkina, D. Meister, F. Dreisbach, and S. Gumma, “Comparison of adsorption isotherms on Cu-BTC metal organic frameworks synthesized from different routes,” *Microporous Mesoporous Mater.*, vol. 117, no. 1, pp. 406–413, 2009.

References

- [156] M. H. Zeng, Y. L. Zhou, M. C. Wu, H. L. Sun, and M. Du, "A unique cobalt(II)-based molecular magnet constructed of hydroxyl/carboxylate bridges with a 3D pillared-layer motif," *Inorg. Chem.*, vol. 49, no. 14, pp. 6436–6442, 2010.
- [157] L.-S. Long, X.-M. Chen, M.-L. Tong, Z.-G. Sun, Y.-P. Ren, R.-B. Huang, and L.-S. Zheng, "A unique open inorganic–organic framework with alternate hexa- and penta-coordinate cobalt(ii) sites. Synthesis, crystal structure and magnetic properties of $[\text{Co}_3(\text{C}_4\text{H}_4\text{O}_4)_2 \cdot 2.5(\text{OH})]_n \cdot 0.5n\text{H}_2\text{O}$," *J. Chem. Soc. Dalton Trans.*, vol. 3, no. 19, pp. 2888–2890, 2001.
- [158] N. Guillou, C. Livage, and G. Férey, "Cobalt and Nickel Oxide Architectures in Metal Carboxylate Frameworks.pdf," *Eur. J. Inorg. Chem.*, pp. 4963–4978, 2006.
- [159] T. Pham, K. A. Forrest, A. Hogan, B. Tudor, K. McLaughlin, J. L. Belof, J. Eckert, and B. Space, "Understanding hydrogen sorption in In-soc-MOF: A charged metal-organic framework with open-metal sites, narrow channels, and counterions," *Cryst. Growth Des.*, vol. 15, no. 3, pp. 1460–1471, 2015.
- [160] P. Deria, J. E. Mondloch, E. Tylianakis, P. Ghosh, W. Bury, R. Q. Snurr, J. T. Hupp, and O. K. Farha, "Perfluoroalkane Functionalization of NU-1000 via Solvent-Assisted Ligand Incorporation: Synthesis and CO₂ Adsorption Studies," *Am. Chem. Soc.*, vol. 14, pp. 20–23, 2013.
- [161] D.-W. Jung, D.-A. Yang, J. Kim, J. Kim, and W.-S. Ahn, "Facile synthesis of MOF-177 by a sonochemical method using 1-methyl-2-pyrrolidinone as a solvent," *Dalton Trans.*, vol. 39, pp. 2883–2887, 2010.
- [162] A. Carton, A. Mesbah, T. Mazet, F. Porcher, and M. François, "Ab initio crystal structure of nickel(II) hydroxy-terephthalate by synchrotron powder diffraction and magnetic study," *Solid State Sci.*, vol. 9, no. 6, pp. 465–471, 2007.
- [163] a. K. Tripathi, a. Sahasrabudhe, S. Mitra, R. Mukhopadhyay, N. M. Gupta, and V. B. Kartha, "QENS and FTIR studies on binding states of benzene molecules adsorbed in zeolite HZSM-5 at room temperature," *Phys. Chem. Chem. Phys.*, vol. 3, no. 19, pp. 4449–4455, 2001.
- [164] P. K. Prabhakaran and J. Deschamps, "Room temperature hydrogen uptake in single walled carbon nanotubes incorporated MIL-101 doped with lithium: effect of lithium doping," *J. Porous Mater.*, vol. 22, no. 6, pp. 1635–1642, 2015.
- [165] C.-W. Tang, C.-B. Wang, and S.-H. Chien, "Characterization of cobalt oxides studied by FT-IR, Raman, TPR and TG-MS," *Thermochim. Acta*, vol. 473, no. 1–2, pp. 68–73, 2008.
- [166] P. Mukherjee, M. G. B. Drew, V. Tangoulis, M. Estrader, C. Diaz, and A. Ghosh, "Facile strategies for the synthesis and crystallization of linear trinuclear nickel(II)-Schiff base complexes with carboxylate bridges: Tuning of coordination geometry and magnetic properties," *Polyhedron*, vol. 28, no. 14, pp. 2989–2996, 2009.
- [167] Y. Kuwahara, D. Y. Kang, J. R. Copeland, P. Bollini, C. Sievers, T. Kamegawa, H. Yamashita, and C. W. Jones, "Enhanced CO₂ adsorption over polymeric amines supported on heteroatom-incorporated SBA-15 silica: Impact of heteroatom type and loading on sorbent structure and adsorption performance," *Chem. - A Eur. J.*, vol. 18, no. 52, pp. 16649–16664, 2012.

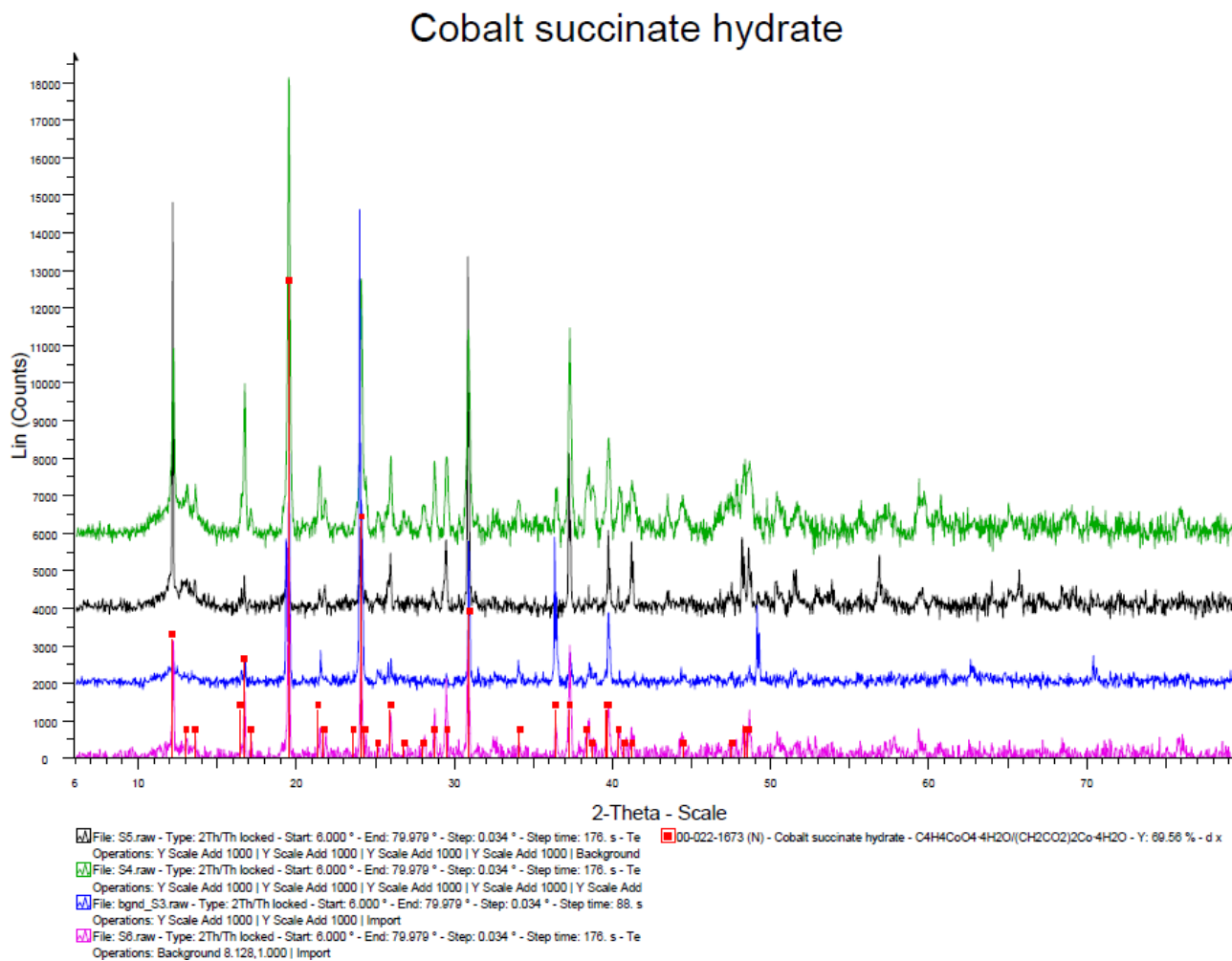
References

- [168] M. Dey, C. P. Rao, P. K. Saarenketo, and K. Rissanen, "Mono-, di- and tri-nuclear Ni (II) complexes of N-, O-donor ligands: structural diversity and reactivity," *Inorg. Chem.*, vol. 5, no.11, pp. 924–928, 2002.
- [169] C. M. Lu, J. Liu, K. Xiao, and A. T. Harris, "Microwave enhanced synthesis of MOF-5 and its CO₂ capture ability at moderate temperatures across multiple capture and release cycles," *Chem. Eng. J.*, vol. 156, no. 2, pp. 465–470, 2010.
- [170] Z. Liang, M. Marshall, and A. L. Chaffee, "CO₂ adsorption-based separation by metal organic framework (Cu-BTC) versus zeolite (13X)," *Energy and Fuels*, vol. 23, no. 5, pp. 2785–2789, 2009.
- [171] S. R. Miller, P. A. Wright, T. Devic, C. Serre, P. L. Llewellyn, R. Denoyel, L. Gheberova, and Y. Filinchuk, "Single Crystal X-ray Diffraction Studies of Carbon Dioxide and Fuel-Related Gases Adsorbed on the Small Pore Scandium Terephthalate Metal Organic Framework, $Sc_2(O_2CC_6H_4CO_2)_3$," *Am. Chem. Soc.*, vol. 2, no. 9, pp. 3618–3626, 2009.
- [172] J. An, S. J. Geib, and N. L. Rosi, "High and Selective CO₂ Uptake in a Cobalt Adeninate Metal - Organic Framework Exhibiting Pyrimidine- and Amino-Decorated Pores," *Am. Chem. Soc.*, vol. 132, pp. 38–39, 2010.
- [173] A. R. Millward and O. M. Yaghi, "Metal Organic Frameworks with Exceptionally High Capacity for Storage of Carbon Dioxide at Room Temperature," *J. Am. Chem. Soc.*, vol. 127, no. 51, pp. 17998–17999, 2005.
- [174] B. Chen, N. W. Ockwig, A. R. Millward, D. S. Contreras, and O. M. Yaghi, "High H₂ adsorption in a microporous metal-organic framework with open metal sites," *Angew. Chemie - Int. Ed.*, vol. 44, no. 30, pp. 4745–4749, 2005.

UNIVERSITY of the
WESTERN CAPE

APPENDIX

Figure A1: XRD spectra of CoS., CoS-Ac, CoS-Th, and CoS-Sn matching with cobalt succinates from JCP2 data from iThemba lab.



Appendix

Table A1: 2-theta peaks of cobalt succinates hydrated from JCPDS

Pattern : 00-022-1673		Radiation = 1.540600		Quality : Not Indexed			
C ₄ H ₄ CoO ₄ ·4H ₂ O /(CH ₂ CO ₂) ₂ Co·4H ₂ O Cobalt succinate hydrate		2θ	I	h	k	l	
		12 048	25				
		12 513	5				
		13 578	15				
		16 341	10				
		16 410	20				
		17 038	5				
		19 453	100				
		21 290	10				
		21 448	5				
		23 517	5				
		24 033	50				
		24 270	5				
		25 064	5				
		25 879	10				
		26 750	5				
		27 047	5				
		28 821	5				
		29 455	5				
		30 660	30				
		32 060	5				
		36 343	10				
		37 217	10				
		38 320	5				
		38 660	5				
		39 690	10				
		39 673	10				
		40 340	5				
		40 701	5				
		41 487	5				
		44 479	5				
		47 516	5				
		48 376	5				
		48 541	5				
Lattice : Not assigned S.G. : (0)		Mol. weight = 247.07					
Color: Violet-red Data collection flag: Ambient.							
My et al., C. R. Seances Acad. Sci., Ser. C, volume 268, page 406 (1969) CAS Number: 23188-11-6							
Radiation : CoKa Lambda : 1.79020		Filter : Beta d-sp : Not given					

UNIVERSITY of the
WESTERN CAPE

Appendix

Table A2: 2-theta peaks of anhydrous crystalline cobalt succinate which match with CoS-Pr1, CoS-Pr2, and CoS-Pr3 obtained from JCPDS.

<i>Pattern</i> : 00-022-1672		<i>Radiation</i> = 1.540598					<i>Quality</i> : Not indexed					
$C_4H_4CoO_4$ $/(CH_2CO_2)_2Co$ Cobalt succinate		2th	i	h	k	l						
		9.302	80									
		10.101	100									
		19.238	20									
		20.305	20									
		25.354	20									
		31.937	10									
		33.797	10									
		35.108	15									
		38.993	15									
Lattice : Not assigned S.G. : (0)		Mol. weight = 175.01										
Reason 'O' quality was assigned: O assigned because of small number of lines. (Ed.) Data collection flag: Ambient.												
My et al., C. R. Seances Acad. Sci., Ser. C, volume 268, page 406 (1969) CAS Number: 3267-76-3												
Radiation : CoKa Lambda : 1.79020		Filter : Beta d-sp : Not given										